TRIBOEMISSION FROM CERAMICS: CHARGE INTENSITY AND ENERGY DISTRIBUTION CHARACTERIZATIONS

Gustavo J. Molina

Dissertation submitted to the Faculty of
Virginia Polytechnic Institute and State University
in partial fulfillment of the requirements for the degree of

Doctor of Philosophy
in
Mechanical Engineering

Michael J. Furey, Chairman
A.L.Ritter
Czeslaw Kajdas
Brian Vick
Norman S. Eiss

July 3, 2000

Blacksburg, Virginia

Keywords: Triboemission, Exoemission, Tribochemistry, Tribopolymerization, Convoluted Poisson Distribution

TRIBOEMISSION FROM CERAMICS: CHARGE INTENSITY AND ENERGY DISTRIBUTION CHARACTERIZATIONS

by

Gustavo J. Molina

Michael J. Furey, Chairman

(ABSTRACT)

Lubrication of ceramics is a difficult and not completely solved problem. Ceramics do not respond to conventional lubricants which are designed to function by a chemical reaction with the surface. There is, accordingly, increased interest in the development of lubrication alternatives for ceramics, and in understanding the tribochemical fundamentals by which new lubrication processes can be designed and controlled. In particular, the mechanism of tribopolymerization for some addition-type monomers is thought to be initiated and controlled by triboemitted low-energy electrons.

This Ph.D. dissertation presents the experimental work carried out at the Virginia Polytechnic Institute and State University for the characterization of charge intensity and energy distribution of charged-particles triboemitted from sliding contacts of ceramics.

A review is presented of research work on tribochemistry and, in particular, on tribopolymerization as a lubrication mechanism. Relevant literature is also reviewed on the phenomena of exoemission, triboemission and fractoemission of charged-particles. The design, construction and development of a new instrument and data acquisition system to carry out triboemission measurements under high vacuum and for controlled load, sliding speed and retarding grid-voltage is described.

The charge intensity is characterized of the particles triboemitted from two related ceramics, alumina and sapphire, and from one metallic material, i.e., aluminum, when scratched by a diamond pin.

In the case of alumina, triboemitted-charge intensity also is studied by sliding contact of an alumina ball. Burst-type negatively-charged particle triboemission was observed from diamond-on-alumina, diamond-on-sapphire, and alumina-on-alumina sliding contacts. The different crystalline structure, i.e., of alumina and sapphire, does not appear to be a factor in electron triboemission. In general, large bursts of electron triboemission may appear superimposed on a constant lower level of small-burst emission. This constant level, being higher than background-noise, does not vary between different ceramic specimens, while maximum levels of triboemission-bursts differ by two orders of magnitude between different specimens. The characteristic decay-time of the triboemission bursts is found of about 100ms. Lower-level decaying post-contact emission of negatively-charged particles from ceramics is observed.

Low negatively-charged triboemission was observed from diamond-on-aluminum sliding contacts. The positively-charged triboemission from these sliding material systems was also measured. Low positive-ion emission, barely above background level, was observed for the diamond-on-ceramics and alumina-on-alumina systems.

The retarded-energy spectra of the negatively-charged particle triboemissions from ceramics were also obtained. Such spectra show decaying rates of triboemission for increasing minimum energy of the triboemitted particles: an important fraction of the total electron triboemission is produced in the zero to 5eVolts energy-range, with a decaying tail extending beyond the test maximum level of 48 Volts.

These experimental measurements are discussed with a focus on the possible role of triboemitted charged-particles in tribopolymerization as a mechanism of ceramic lubrication. It is concluded that low-energy electrons are emitted in bursts from ceramics under sliding contact, the essential first step in the hypotheses of tribopolymerization of certain addition-type monomers, while positively-charged emission is negligible. These findings strongly support tribopolymerization results from previous research.

A frequency domain analysis of the triboemission data is carried out. For the electron-triboemission outputs, a characteristic pattern is found for the experimentally estimated frequencies of occurrence of the triboemitted particles. A new probability distribution, called "Convoluted Poisson" is developed to describe this triboemission data. Good agreement is found between the probabilities of triboemitted-particle occurrence, as predicted by such distribution, and the experimental probabilities estimated from triboemission outputs. The significance of the two parameters defining this "Convoluted Poisson" distribution is explored and discussed with a focus on basic surface-change phenomena.

ACKNOWLEDGMENT

I wish to express my sincere gratitude to Dr. Michael J. Furey, Chairman of my advisory committee, for his invaluable suggestions, guidance, continuous encouragement and help during the course of this research.

I would also like to thank Dr. A. L. Ritter, Dr. Czeslaw Kajdas, Dr. Brian Vick and Dr. Norman Eiss for serving on my advisory committee. Their recommendations during this research work proved extremely useful. I am specially indebted to Dr. Ritter and Dr. Kajdas for their generous assistance, support and advice, which played a big role in the success of this study, and to Dr. Vick, for his suggestions during numerous meetings we had. I would also like to thank Dr. Roman Kempinski for his involvement with this project.

I am very grateful to the National Science Foundation, Surface Engineering and Tribology Program for the financial support provided for this research.

I would also like to express my acknowledgments to the staff of the Department of Mechanical Engineering, and to the staffs of the Machine Shop and the Electronics Shop at the Department of Physics for their key assistance to the success of this research. I specially acknowledge the assistance of Ms. P. Malosse in taking wear measurements related to this dissertation research. I also thank Dr. L. Berrien, Dr. A.C. Christiaen, Mr. D. Mazilu, Mr. S. Talluri, Mr. K. Iskandar, Mr. M. Owellen and Mr. J. Valentino, who were with me during laboratory work; working with them was an enjoyable experience.

Finally, I wish to give a special thought to my wife Virna for her love, support, patience and understanding.

TABLE OF CONTENTS

Page

LIST OF FIGURES

Page

LIST OF TABLES

Page

CHAPTER 1. INTRODUCTION

1.1. Problem statement and rationale

Ceramics are increasingly employed over conventional materials in tribological systems. Because of their outstanding thermo-mechanical properties (e.g., strength, hardness, thermal resistance) and their chemical inertness, ceramics are ideal candidates for applications in engine and turbine components, bearings, pump seals, etc. However, such practical applications demand a better understanding of friction and wear in ceramic-material system. Ceramics present challenging tribological problems which require entirely different solutions.

Ceramic chemical inertness, in addition to being a design advantage in critical applications, constitutes a lubrication problem: ceramics do not respond to conventional lubricants, which are designed to function by a chemical reaction with the surface. The lubrication of ceramics is a difficult and still not completely solved problem. There is, accordingly, increased interest in the development of lubrication alternatives for ceramics, and in the understanding of tribochemical fundamentals by which new lubrication processes can be designed and controlled.

Tribopolymerization, a mechanism developed by Furey and Kajdas [1] and reviewed in subsection 2.1.2 of this dissertation, provides boundary lubrication to ceramics by the continuous formation of a protective polymeric film on rubbing surfaces. In particular, tribopolymerization for addition-type monomers is thought to be initiated by low-energy electrons. These so-called exoelectrons are emitted when ceramic or surface oxides are perturbed during tribological contact. Triboemitted charged-particles (both ions and electrons) are one important aspect of the more general phenomenon of triboemission, which is reviewed in section 2.3. Triboemitted particles may have a dramatic, if not controlling, influence on some tribochemical reactions which occur in the contact region.

Although a number of studies have demonstrated that charged particles are emitted from mechanically activated surfaces, including ceramics, the experimental picture relating triboemission to sliding-contact variables is unknown. In particular, fundamental experimental knowledge is needed on the charge intensity and energy distribution of

charged-particles triboemitted from ceramics, as well as on eventual relations of the triboemission level to the operational and material variables. Such knowledge can be of key importance in understanding the role of particle emission in tribochemical processes and, in particular, in tribopolymerization as a mechanism of ceramic lubrication.

The research work reported in this dissertation carried out fundamental experimental measurements of triboemitted charged-particles. It was conducted for the project "Triboemission of Charged Particles from Ceramic Surfaces and Their Role in Tribochemistry" [2], funded by the National Science Foundation, Surface Engineering and Tribology Program. This project is being developed in the Department of Mechanical Engineering and the Department of Physics at the Virginia Polytechnic Institute and State University, and also involves scientists from the Warsaw University of Technology, Institute of Chemistry in Plock, Poland.

The principal investigators of this project are Dr. Michael J. Furey in the Department of Mechanical Engineering, Dr. A. L. Ritter in the Department of Physics, Virginia Polytechnic Institute and State University, and Dr. Czeslaw Kajdas from the Warsaw University of Technology, Poland. Dr. Brian Vick in the Department of Mechanical Engineering, Virginia Polytechnic Institute and State University, and Dr.Roman Kempinski from the Warsaw University of Technology, Poland, have actively participated in this project in, respectively, modeling and calculations of friction-generated surface temperatures and carrying out tribopolymerization tests and surface examinations.

1.2. Research questions of interest

Among the several unknowns regarding triboemission phenomena, the following research questions of interest are addressed by this research work.

What are the experimental conditions required for the measurement of triboemitted charged-particles?

What are the basic characteristics of charged-particle triboemitted from ceramic systems scratched by diamond (A-on-B systems)?

Are charged-particles emitted from sliding friction of same-ceramic systems (A-on-A ceramic systems)? If so, how does charge intensity relate to that of triboemissions from A-on-B ceramic systems?

Are both positively- and negatively-charged particles triboemitted from ceramic contacts? If so, what is ratio of positively- to negatively-charged triboparticles?

What is the energy distribution of these triboemitted charged-particles?

What is the time dependency of charged-particle triboemission intensity in ceramics?

Does charged-particle triboemission from ceramics relate to the operational variables, e.g., applied load and sliding velocity? Does it relate to ceramic wear?

If triboemission from a ceramic system is significant, are charged-particles also emitted during sliding friction of the related metal (e.g., triboemission from alumina as compared to that from aluminum)?

Does charged-particle triboemission from ceramics relate to the so-called fractoemission from surface-oxides?

Is it possible to describe the occurrence of particle triboemission by classic probability models? Is it possible to describe triboemission phenomena in terms of basic exoemission phenomena from mechanically-excited surfaces?

1.3. Objectives and Plan of the Research

The main goal of this dissertation research is to obtain fundamental knowledge about the charge intensity and energy distribution of charged-particles triboemitted from sliding contacts systems, in particular, from ceramics. Such knowledge is needed for a better understanding of the role of particle emission in tribochemical reactions. To the purpose of such main goal, the following objectives are sought:

(i) To design and develop an instrument adequate for charged-particle triboemission measurements.

(ii) To carry out observations and measurements of charged-particle triboemission outputs from sliding contact systems, in particular, from ceramic systems.

(iii) To investigate relations of the charged-particle triboemission to operational (e.g., load, sped, time) and material-system variables.

(iv) To seek characterizations of the charge intensity and energy distribution of charged-particles triboemitted from sliding contacts.

(v) To explore connections between the observed triboemission phenomena and the surface modifications resulting from friction and wear.

(vi) To obtain fundamental knowledge for the understanding of the role of particle emission in the tribopolymerization mechanism for ceramic lubrication.

The experimental work seeking the above objectives will be carried out according to the following plan of research:

(a) A new triboemission instrument and system will be designed, constructed and developed. The design of this instrument should be based on tribological criteria for maximizing the detected emission and obtaining adequate control of relevant tribological variables. Different particle-detection alternatives (e.g., a picoammeter, a channel electron multiplier) and experimental environments (e.g., ambient, vacuum) will be

explored. Prototype instruments designs will be developed and tested to determine the conditions for efficient detection of triboemitted charged-particle and appropriate acquisition of triboemission signals.

(b) After an adequate instrument is developed, initial tests will be carried out to explore basic features of triboemission (e.g., charge intensity levels and characteristic-time of triboemission outputs) from the sliding contact of ceramic systems. Appropriate measurement techniques should be designed and developed on the basis of such preliminary information.

(c) Experimental measurements will be performed by such instrument of both negatively-charged and positively-charged triboemission intensity from ceramics, and of energy-distributions of these triboparticles. Comparative measurements of triboemission outputs will be carried out for ceramics of same chemical composition but different crystalline structures and for the related base metal (i.e., for alumina, sapphire, and aluminum). Different tribological contacts will be used: a diamond-pin scratching a softer ceramic-surface, and a ceramic ball sliding on the same ceramic-material.

(d) Characterizations will be explored of the triboemission outputs in both the time and the frequency domains of representation. Descriptive models of the data will be proposed and their fits to triboemission outputs will be tested.

(e) Connections will be discussed between the observed triboemission phenomena and the surface modifications resulting from friction and wear.

(f) The role of charged-particle emission in tribopolymerization will be discussed with a focus on Furey and Kajdas' experimental results and hypotheses.

1.4. Presentation of the research work in this dissertation

Triboemission phenomena are of interest in this dissertation research because triboemitted charged-particles may relate to key tribochemical reactions for the lubrication of ceramics surfaces. Chapter 2 presents a literature review on the chemistry of tribological contacts: tribological contact promotes chemical reactions which may be

different and/or may initiate for different conditions than those observed in glassware studies. In particular, the review in Chapter 2 examines the tribopolymerization mechanism for reducing wear of ceramics.

Chapter 2 also presents a review on the emission of charged-particles from solids subjected to mechanical action. There is evidence that the tribopolymerization mechanism, at least in the case of addition-type monomers, is connected with low-energy electron emission. Therefore, this chapter also reviews the so-called exoemission and the charged-particle triboemission phenomena. Chapter 2 finally discusses particle fractoemission from mechanically strained oxides, as it may relate to triboemission.

A new instrument was needed to carry out the triboemission measurements. Chapter 3 thoroughly reports the design, construction and development of this triboemission instrument and its data acquisition system. It also describes the contact geometries and material-systems employed, and the methodologies for experimental testing.

The experimental measurements of charge intensity and energy distribution of particles triboemitted from ceramics are presented in Chapter 4. This chapter also deals with the preliminary characterization of some basic triboemission features, e.g., general triboemission levels and time-characteristics. It also explores relations of triboemission to operational variables and material systems, the knowledge of which was needed for further measurement development.

Chapter 5 discusses the experimental findings on triboemission with a focus on the possible role of triboemitted charged-particles in tribopolymerization as a mechanism of ceramic lubrication. This chapter also presents a frequency domain characterization of triboemission data and proposes a model to describe such data from basic probability distributions. Conclusions and recommendations for future research are presented in Chapters 6 and 7, respectively.

CHAPTER 2. LITERATURE REVIEW

2.1. Mechanochemistry, tribochemistry and tribopolymerization

2.1.1. Mechanochemistry and tribochemistry

Wear of materials occurs by different mechanisms, the occurrence of any mechanism depends on the system (e.g., materials, environment, operating conditions, and the geometry of the wearing bodies). Wear mechanisms are mainly determined by the mechanical properties of solids and the chemical behavior of surfaces [3]. In this, chemistry of tribological wear and friction, which is also called tribochemistry, and its relation to tribophysics have been recently discussed by Kajdas [4]. Tribochemistry can be defined as the branch of chemistry dealing with chemical and physico-chemical changes in rubbing solids [5].

Tribochemical reactions are promoted by mechanical-energy input from the sliding contact between solids: Friction and wear initiate and accelerate chemical reactions that would take place at much higher temperatures or will not initiate in glassware [5]. Although friction may locally produce high temperatures, wear exposes new surface which is known to be extremely reactive. Also, tribochemical reactions affect surface properties, which ultimately determine friction and wear changes.

The importance of tribochemical reactions as controlling factors in friction and wear is apparent in the boundary lubrication regime in particular. In this lubrication condition, friction and wear between the rubbing surfaces are determined by the surface properties and the chemical nature of the lubricant [6].

The feasibility that chemical reactions in solids can be initiated by mechanical deformation and/or tribological contact has been considered for over 100 years. Probably the first work pertinent to the so-called mechanochemistry was performed by Carey-Lea [7-10] in 1892. He showed that shearing action was more effective than

simple hydrostatic pressure to produce halogens from silver halides. Also, by grinding of the latter compounds he made them react with moisture to obtain the corresponding acid. Later, Parker [11] demonstrated the efficacy of mechanical shearing in bringing about chemical reactions. More recently, Gilman [12] discussed the mechanochemical importance of shearing action on the reactivity of solid molecules of various inorganic and organic compounds, ruling out any concurrent effect from thermal energy.

The reactions of freshly created surfaces with the surrounding environment are of particular importance in mechanochemistry. Shaw [13] in the early forties reported on the chemistry involved in metal cutting and employed cutting fluids. Some ten years later, Grunberg [14] showed that metal-cutting under water can produce hydrogen peroxide. St.Pierre et al. [15] demonstrated the importance in lubrication of freshly-formed surfaces. He showed the reactivity of fresh aluminum surfaces in 1-cetene lubricant. Rosenfeld [16,17] reported hydrogen as a by-product from some lubricating oils during sliding wear experiments. He concluded that hydrogen resulted from reaction between lubricating oils and the fresh metal surfaces.

Comprehensive reviews on mechanochemistry can be found in [3-5,18]. The concurrent influence of both mechanics and chemistry in sliding contacts was also reviewed by Singer [19]. A review on the area of tribo-electrochemistry in metal friction was reported by Preis and Dziub [20]. Tamai [21] discussed the role in the activation of polymerization of the so-called exoelectrons – a phenomenon which is reviewed in subsection 2.2.2 – which were emitted from milled metallic-powders. The importance of such electron-initiated reactions will be apparent in the following review of the tribopolymerization mechanism.

2.1.2. Tribopolymerization

Lubrication of ceramics is an example of the importance of tribochemistry. Conventional and often ineffective approaches to ceramic lubrication seldom accounted for the tribochemistry of the surfaces. They included incorporation of lubricant materials in the ceramic matrix, surface treatments and coating, dispersed solid lubricants and antiwear

additives in a conventional lubricant. Ceramic-lubrication remains, however, a difficult and not completely solved problem.

A new approach to the lubrication of ceramics was the introduction by Furey and Kajdas [22] of the mechanism of tribopolymerization: it can be defined as the planned and continuous formation of protective polymeric films directly on tribological surfaces by the use of minor concentrations of selected monomers capable of forming polymer films "in situ" either by polycondensation or addition polymerization. In this mechanism the monomers are incorporated in a carrier (e.g., a liquid hydrocarbon or an inert gas for vapor phase). Due to high temperatures and/or charged-particle emission in regions of greatest contact, the monomers will polymerize "in situ" where they are needed. The mechanism will continue until reduction of friction and wear will cause the rate of film formation to decrease. If the formed film is eventually worn away, this formation rate will increase. The tribopolymerization process therefore constitutes a self-controlled continuous protective-film deposition in a forming/removal/replenishment cycle.

Development of the tribopolymerization mechanism began with conventional metal systems. Initial research by Furey [23,24] showed the anti-scuffing effect of partial monoesters made by reacting long-chain C_{36} dimer-acids with glycols. He also proved the effectiveness of adding the embryonic condensation-type monomer on the rubbing surface by a carrier rather than as a pre-formed polymer. Further research by Furey and Kajdas [25-27] demonstrated the same condensation-type monomer and also some addition-type monomers polymerizing according to an anionic mechanism (e.g., lauryl methacrylate, diallyl phthalate, vinyl acetate) significantly reduced alumina wear. However, an addition-type monomer polymerizing according to a cationic mechanism (e.g., vinyl octadecyl ether) did not significantly reduce alumina wear. A follow-up of the same work [28] proposed an explanatory mechanism of initial chemical reactions with the surface, followed by formation and growth of oligomer/polymer chains.

Furey and Kajdas also studied [29] the effects of tribopolymerization on different substrates by comparison of metal (e.g., steel-on-steel) and ceramic (e.g., alumina-on-alumina) systems. They showed that the tribopolymerization mechanism worked for both condensation-type (e.g., dimer-acid/glycol monoester) and addition-type monomers (e.g., lauryl methacrylate, diallyl phthalate, vinyl acetate), when they are added as minor

concentrations in a carrier. However, the monomers were generally more effective with alumina than with steel. Analysis of the wear tracks by Fourier Transform Infrared Microscopy indicated the details of tribopolymerization could be more complex than originally suggested. Evidences from two surface reactions were found: from the planned formation of oligomeric/polymeric species on the rubbing surfaces and from a chemical reaction with the substrate to form a soap. The anti-wear effect of the latter was unknown. Furey and Kajdas identified two main factors believed to control tribopolymerization: surface temperature and exoelectron emission. The latter phenomenon is reviewed in sections 2.2 and 2.3.

Another Furey and Kajdas' study [30] investigated tribopolymerization under fretting contact conditions for a steel ball-on-softer steel and -on-aluminum. The steel-on-steel system was chosen for a higher calculated temperature rise than that of steel-on-aluminum. The authors found evidence that condensation-type monomers polymerized only under the higher temperature conditions, while only the addition-type monomers worked for the low-temperature case (e.g., for a 10C to 40C temperature increase). They relate the latter observation to the tendency of aluminum to oxidize, and to the phenomenon of exoelectron emission – reviewed in following sections 2.2 and 2.4 – from mechanically-excited aluminum-oxide layers. Furey and Kajdas [30] also hypothesized that the effect of surface temperature would be important to initiate condensation-type tribopolymerization, i.e., in the case of severe load and/or sliding speed conditions. Meanwhile, exoelectron emission from oxides was proposed as a major factor in the tribopolymerization of vinyl monomers.

A Furey and Kajdas exploratory study [31] investigated the effect on alumina systems (e.g., balls on rotating disks) of tribopolymer forming compounds (e.g., diallyl phtalate, lauryl methacrilate and vinyl octadecyl ether) in the vapor phase using an inert gas carrier, dry N_2. Alumina wear reductions as high as 99% were observed for the alumina balls, and of over 70% for the total wear (i.e., ball and disk). However, significant wear reduction was observed for vinyl octadecyl ether, a compound that polymerizes by a cationic mechanism. These results show that some tribopolymerization reactions may be related not only to exoelectron emission. Recent research work by the same researchers [32] showed that tribopolymerization may be ineffective in reducing wear for alumina-on-alumina at high sliding-speed conditions (e.g., 1.0 m/sec). They suggested

that the higher surface temperatures led to thermal degradation of the polymeric films, indicating a limit for the antiwear action of the monomers used.

The reviewed research works by Furey, Kajdas et al. concluded that high surface temperatures play an important role in tribopolymerization of condensation type monomers, while emission of charged particles from surfaces may be the main factor in initiating and controlling such process for addition-type monomers. A distinction is made between addition-type monomers polymerizing by an anionic mechanism and those polymerizing according to a cationic mechanism. The former are expected to form tribopolymers on rubbing surfaces producing mainly negative particles (e.g., electrons), while the latter will develop tribopolymers only from the emission of positive particles (i.e., cations). However, the experimental differences found between monomers in a liquid carrier (e.g., in hexadecane [27]) and same compounds in vapor phase [31] show that the initiating mechanisms for tribopolymerization are still unclear.

The chemistry details of tribopolymerization can be modeled by Kajdas' concept of the formation of negative-ion-radical reactive intermediates, which were originally applied to lubricant components [33-35]. This basic negative-ion concept hypothesizes the ionization effect caused by the action of electrons of low energy (e.g., of 1 to 4 eV), on the assumption that these electrons are spontaneously emitted from fresh surfaces formed during sliding contact. The following hypothesis in the concept is that lubricant components form anions which are then chemisorbed on the positively charged areas of rubbing surfaces.

This application of the negative-ion concept and its further development into the Negative-Ion-Radical-Action-Mechanism (NIRAM) [36] explain the role of exoelectrons in tribopolymerization of addition-type monomers. The NIRAM comprises the following major stages:

(i) Low-energy electron emission process and creation of positively-charged spots, generally on tops of asperities.

(ii) Action of the emitted electrons with the lubricant causing the formation of negative ions and radicals components on the rubbing surfaces.

(iii) Reaction of negative ions with metal surface, and other reactions, e.g., free radical reactions, forming an organometallic (or inorganic) film, which protects the rubbing surfaces from wear.

(iv) If shear strength is high, it can cause cracking of chemical bonds producing inorganic films and further radicals.

(v) Eventual destruction of protective layer by wear, followed by electron emission and subsequent formation of a new protective film according to stages (i) through (iv).

In summary, this boundary lubrication model proposes the formation of protective organometallic and inorganic layers on rubbing surfaces – according to an anionic-radical reaction – connected with exoelectron emission processes, and the eventual destruction of the inorganic layer in a formation/destruction cycle. The reaction cycle can be expressed in terms of a reduction-oxidation process [36]. A discussion of the NIRAM in addition-type tribopolymerization can be found in reference [37]. A discussion of this mechanism in the relevant case of alumina-on-alumina sliding contact was reported in reference [38]. A comprehensive report on relevant developments of the tribopolymerization concepts can be found in [39].

The surface-temperature case of condensation-type tribopolymerization was recently discussed in reference [40]. In this, comparisons of experimental temperature measurements, using an infrared microscope, and the theoretical predictions of temperature rise were discussed by Vick et al. [41]. A study of the predicted temperature rise from frictional contacts of several ceramics was recently presented by these authors [42].

The review in this subsection reveals that tribochemistry and interactions occurring within the sliding-contact environment may be used to reduce the wear of ceramics by the tribopolymerization mechanism. There is evidence that this mechanism, in the case of addition-type monomers, is connected with low-energy electron emission. The following sections review the phenomenon of exoelectron emission and the particular case of charged-particle emission from tribological contacts.

2.2. Electron emission and exoemission

2.2.1. Conventional electron emission processes

The conventional electron emission processes are analogous to that of ionization of a free atom. As the energy of electrons in the atom is lower than that of an electron at rest in vacuum, some energy must be added to obtain the release of electrons. The electron emission process is, therefore, the ejection of electrons from a substance as a consequence of excitation by some external source of energy. Given the appropriate level of external excitation, any solid may emit electrons from its surface.

Conventional processes of electron emission from solids include thermionic emission, photoemission and field emission. They correspond to the different energy sources, i.e., heating, photon illumination, and external electric field, respectively, which may conventionally produce high-energy electrons from a solid surface. However, these mechanisms do not concern the experimental research in this dissertation. Reviews on thermionic emission, photoemission and field emission can be found in references [43], [44] and [45], respectively. The following subsection focuses on the less understood low-energy exoelectron emission phenomenon, which more closely relates to this dissertation research.

2.2.2. Exoemission

When solid surfaces are subjected to mechanical work or tensile deformation they show emission of electrons. These electrons, whose emission rate may decrease with time after the excitation ceases, are called exoelectrons [5]. Exoelectrons are typically electrons of low energy, which may be spontaneously emitted from most fresh surfaces under certain excitation conditions. The particular and not well-understood feature of exoelectron emission is that it would proceed for external excitation lower than the work function of the bulk material. Changes of the surface work-function are thought to explain such behavior.

Because no general description of the exoemission phenomenon exists, nor a clear explanation for its mechanisms is available, definitions of exoelectron emission are not more specific than the following:

> “Exoelectron emission is a transitory phenomenon of low-energy electron emission by substances after their excitation of some kind (called the primary excitation), or after the spontaneous stimulation, or due to the energy that is below the work function of substances (called the secondary excitation)” [46].

The above definition suggests that exoelectron emission might be excited by a variety of physical and chemical phenomena. At present, however, the term exoelectron emission is used as an inclusive term for emission phenomena that proceed from changes in the work function. These work-function changes are experimentally related to excitation by input of physico-chemical energy input. Although exoelectron emission has been observed from both metals and non-metals, there is strong evidence that the existence of oxides or other non-metallic surface layers is necessary for exoelectron emission [47].

Evidences of exoelectron emission were reported as early as 1902, in the work of McLennan [48]. He reported emission from several mineral salts after irradiation with cathode rays, although he interpreted those results as "acquired radioactivity". The term exoelectron emission (EE and also exoemission) originated from the investigations of Kramer [49] of the emissions from freshly treated metals, which he interpreted as a consequence of exothermal transformation processes of the surface (e.g., recrystallization and/or phase transformation).

Nakayama et al. [50] investigated EE from the cutting of several metals in vacuum and in gases N_2 and O_2. They reported a correlation between the heat of formation for oxides of the pertaining metals and the exoemission intensity: the emission of exoelectrons increased for increasing heat of formation. They also computed a minimum value of heat of formation below which exoemission did not occur for the tested metal.

Such threshold value was found, however, smaller than the values of work function for the oxidized metal surfaces. They concluded that work function values for freshly-formed surfaces were lower than those for oxidized surfaces, and that exoelectrons resulted from complex exothermic reactions of fresh metal-surfaces with surrounding gas species.

The evidence that EE also occurs when highly energetic chemical reactions, which would reduce work function, take place on metal surfaces, made some authors to call it “chemically stimulated exoelectron emission” [51] or “chemi-emission” [52]. In this research field, Gessel et al. [53] investigated “chemisorptive stimulation” of the exoelectron emission from fresh magnesium surfaces. They concluded that the excitation energy for exoelectrons was derived from the reaction of oxygen and water with freshly exposed magnesium surfaces. They also found [54], using photoelectron emission measurement, a decrease on the work function of 1.8 eVolts for oxygen adsorption on magnesium. Ferrante [55] observed exoemission from a clean well-annealed magnesium single-crystal upon exposure to oxygen in ultra high vacuum. This emission was found to depend on the oxygen flux to the surface.

Although the above-reviewed research may suggest that surface chemical reactions are the exclusive source of exoemission, there is strong evidence that EE also depends on mechanical alteration of surfaces. In general, surface changes produced by plastic deformation, wear and material fatigue were shown to be connected with exoelectron emission [56-58].

Several experimental works suggest that EE may be associated with defect formation in mechanically-altered solids. In this, the work of von Voss and Brotzen [59] hypothesized that EE from metallic surfaces may be attributed to a diffusion-controlled process of point imperfections (e.g., vacancies) in non-conducting surface layers. The mechanisms for exoemission, being of either chemical or physical origin, are, however, not well understood. Research in the field of exoemission from mechanically-altered surfaces is reviewed in following sections 2.3 and 2.4.

Another interesting feature of EE is that, already in the presence of physical or chemical excitation, it may be enhanced by irradiating light of suitable wavelength [18,60-62], by heating [63,64], and by applying an electric field [65,66], respectively referred as photostimulated, thermally stimulated, and field stimulated exoelectron emission.

In a comprehensive study, Enomoto et al. [67] measured photostimulated EE for twenty different metals after polishing by emery paper in a controlled-humidity atmosphere. Initial maxima of emission were reported, except for the silver surface, as being followed by a monotonical decrease. They found a strong influence of oxygen and water surface-adsorption on the observed exoemission. A comprehensive review on thermally stimulated EE can be found in [68].

The enhancement of EE by light, heat and electric field is not, however, well understood. Shigekawa et al. [69] showed that during the measurement of photostimulated EE from scratched aluminum, the interruption of photostimulation resulted in a transient enhancement of exoelectron yield. In further research [70] they studied conventional photoemission after abrasion from both aluminum and zinc specimens, by continuously shifting the stimulation wavelength from that of visible light to that of UV. The EE dependence on the wavelength was found considerably different before and after scratching. After scratching, the EE peak was observed at longer wavelength (i.e., for lower energy) than the peak wavelengths for both undamaged aluminum and zinc. It was also found that the EE-peak wavelength was independent of both the time after scratching and the intermission period between illuminations.

Most of the reviewed research investigated EE as it related to a single source of external excitation. However, the physics and chemistry of EE may be more complex, as demonstrated by Kreigseis and Sharman [71]. They showed that intense thermally stimulated EE from ZnO required simultaneous chemisorption of both oxygen and water. It is likely that simultaneous energy inputs (e.g., mechanical, chemical, adsorption, heating, radiation and electric field) have a combined effect on the surface work-function and, therefore, on the EE output. Several extensive surveys exist on exoemission phenomena [72,73].

The literature review of this section reveals that the exoelectron emission process can be described as a phenomenon producing low-energy electrons from physically and/or chemically treated solid surfaces, the intensity of exoelectrons can be enhanced by light, heat and electric field application.

2.3. Triboemission

Friction and sliding contact of solid surfaces may produce a variety of material and energy outputs, e.g., material debris, heat, acoustic emission, charged particles and various radiation. In general, several energy outputs may result from transformation of the mechanical energy, which is input by rubbing, into other forms of energy. This energy input also provides the driving force for a number of physical and chemical changes of the surface, the so-called triboemission among them. It is apparent that energy transfer and rubbing-surface interaction – which may eventually result in surface damage and/or transformation – are needed for triboemission to occur.

From this general point of view, the term triboemission may be applied to all energy and material tribological outputs. The term triboemission is reserved, however, for the emission of electrons, ions, neutral particles, photons, radiation and acoustic emission under conditions of tribological damage. Triboemission of charged particles and friction-generated heat are considered the most important factors in some tribochemical mechanisms, in particular, in the mechanism of tribopolymerization, which was reviewed in subsection 2.1.2.

Triboemitted electrons, which are thought to be of low-energy (e.g., from 1 to 3 eVolts) [46], play a significant role in some models of boundary lubrication, notably the Negative-Ion-Radical Action Mechanism (NIRAM) [36], which was discussed in subsection 2.1.2. Although the detailed physics by which charged-particle triboemission proceeds is unknown, triboemitted electrons are known to pertain to the general phenomena of exoelectron emission, and they are also called triboemitted exoelectrons.

Triboemission of electrons and other charged particles particularly concerns the experimental research in this dissertation. Triboemission of charged particles, among them exoelectrons, was reported from early experimentation on exoemision. Kramer [49] found that metal surfaces which had been subjected to abrasion produced pulses similar to those of radio-active materials. He interpreted that effect as electrons spontaneously emitted from the abraded surface, whose work function would have been reduced by the abrasion treatment.

Ramsey [74] reported that photostimulated exoelectron emission from aluminum peaked immediately after abrasion by steel in O_2 , N_2 , humid and dry air, to be followed by an exponential decay. He also investigated [75,76] the in-vacuum effects of residual pressures of air, oxygen, nitrogen and water vapor on such abrasion systems. They concluded that the presence of oxygen and water vapor was needed for the observed triboemission to occur: Water vapor would lower the surface work-function and triboemission would correspond to building of an oxide film.

Momose and Noguchi [77] measured electron triboemission, using a Geiger counter, from the simultaneous abrasion of solid polymers by metals. While they reported increasing emission for increasing sliding speed around 0.1 m/sec, they found that emission decreased with externally-input temperature increases. This kind of evidence shows that triboemission is an exoelectron emission mechanism substantially different from conventional thermionic emission. March and Rabinowicz [78] investigated UV-enhanced electron triboemission from surface cracks on steel-balls after four-ball surface-fatigue wear tests. They correlated emission-peaks with the position of surface cracks. More recently Tagawa et al. [79] reported UV-stimulated triboemission of electrons from a steel pin sliding on polycrystalline graphite.

Extensive research was carried by Nakayama et al. [80-91] on charged-particle and photon triboemission from several material systems. In an early work [80] they reported burst-type UV-stimulated exoelectron emission from an aluminum disk scratched by a steel blade, and no emission after scratching ceased. For electron measurement they used a ceramic-surface continuous electron multiplier in vacuum of 10^{-3} Pa.

In a series of following papers Nakayama et al. [81-89] reported measurements of currents from a system of a scratching diamond-stylus on a rotating disk of the pertaining material (e.g., metals, ceramics and semiconductors). The Faraday-cup employed, however, may have detected charges both emitted and of electrostatic origin.

This measurement of charges was carried out by “collecting” them in ring-shape metal pieces mounted on the stylus. The voltage between the collectors and the reference emitting surface was amplified and processed, and the output signals were usually measured in arbitrary units. By biasing the collectors +15V and -15V from reference, the collected signals would represent negative and positive charges respectively. No simultaneous measurements of both type of charges was performed. In the cases when photons were simultaneously detected [82-84,86,87,89], a photon multiplier tube was employed.

In Nakayama's investigations both negative and positive charge outputs were burst-type. Signal-level was well above the background level (e.g., that obtained during disk rotation without scratching). The experimental setup allowed different environments, including low vacuum, for the tribological contacts. Standard atmosphere, reactive and inert gases and hydrocarbon liquids and gases were investigated for their influence on the charge measurement. Some general features and findings from those experimental works [81-89] are summarized as follows:

(i) Conditions of severe wear were used for the experiments (i.e., scratching of a rotating disk by a diamond stylus).

(ii) Burst-type signals started immediately with scratching and abruptly dropped when scratching ceased.

(iii) Higher negative-charge intensity was measured than that of positive-charge for same material.

(iv) Increases of negative-charge intensity were observed for increasing electrical resistance of materials [82,83] in the order:

conductor < semi-conductor < insulator

(v) Photon emission was also observed and it followed the same trend of the above (iv) [83,84,86].

(vi) Coefficient of friction did not correlate with charge intensities [81-86,88-91].

(vii) Variables that may relate to wear phenomena (i.e., sliding speed [81], normal load [82], hardness [83]) correlated with charge intensities. For insulators, the intensity of both negative and positive charges decreased for increasing hardness.

(viii) Conditions that may lower wear under boundary lubrication conditions (i.e., hydrocarbon lubricants [88]) reduced charge intensities.

(ix) Increasing charge intensities correlated with oxide-film thickness on metal substrates [81] .

(x) Charge intensities from ceramics (e.g., Si_3N_4, Al_2O_3, ZrO_2 and soda lime glass) were affected by different gas species atmospheres (e.g., wet and dry air, O_2, N_2, Ar and He) at same pressure [84].

(xi) Charge intensities from ceramics reached a maximum for a characteristic value of gas-species pressure (i.e., of He, Ar and O_2) in the range 10^1 Pa to 10^5 Pa [86].

(xii) Under boundary lubrication with hydrocarbons, charge intensities from ceramics correlated with hydrocarbon chain-length. In this, charge intensity decreased for increasing chain-length [85, 87-89].

Although of importance to the field of triboemission, the above-reviewed research works by Nakayama et al. can be criticized in the following aspects: the charge-detector used

must be sensitive, in addition to actually emitted particles, to build-up of electrostatic-charge on the contact surfaces. In this, the latter phenomenon may be critically important for insulating materials. Although different-material (A-on-B) contacts were investigated, no research was conducted for the relevant case of triboemission from same-material (A-on-A) contact, and energy of particles was not investigated.

A model was proposed by Nakayama and Hashimoto [84,86] for triboemission from ceramic sliding dry-contacts, in gas pressures of about 10^5 Pa of Ar, He, N_2, O_2, dry air and wet air. The model is concerned with ion emission, and it is based on the ionization of surrounding gases due to surface damage. In particular, electron emission would be excited by electric fields within surface cracks. Those electric fields might be created by charge separation, in a similar way to that of Dickinson's charge-separation model [92], which is reviewed in the following section 2.4.

In their model, Nakayama et al. presented an argument [84] to conclude that sparking from dielectric breakdown would originate charged particle emission, which would be mainly constituted by negative ions (and not electrons). This model might also explain [86] the higher intensity of negatively-charged particles, with respect to that of positively-charged ones, from the higher mobility and drift velocity of the former. These properties would allow negative charges an easier reaching of the detector. However, this triboemission model is limited to a relatively narrow range of gas pressures. It also implies that emission from dry ceramic contact surfaces comprises mostly charged ions (and no electrons). There is no plausible evidence, however, to rule out electron emission in that case. This model does not explain charge measurements at very low pressure: they also observed [86] that charge emission significantly increased when gas pressure was lowered below 1 Pa.

Nakayama et al. also carried research [90,91] on charged-particle triboemission from an alumina-ball sliding on hydrogenated and amorphous carbon films. The particle-detector was a secondary-electron multiplier in vacuum (Extensive discussion on the use of such detectors is found as part of this dissertation research, in chapters 3 and 4).

They found burst-type electron emission, whose intensity depended on the H_2 content in the sputtering gases employed for film preparation. While they found a strong correlation between electron emission and carbon-film wear, no correlation was observed of emission and coefficient of friction. Most of Nakayama's findings were briefly reviewed in [93,94].

Dickinson et al. recently presented some relevant research on triboemission. They investigated electron and photon emission from simultaneous reciprocating scratching of MgO with diamond [95]. Electron and photon emission were respectively measured by a channel electron multiplier and a photomultiplier tube. They found significant burst-type electron and photon emissions as high as, respectively, $3x10^6$ counts/sec and $2x10^4$ counts/sec (for 0.1 N load, and 4 cm/sec average sliding speed). In this, Dickinson et al. observed differences, for both emission types, as high as three orders of magnitude between the highest spike level and the average emissions (in the whole contact period).

Photon emission for this diamond-on-MgO system decayed on the millisecond scale after each burst, returning to near-zero between spikes. Electron emission, however, showed a characteristic decay-time of about 100ms after each spike, being the signal envelope quasi-continuous. Evidences were reported of emission after the contact ceased, although of longer decay period for electron emission than that for photon emission. While they found correlations between minima of photon emission, and both electron emission and coefficient of friction, they observed a 5 to 10msecond-lag for the rise of electron emission with respect to that for photon emission. They related such observation to stick-slip behavior in the plowing process.

An interesting finding from this research [95] was that, during pure indentation (i.e., without relative motion) of MgO by diamond, photon emission was observed from the onset of contact and deformation, while electrons were emitted only after surface fracture occurred. They hypothesized that photon emission was mainly originated from dislocation during motion in both plastic and fracture behavior, while electron emission corresponded to fracture only, after periods of extensive plastic deformation.

Dickinson et al. [96] also reported research on the kinetic-energy of electrons triboemitted from diamond-on-MgO contact. Using the retarding-grid method (which is thoroughly described in Chapter 3) they measured the rate of electron emission (as counts/sec) vs. the retarding-grid voltage. The general trend appeared as an exponential-decaying function: electron emission abruptly dropped from a maximum rate for all the emitted particles (i.e., at zero-Volt grid) to a fraction smaller than 10% (of that maximum) at -100V. Grid voltages up to -1,000V were not enough to completely stop the emitted electrons. They assumed such electrons were actually emitted with low energy of about 1eV, to be further accelerated by the electrostatic potential of charged patches on the rubbing surfaces.

The same work by Dickinson et al. [96] reported experimental research to determine which of the contact surfaces emitted the electrons: both diamond and MgO were found to eject them. On the fact that diamond does not present any known defects that could serve as exoelectron sources, they hypothesized that diamond emission could proceed from diamond contamination by MgO transfer. However, when net surface-charge was measured (using a charge probe feeding an electrometer), diamond and MgO were found respectively negatively- and positively-charged. Their explanation to the emission of electrons from both surfaces was the coexistence of opposite-charge patches on the same surface. Unfortunately, they did not investigate the emission of positive particles from the system, that could have helped to understand the phenomenon.

A new technique for triboemitted-charge measurement was recently reported by Dickinson et al. [97] of using a Cu collector feeding a "floated" electrometer. The charges, generated by reciprocating scratching of single crystal MgO, quartz, sapphire and amorphous silica with diamond, were carried by a gas stream towards the detector. The gases employed were dry air, N_2 and O_2 with 10% to 30% relative humidity, at about one atmosphere. They demonstrated the feasibility of gas electrification from positively- and negatively-charged triboemission and of charge-transport to cm-distances by gas molecules. Also, gas humidity of 30% or greater showed to decrease the measured emission. This triboemission intensity was dependent on material, and decreased in the order: MgO, amorphous silica, quartz and sapphire. They pointed out the fact that this order correlates with increasing hardness, suggesting the existence of a relation of triboemission to wear.

Table 2.1. Summary of setup features and outputs for research on triboemission.

Ref.	Material System and Atmosphere	Force Speed	Maximum Charged-Emission Intensity	Detection System
[74 - 76]	Stainless steel brush abrading high purity Al. Air, O_2 and N_2 at 10^{-8} to 10^{-5} Torr.	(NR) (NR)	$6.5x10^{-16}$ A for 10^{-5} Torr vacuum.	(a)
[79]	Stainless steel pin on graphite-disk followed by UV-irradiation. 10^{-8} Torr vacuum.	7.9N 0.6cm/s	$4x10^{-15}$ A	(d)
[81]	Diamond stylus scratching Aluminum oxide film. Ambient atmosphere.	1.0N 5.5cm/s	Arbitrary units	(b)
[82]	Diamond stylus scratching metals and ceramics. Ambient atmosphere.	0.5N 6.3cm/s	Arbitrary units	(b)
[83]	Diamond stylus scratching metals and ceramics, glass, $Al_2 0_3$ films, polymers and mica. Various atmospheres.	0.5-1.5N 7-12cm/s	Arbitrary units	(b) and (c)
[84]	Diamond stylus scratching ceramics. Ar, He, O_2 , N_2 and dry air atmospheres at 10^5 Pa.	1.5N 3cm/s	Arbitrary units	(b) and (c)
[85] [88]	Diamond stylus scratching metals, ceramics, polymers and semiconductors. Submerged in HC liquids.	1N 5.3cm/s	70 pC/s (i)(h)	(b)
[87]	Diamond stylus scratching Al_2O_3 , Si_4N_3 and ZrO_2 . Hydrocarbon gas atmospheres at 10^5 Pa	1.5N 3cm/s	350pC/s (negative) (i) 160pC/s (positive)(h)	(b) and (c)
[86]	Diamond stylus scratching Al_2O_3 , Si_4N_3 and ZrO_2 . He, Ar and O_2 atm. at 10^{-2} to 10^5 Pa.	1.5N 6cm/s	1,150pC/s (negative)(i) 950pC/s (positive) (h)	(b) and (c)
[89]	Diamond stylus scratching Al_2O_3 and Si_4N_3 (g). N-butane gas atmospheres at 1 to 10^5 Pa.	1.5N 6cm/s	600pC/s (negative) (i) 500pC/s (positive) (h)	(b) and (c)
[90] [91]	Alumina ball sliding on amorphous and hydrogenated carbon films. Dry air at 5mPa.	0.44N 2.2cm/s	500 counts/sec for negative emissions	(e)
[93]	Alumina ball sliding on amorphous and hydrogenated carbon films. Dry air at 5mPa.	0.2N 5.2cm/s	160 pC/s for negative emissions (i)	(b) , (c) and (f)
[95]	Diamond stylus on MgO disk. Vacuum below 10^{-4} Pa.	0.1N 0.25cm/s	3 x 10^6 counts/s.	(e) and (c)
[96]	Diamond stylus on reciprocating MgO, SiO_2, sapphire, and α-quartz. Air, N_2 and O_2 flow at 1.4 atmosphere.	30-100N (NR)	24 pA , negative emissions	(j)

(NR) Non reported.

(a) Be-Cu particle multiplier feeding electrometer.

(b) Electrode on diamond stylus at 0.5mm from surface. ± 15 V biasing w.r. to surface.

(c) Photon measurement by photon multiplier tube.

(d) Microchannel Plate feeding a picoammeter.

(e) Secondary electron multiplier and rate counter.

(f) Electrostatic voltmeter for surface potential.

(g) 4mm alumina ball sliding on alumina and Si_4N_3 for photon emission (6N load).

(h) Emission for scratched alumina.

(i) Accumulated charges for reported period.

(j) Cu collector feeding floated electrometer.

A summary of employed material and techniques, and of results obtained for the most relevant research works on triboemission is presented in Table 2.1. The diversity of employed experimental conditions (e.g., materials, tribological excitations, detection systems and units of measurements) in the reported research works makes difficult any comparison of results.

The core of this dissertation, presented in Chapter 4, is an experimental characterization of the charge and energy of particles triboemitted from ceramics surfaces. The following section presents a review on the phenomenon known as fractoemission, as it may relate to triboemission. The triboemission research works reviewed in this section provide good evidence that materials, in particular insulators, emit both negatively- and positively-charged low-energy particles in conditions of tribological wear.

2.4. Fractoemission

The triboemission phenomena, which was reviewed in section 2.3, may relate to the exoemission process known as fractoemission. The latter concerns the emission of negatively- and positively-charged particles, neutral particles, photons and various radiation from materials subjected to mechanical strain. The fact that fractoemitted particles are produced by mechanical alteration and certainly from strained surfaces, strongly suggests a relation to the triboemission phenomena, for which some surface damage (e.g., from sliding contact) is also needed. In this, is not unusual that triboemission research references to findings in the fractoemission field.

Early interest in the emission of exoelectrons from freshly-deformed metal surfaces was reviewed by Grunberg [98]. He concluded that fractoemission was associated with the disruption of oxide surface layers. Von Voss and Brotzen [59] investigated light-stimulated electron emission from aluminum under tensile-strain by means of a Geiger counter. They found a strong correlation between the emission rate and tensile strain.

To study the same material system under tension, by means of an electron multiplier as detector, Sujak and Gierozynski used simultaneous external excitations, e.g., photostimulation [99,100] and previous electron bombardment [101], to produce the observed exoemission. They later realized, however, that no added excitation was needed for surface-oxidized aluminum [102] and nickel [103] to emit electrons under tension.

Rosemblum et al. [104] carried comprehensive research to confirm that fractoemission from tensile-strained aluminum occurred without any additional external stimulation. They determined that emission showed in bursts and depended on continuous deformation. Fractoemission was observed only at non-zero strain rates, and ceased abruptly once deformation stopped. They also reported a rough determination of the retarded-energy distribution for fractoemitted electrons, which showed that a large fraction of the energy-spectrum would be in the zero to two eV range.

In general, the above reviewed research works concluded that fractoemission was related to diffusion of point imperfections and/or micro-fracture in the oxidized surface. Another line of thought [105], however, assumed that such mechanical alterations would be the origin of exoemission only in the condition of no added excitation. But under tension with external photostimulation, gas adsorption on freshly exposed metal surfaces would produce the exoelectrons. As pointed out in subsection 2.2.2, however, simultaneous external inputs may have a combined effect on surface work function, and on fractoemission.

Dickinson et al. [106-121] carried relevant research on fractoemission from several materials with varied mechanical excitation sources. Their research works showed several approaches to measure fractoemitted electrons, negative ions, positive ions, neutral gas species, photons, and simultaneous acoustic emission. Although tensile strain of the material was the usual mechanical excitation, interface debonding [115,116,118] and indentation [122] also were sources of fractoemission. In general, the particle-measurement systems employed were based on channel electron multipliers in the pulse-counting mode, which were operated in medium to high vacuum.

The various fractoemission features studied by Dickinson et al demonstrated that oxide-covered aluminum [106-110], polymers [112,117] elastomers [111], ceramics [119], alkali halides [113,114], and polymer-matrix composites [115,116] produced fractoemission. In the case of metals, a surface oxide layer was required for fractoemission: for the extensively studied case of aluminum under tensile strain [104-110] a correlation exists between the oxide-layer thickness and the fractoemission intensity.

In a relevant research work Dickinson et al. [108,109] demonstrated a relationship between crack initiation and propagation, and the simultaneous fractoemission. They found that the onset of plastic deformation and surface-oxide cracking in aluminum, which was detected by acoustic emission, was simultaneous with a series of bursts of electrons and positive ions. Emission began and was most intense during fracture. Also, fractoemission decayed after the initiation of surface cracking, if no added strain were applied, indicating that the fractured surfaces remained in an activated state. In this, an exponential decay of the electron emission was observed with a relaxation mechanism slower than that of most electron emission processes [108].

Some comprehensive reviews by Dickinson et al. concern fractoemission from adhesive failure [118], steel-epoxy interface failure [116] and fractoemission as a probe for fracture, wear and deformation [119]. They also presented a discussion on chemisorption as a alternative source of electron emission from plastically deformed reactive metals [120].

One of Dickinson's earliest explanations for the phenomenon of fractoemission, although probably limited to oxide layers on metal substrates, is the so-called "model of charge separation" [92]. This conceptual model proposes that fractoemission from strain of oxide-metals would proceed by a complex series of basic physical and chemical mechanisms, which are summarized as follows:

(i) Charge separation (and corresponding electric field) results from fracture;
(ii) Desorption of gases raises the local pressure in the crack tip;

(iii) Gas discharge occurs, producing local electron-discharge, and photon and electromagnetic emissions;
(iv) Electron bombardment of freshly created surfaces excites primary excitations in the form of electron-hole pairs, followed by thermal stimulation and electron migration until;
(v) Electron-hole recombination occurs, yielding an emitted electron or a photon;
(vi) Some emitted electrons may eventually strike gas species, to emit charged ions.

The model of charge separation proposes a detailed sequence for the fractoemission of exoelectrons and postulates that positively-charged particles are a marginal effect of such electron emission. It is not clear, however, if such model could work for materials other than oxides on metal substrates. It is also apparent that a plastically strained surface may grow surface defects from dislocation motion. Such processes may locally reduce the work function to emit electrons, without the simultaneous charge separation proposed by the model, as pointed out by Dickinson et al. themselves in recent research [95]. Therefore, there may be more than one mechanism to explain different sources of fractoemission. In another line of thought, Dickinson et al. presented a model of molecular recombination on fractal lattices to explain fractoemission over long-time scales [121].

Table 2.2 summarizes the variety of experimental setups that these and other researchers employed to examine fractoemission. Because a diversity of materials and experimental conditions were employed for such research works, any comparison of results is difficult.

Although the detailed physics of fractoemission is still unclear, it is apparent from this review that fractoemission constitutes a phenomenon of less complexity than that of triboemission. The simpler mechanical input and the cleaner experimental environment that is needed in fractoemission facilitate the analysis. In general, the findings and models derived from fractoemission research might help understanding some of the basic interactions in the triboemission, specially the connection between contact damage and produced triboemission. Fundamental knowledge on the role of micro-fracture and/or fresh-surface creation in fractoemission might be applied to understand triboemission: fracture and surface creation are thought originate both phenomena.

Kajdas et al. [122] recently presented a comprehensive review relating the phenomena of exoemission, triboemission and fractoemission, with a focus on the possible role of low-energy electrons in the boundary friction regime.

Table 2.2. Summary of setup features and outputs for research on fractoemission.

Ref.	Material System and Atmosphere	Stress type Strain rate	Measurement System	Maximum Emission
[58]	"Commercial" and "high purity" aluminum. Mixture atmosphere of 1% methane and 99% He.	Tensile 0.06-0.16in/min	Geiger-Muller counter.	200 counts/s
[104]	Oxide-covered Al, Ni and Ti. Vacuum of 10^{-8} Pa.	Tensile 0.5 -10^{-4} s^{-1}	Single-event CEM and energy spectrometer.	450 counts/s
[106] [110]	Bare and oxide-covered 2024 Al-alloy. 10^{-6} Torr vacuum.	Tensile until rupture. 0.014% s^{-1}	Single-event CEM.	1,100counts/s
[107]	Bare and oxide-covered 2024 Al-alloy. Vacuum less than 10^{-7}Pa.	Tensile. Constant strain rate (NR)	Bayer-Alpert gauge (total pressure) and quadrupole spectrometer (partial pressure).	1.6x10^{-7} Torr total pressure increase
[108]	Anodized 1350 Al-Alloy. 10^{-4} Pa vacuum.	Tensile 0.014-25% s^{-1}	Single-event channel electron-multiplier.	50 counts/s
[109]	Anodized 1350 Al-Alloy. 10^{-4} Pa vacuum.	Tensile 0.2% s^{-1}	Single-event CEM.	8 counts "per burst"
[92] [113]	Alumina-filled epoxy, glass bead filled polybutadiene, sucrose, SiO_2 and MgF_2. 10^{-5} Pa vacuum.	Tensile and three-point bending until fracture (NR)	Single-event CEM.	Bursts as high as 14,000 counts/s for sucrose
[122]	Alkali-halides LiF and CaF_2 Up to 400ºC in air.	2 min indentation (98-294N).	Electro-conductive tip with ± 15 V bias.	Arbitrary units.
[114]	Alkali-halides LiF and NaF_2	Three-point bending. 70 μm s^{-1}	20V-floated ion collector feeding electrometer.	170 nA
[115] [116] [118]	Stainless-steel rod imbedded in epoxy. 10^{-5} Pa vacuum.	Rod pullout. 2 mm min^{-1}	Electro-optics CEM.	2,000 counts/s
[117]	High density polyethylene.	Tensile. 30% s^{-1}	Two CEMs.	1,100 counts/s

(NR) Not reported.

CHAPTER 3. NEW TRIBOEMISSION INSTRUMENT AND EXPERIMENTAL METHODOLOGIES

The broad objectives of the research in this dissertation are to make fundamental experimental measurements of charged-particles triboemitted from ceramics. These particles are believed to be important in tribochemical reactions and, in particular, in tripopolymerization as an effective antiwear mechanism. To accomplish these experimental measurements, a new instrument was needed. This chapter presents the design, construction and development of the new device and data acquisition system, and the general experimental techniques for the triboemission measurements. It also describes the material systems and contact geometries used for the measurements.

3.1. New triboemission instrument

3.1.1. Design criteria for the triboemission instrument

To carry out measurements of triboemitted charged-particles, the testing instrument should satisfy both tribological and triboemission requirements. The following criteria were accordingly applied for the design of such instrument:

(i) Since the influence of contact geometry on the triboemission output and on the measurement was unknown, the instrument should be able to accommodate different geometries, including the classical pin-on-disk. Also, these geometries should be contact pairs of both different (A-on-B) and same material (A-on-A) systems.

(ii) It should be possible to vary and control the applied load and sliding speed in a broad range of contact conditions.

(iii) The instrument should allow measurements of charge intensity for both negatively-charged and positively-charged particles, and of kinetic energy of such triboemitted particles.

(iv) The emitting area and the unobstructed solid angle into which the charged particles are emitted should be as large as possible.

(v) Although some research claimed to observe triboemission in atmospheric conditions [82], the system should provide a good vacuum between the emitting surface and the particle detector, in order to observe low-energy particles.

(vi) Sufficient flexibility should be incorporated to modify the instrument for the measurement of mass of emitted particles, as well as for the detection of other forms of triboemission (e.g., photons).

(vii) It should be possible to modify the instrument for the control of atmospheres.

This set of criteria was established on the basis of previous research works from the literature review and on the experiences obtained from some initial instrument-designs, which are described in the following subsection.

3.1.2. Initial instrument designs

An initial instrument-design consisted of a rotating alumina ball spinning within an alumina cone specimen, the tip of which was open. An schematics view of such geometry is shown in Figure 3.1. Charged-particles were expected to be emitted within a cone of trajectories from the ball-in-cone area of contact. Sliding contact and unsuccessful charge-detection were performed in atmosphere.

Triboemitted charged particles were expected to be emitted from the cone opening to a Faraday-cup detector, which fed an picoammeter (Keithley model 480 feedback picoammeter) through coaxial cables. This system would measure the total current of triboemitted charged-particles. However, no measurement was effectively carried out with this instrument.

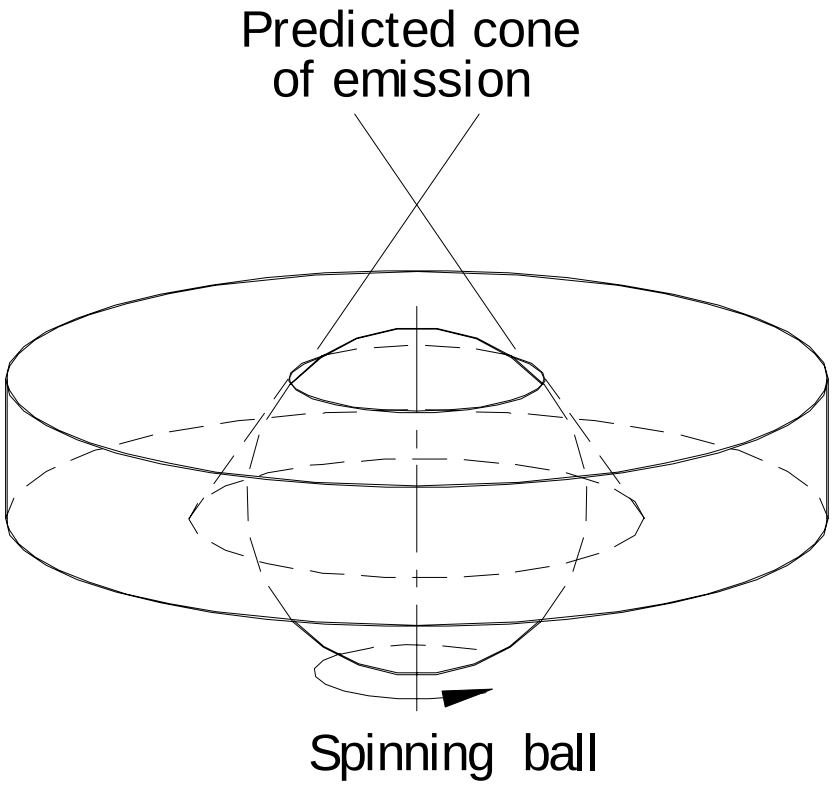

Figure 3.1. Schematic view of the ball-in-cone geometry.

Several operational limits and measurement problems were found in the use of Faraday-cups to detect the low-level currents which result from triboemission. A picoAmp-level current was indeed observed for spinning contact of the ball in the cone: this current linearly increased during ball spinning (about the ranges of 50N load and 0.6 m/s sliding speed), and it peaked immediately after the spinning stopped, to then decay with a large time-constant of about 30 minutes. Although this could appear as evidence of triboemission, that current was traced to temperature-dependent leakage-paths through the Faraday cup assembly: Leakage current increased in time as the Faraday-cup was heated from the ball-in-cone frictional contact, to decay after the sliding ceased with a large time-constant pertaining to cooling. The problem of picoAmp leakage-current could not be solved, however, by the use of high electrical-resistance materials (i.e., alumina, sapphire) to thermally insulate the detector from the frictional contact.

Another measurement problem arose with the low-level signal from the Faraday-cup, which had to be fed to the ammeter through shielded conductors (e.g., coaxial cables). It was found that low-amplitude vibrations in such cables excited picoAmp-level noise currents in the cable itself. These so-called triboelectric currents are generated by internal rubbing (e.g., of the metal wire and the external insulators) in coaxial cables.

Since such noise correlates with sliding contact, it could be mistakenly assumed as triboemisssion. Even special low-noise cables gave unacceptable noise-level [124] for the inherent excitation coming from the tested dry-sliding contacts. This problem could not be solved by insulation of the Faraday-Cup from the mechanical-excitation source (e.g., from the ball-in-cone assembly).

A specific description of this instrument development and the measurement problems can be found in [125]. It was concluded that Faraday-cup assemblies were inappropriate for the intended measurement.

Although some research claimed to observe triboemission in atmospheric conditions [82], an important measurement requirement was apparent at that stage of instrument development: a good vacuum must exist for low-energy triboemitted electrons to reach a detector. Also, the limitations of this initial instrument indicated that a detector other than a Faraday-cup-type was needed for the very low currents involved in triboemission.

These new design criteria, together with those outlined in previous subsection 3.1.1, formed the basis for the new triboemission instrument design which is described in following subsections 3.1.3 to 3.1.6.

Although the new triboemission instrument is described with a focus on the geometry used for the experimental measurements in Chapter 4 of this dissertation (i.e., a diamond pin scratching a ceramic disk, see subsection 3.2.1), the ball-in-cone geometry of Figure 3.1 was initially tested during instrument development. An alumina ball spinning within an alumina cone were employed. This contact geometry was tested in vacuum and with a channel electron multiplier (CEM) as particle detector. A partial schematics of this setup is included in Figure 3.2. Detailed descriptions of vacuum and detector setups used follow in subsections 3.1.3 to 3.1.6. A specific description of this instrument development can be found in [125].

No significant charged-particle emission above background was observed from the sliding contact of this system. However, significant emission was later obtained with a diamond pin on a rotating ceramic disk, and with a small alumina ball on an alumina disk, as reported in Chapter 4. It is possible that the geometry itself in the case of ball-in-cone (i.e., of a narrow ring of contact, see Figure 3.1) and/or wear debris deposited around the area of contact hide and/or stop the eventually emitted charged-particles. It was concluded from this stage of development that the ball-in-cone geometry may not be adequate for the intended measurement.

3.1.3. Mechanical and vacuum system features of the new triboemission instrument .

The new instrument features a vertical rotating-sliding shaft that introduces the mechanical inputs (i.e., load and sliding speed) to the tribological contact, which is placed into a vacuum chamber above. The top end of such shaft carries the revolving tribological specimen (e.g., a disk, a ball, etc.), which is in sliding contact with the non-rotating matching specimen (e.g., a pin, a small ball). This tribological contact is mounted in the center of the vacuum chamber.

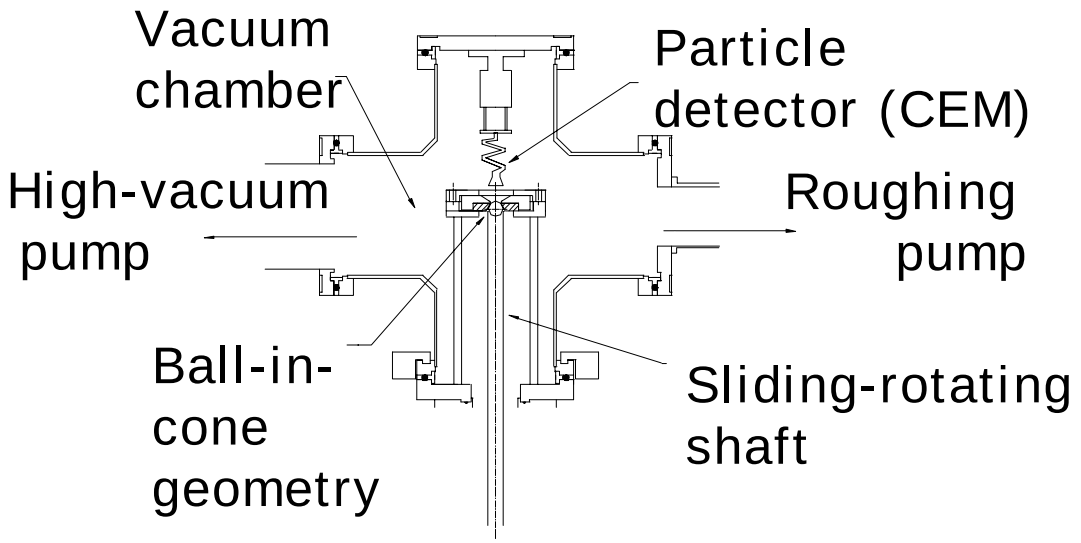

Figure 3.2. Schematic view of the ball-in-cone geometry,
detection setup and vacuum assembly employed during initial instrument development.

A schematic view of the triboemission device is shown in Figure 3.3. A ferrofluidic-seal AFS™-feedthrough model KF40 allows shaft spinning as fast as 2,000rpm, while being compatible with high-vacuum requirements. Such feedthrough is mounted on the vacuum chamber through a stainless-steel low-rigidity bellows, which allows either separating or contacting the tribological surfaces while spin is simultaneously applied to the shaft. Therefore, either contact or non-contact conditions can be alternatively applied to the tribological specimens while the shaft is continuously spinning.

A wide range of loads can also be applied to the tribological contact by a weight and fulcrum, which are connected to the shaft by a thrust bearing assembly. A variable-speed electric motor and connecting timing-belt provide a wide range of rotational speeds for the shaft. The motor (Kollmorgen™ model TT-2042/3004A) and speed control (Kollmorgen™ KXA Servo Amplifier, which is operated in speed mode) feature noise-filtering and grounding adequate for simultaneous particle-measurement.

The top end of the shaft may accommodate different rotating geometries (i.e., disks, balls), while an upper fixture holds either pins or other matching geometries. This allows enough flexibility to test contacts other than the traditional pin-on-disk and contact pairs of both different (A-on-B) and same material (A-on-A) systems. This contact-geometry assembly gives a large unobstructed solid angle into which the charged-particles are emitted and allows close proximity of the particle detector to the emitting surfaces. A detailed description of the charged-particle detector employed in this new triboemission instrument is presented in following subsection 3.1.4.

In the new instrument a good vacuum can be obtained between the emitting surface and the detector to allow the observation of low energy triboemitted particles. Low and high vacuum pumping systems give the required level of vacuum (as low as 10^{-8} Torr).

Roughing pumping is carried by a cryogenic pump to a vacuum-level lower than 10^{-3} Torr. A combination of a Xerox™-Vacion model 011 vacuum ion-pump and baking of the system (at about 110C for a minimum of 12 hours) is needed to reach the 10^{-6} Torr-

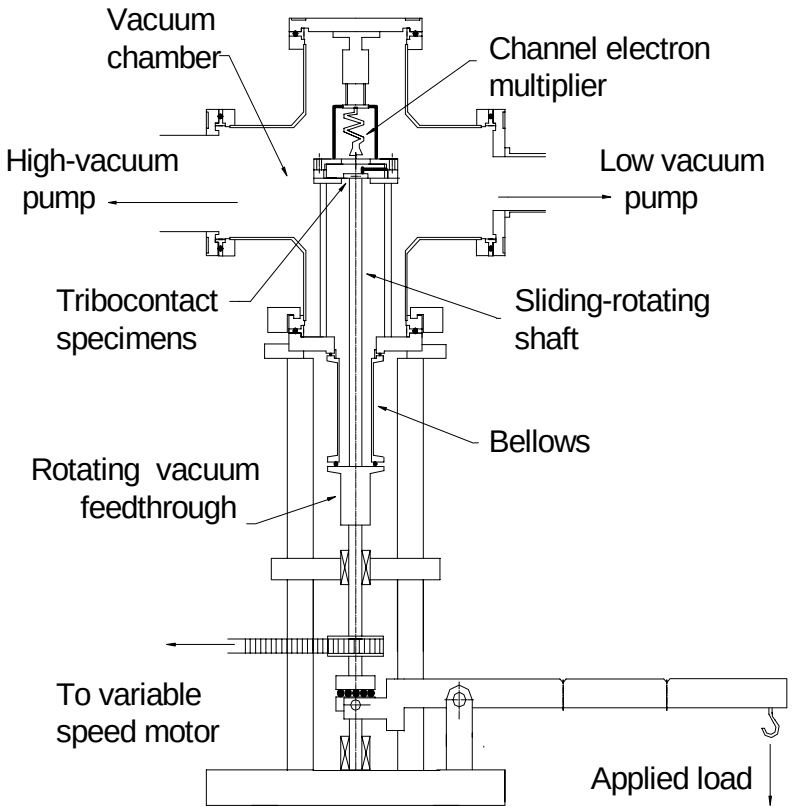

Figure 3.3. Schematic view of the new triboemission device.

level. By intermittent running of a Thermionics™ TLI-COV500 Ti-sublimation pump the pressure is lowered to the final 10^{-8} Torr-level.

Adequate vacuum monitoring can be performed in the whole range of operation: thermocouple measurement is employed between atmosphere and 10^{-3} Torr, while ion-pump current is translated to pressure for the rest of the range. Also, an ion-gauge detector (Spectramass™ model 100A) can be used to monitor total and partial pressure of gas species in the 10^{-4} Torr to 10^{-11} Torr range.

Figures 3.4 to 3.6 show photographs of the triboemission device and some of its important details. The system has also capabilities for simultaneous measurement of motor outputs (e.g., applied motor current and voltage), and of thrust displacement of the sliding shaft by a Schaevitz™ type 100-HR LVDT, which is mounted in the fulcrum assembly and controlled by a Schaevitz™ ATA 101 instrumentation.

The new triboemission instrument can be modified for the mass-measurement of the emitted particles (i.e., by placing a quadrupole mass analyzer between the emitting surface and the particle-detector), as well as for the detection of other forms of triboemission (e.g., photons). Control of atmospheres may be obtained by minor modification of the instrument.

3.1.4. Particle detector

Measurement of the intensity of triboemitted charged-particles is carried out by a Galileo Channeltron™ model 4869 Channel Electron Multiplier (CEM). A CEM is a particle-detection device that makes use of secondary-electron multiplication and cascading effects to amplify the very-low level currents, which correspond to the input of a individual charged-particle, to a mAmp-level pulse as output. A schematic view of the CEM operation is shown in Figure 3.7.

A CEM consists of a hollow coil of a heavily lead-doped glass formulation, which is internally-covered by a semiconductor-layer to enhance secondary-electron production.

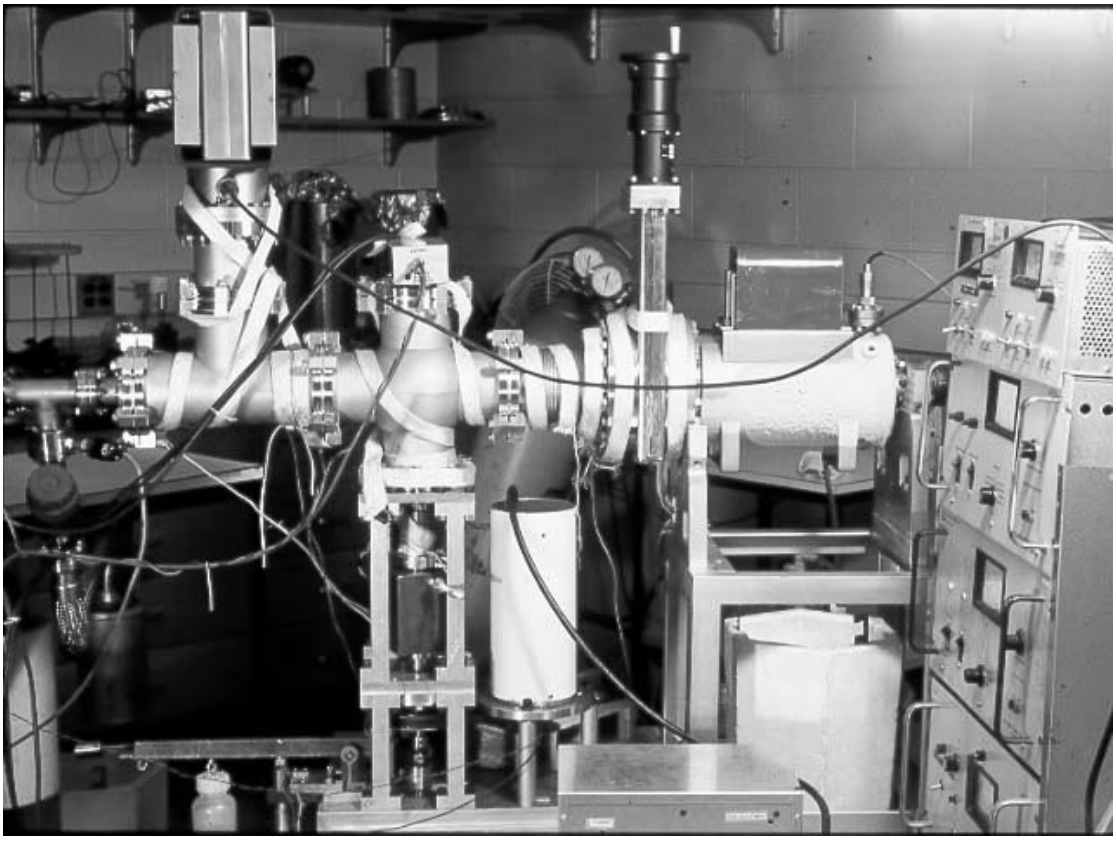

Figure 3.4. Triboemission device. General view of mechanical and vacuum assemblies.

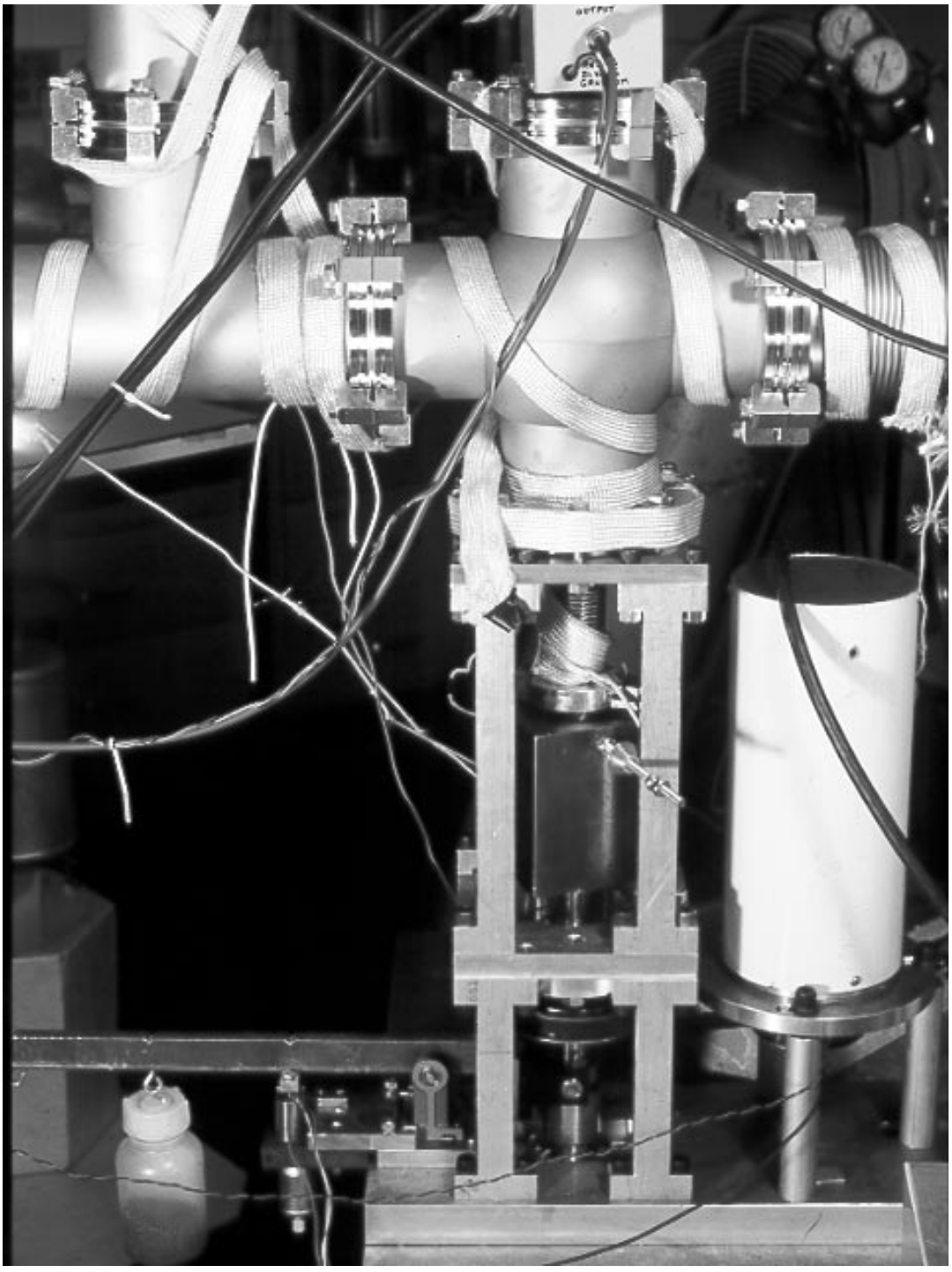

Figure 3.5. Triboemission device. View of mechanical input assembly.

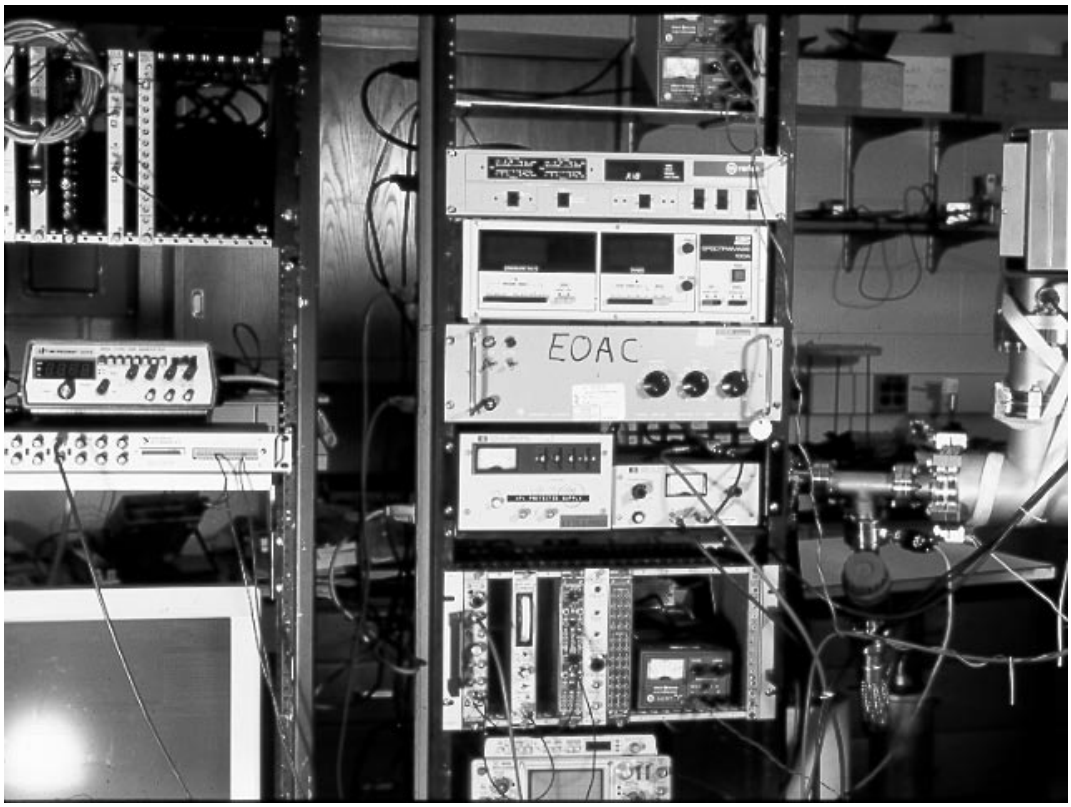

Figure 3.6. Triboemission device. View of instrumentation and data acquisition system.

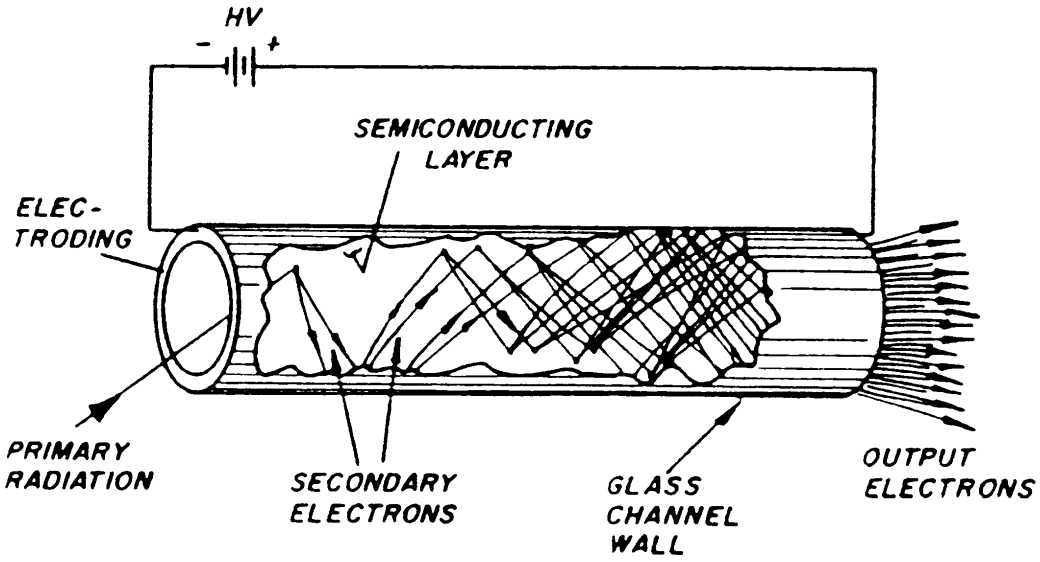

Figure 3.7. Schematic view of the CEM operation.

To prevent some effects of self-generated noise, the tube is given a coil-shape [124]. The high electrical resistance of the CEM material also provides a voltage divider to apply an external high-voltage difference between the input-cathode and the dynode at the other end. CEM operation requires a vacuum of 10^{-6} Torr or better. Both the CEM, which is enclosed in an everdur shielding-cup, and its basic electronics hang from the upper flange of the vacuum chamber (see Figure 3.3). Cathode, dynode and anode input and outputs are made by coaxial-type feedthroughs.

A charged particle, after being accelerated by the cathode voltage into the CEM input, creates secondary electrons by impacting the CEM internal-surface. The dynode-to-cathode voltage replenishes the CEM and further accelerates the secondary electrons to produce additional secondary emission. This repeated process (see Figure 3.5) results in the amplification of the initial single-particle signal to a narrow pulse (of about 10^{-8} second-width) representing the particle at the CEM anode-end. For a 1mm-diameter CEM an overall gain of 10^{+8} can be reached. Therefore, a pulse-signal as high as 2 mVolts can be obtained from an individual electron-input. Comprehensive reviews on CEM characteristics and operation can be found in [126,127].

The fact that a very narrow mAmp-level pulse at the CEM-output represents an individual charged-particle allows particle counting by using the so-called pulse-counting mode of the CEM. Figure 3.8 shows a diagram of the CEM electrical-setup employed for pulse counting in the triboemission instrument. In the pulse-counting mode, the output-pulses from particle-inputs group in a narrow-range of characteristic amplitudes well above noise-pulses. In this, the amplitude of an output-pulse only indicates its source (e.g., either particle-signal or noise), but it does not represent relative input-energy of the detected particles. By setting a low amplitude discriminating-threshold (e.g., of about 50mVolts after preamplification), noise pulses are efficiently filtered out.

An appropriate dynode-to-cathode voltage difference must be set for the highest gain compatible with efficient noise-pulse discrimination. For this, the CEM-characteristics of output count-rate vs. dynode-to-cathode voltage is used. Figure 3.9 shows a plot of such characteristics for the CEM-setup employed in the triboemission instrument. In particular, the input signal to obtain such characteristics was the ion-pump production of

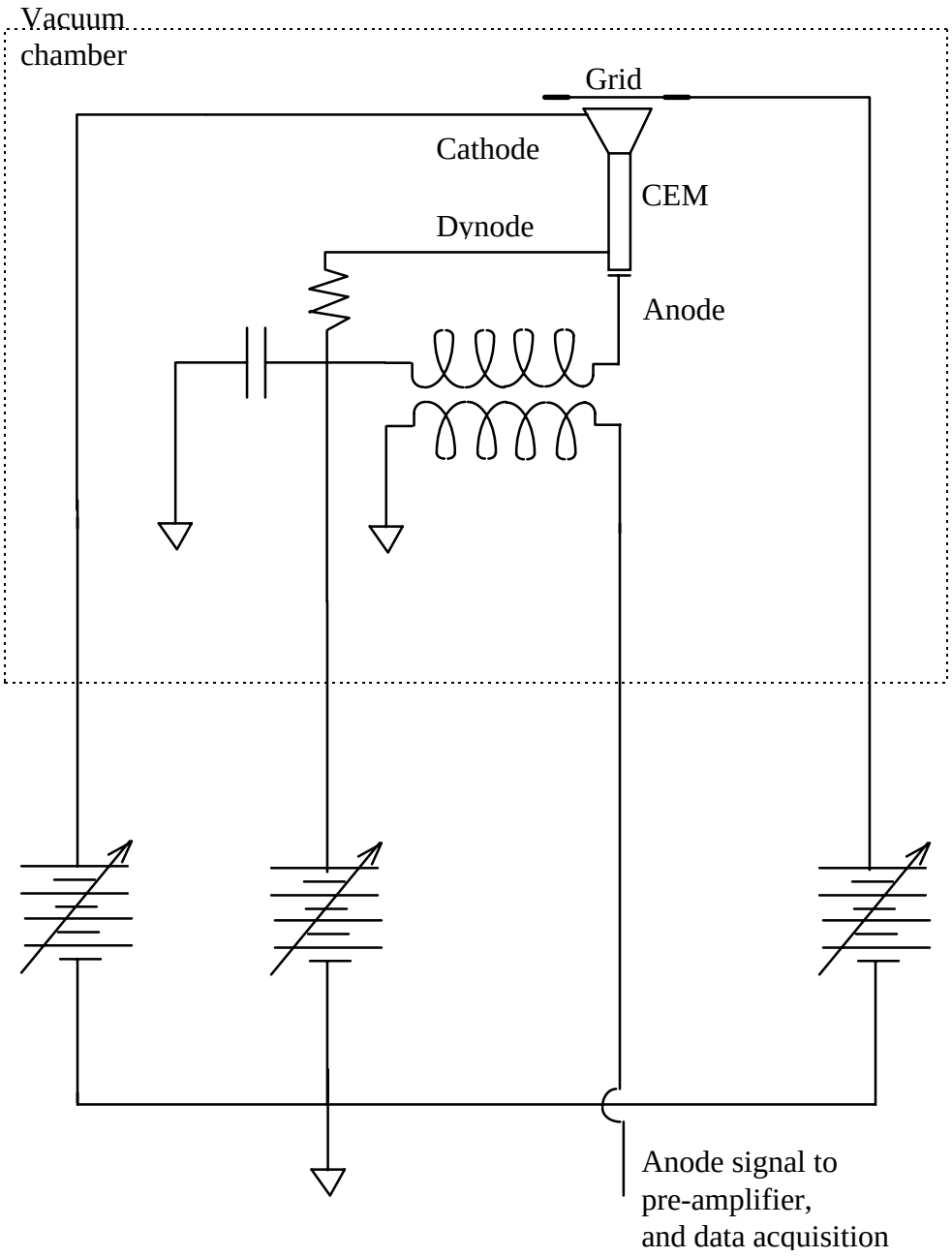

Figure 3.8. Diagram of the employed CEM electrical setup in the pulse-counting mode.

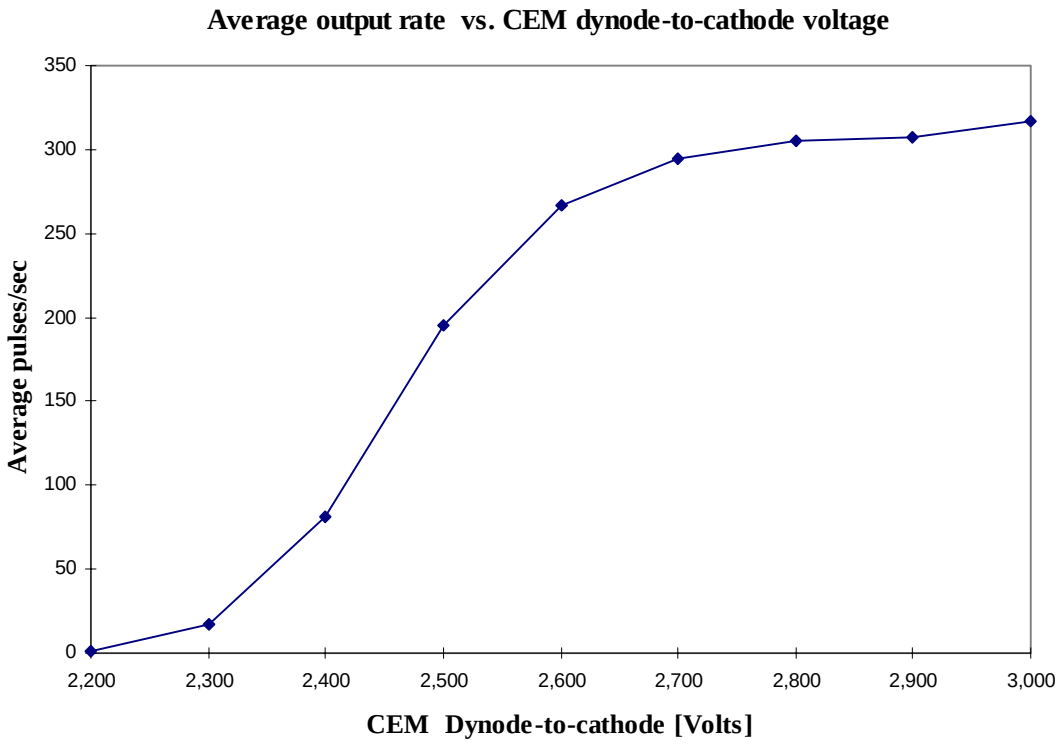

Figure 3.9. CEM characteristics of output count-rate vs. dynode-to-cathode voltage. Input signal: ion-pump particle production at vacuum level 1.5 x 10^{-8} Torr. Cathode voltage: +500Volts.

high-energy particles at a pressure of 10^{-8} Torr. Data acquisition methodology for this characterization is described in subsection 3.2.2. It can be observed in Figure 3.9 that the output count-rate reaches a plateau above a certain dynode-to-cathode difference value, which is called the "knee" of the curve. The operation point should be set for dynode-to-cathode 50 to 100Volts above this “knee”.

Cathode voltage, which is typically between ±500V to ±1,500V with respect to ground and to instrument frame, allows selectively accelerating negative- or positive-charge particles by respectively setting positive and negative cathode voltage. Because of this applied cathode-voltage, the CEM would be able to pick up from the close surrounding particles of charge opposite to the cathode polarity, regardless of particle energy. In particular, it would be able to extract particles from electrostatically-charged surfaces and even charged material-debris from the close tribological contact.

To collect only charged-particles being effectively emitted from the sliding surfaces (e.g., other than electrostatically-charged particles), a retarding grid was placed between the emitting surfaces and the CEM input. Figure 3.10 shows a detailed schematics of the employed CEM and grid assembly as they were placed in the case of a contact geometry consisting of a diamond pin on a revolving disk.

By grounding the retarding grid, the electric field from the cathode potential does not extend beyond the grid (i.e., the cathode potential does not reach the emitting surfaces): the accelerating CEM cathode-voltage is restricted to the space above the grid. Therefore, emitted particles need a minimum energy to leave the surface and to overcome the grid (depending on grid potential), to be then accelerated to the detector. A copper 100-mesh-size, of 0.0045 inch-diameter wire and 64% open area, was employed for the grid. The grid can be set to potentials other than zero (i.e., other than ground reference) to perform particle-energy spectroscopy, as explained in the following subsection 3.1.6. Following Table 3.1 summarizes the capabilities of the new triboemission instrument.

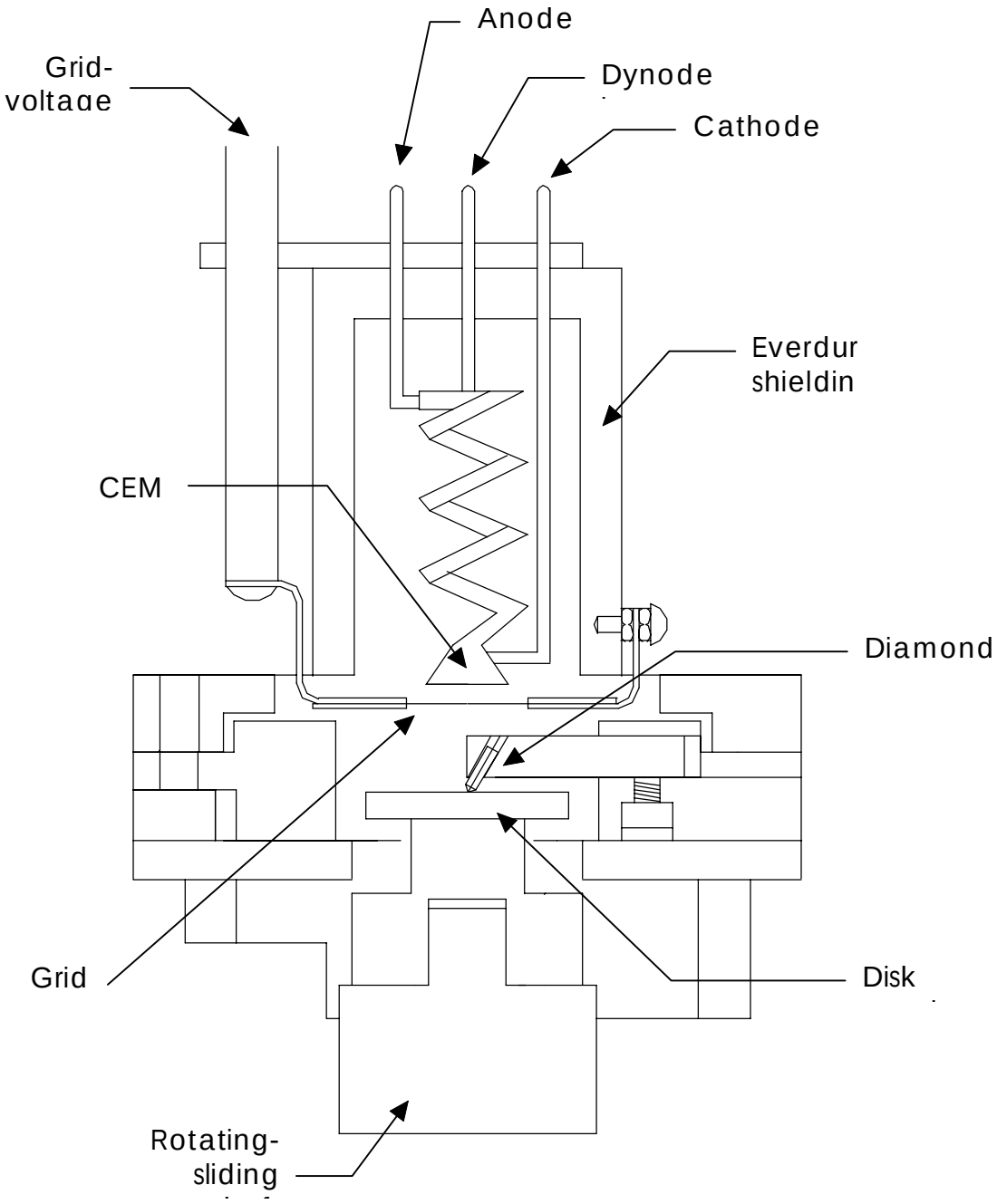

Figure 3.10. Schematics view of the CEM and grid assemblies for contact geometry of diamond-pin on rotating-disk.

Table 3.1. Features and operation ranges of the triboemission instrument.

Applied load	2 to 200 N
Rotary speed	2.5 to 2,000 rpm
Sliding velocity(*)	0.12 to 94 cm/s
Environment	Ambient, vacuum to 10^{-8} Torr, controlled atmosphere.
Material system	A-on-B or A-on-A.
Measurement capabilities	Charge intensity, retarded energy of particles, total and partial pressures of environment species.

(*) For 0.9cm-diameter track in a pin-on-disk setup.

3.1.5. Data acquisition system

Standard instrumentation is used for pre-amplification, fraction discrimination and conditioning of CEM-pulses. Pulses from the CEM-anode are pre-amplified with a gain 10. A LeCroy™ VV100B preamplifier is employed. Pre-amplified pulses are noise-filtered by a Camberra™ Constant Fraction Discriminator model 1428A. A 50 mVolt-threshold was found appropriate for this noise-filtering in the ranges of operation.

Pulse conditioning is carried by means of a LeCroy™ Dual Gate Generator model 222. In this, pulse amplitude and width are set to obtain identical TTL-pulses for counting purposes. For the employed data-acquisition electronics and sampling-rates, the TTL-pulse amplitude was set at 2 Volt peak-to-peak, and pulse width of 1 microsecond was chosen.

The conditioned analog square-pulses, each representing a single particle reaching the CEM, are fed to a data acquisition board National Instrument™ model PCI-MIO-16E-4. The board is controlled by a personal computer and appropriate software. This computer-based data acquisition system provides analog-to-digital conversion, fast-rate accumulated pulse-counting and storage of data. Figure 3.11 presents a block-diagram of the above described data-acquisition system.

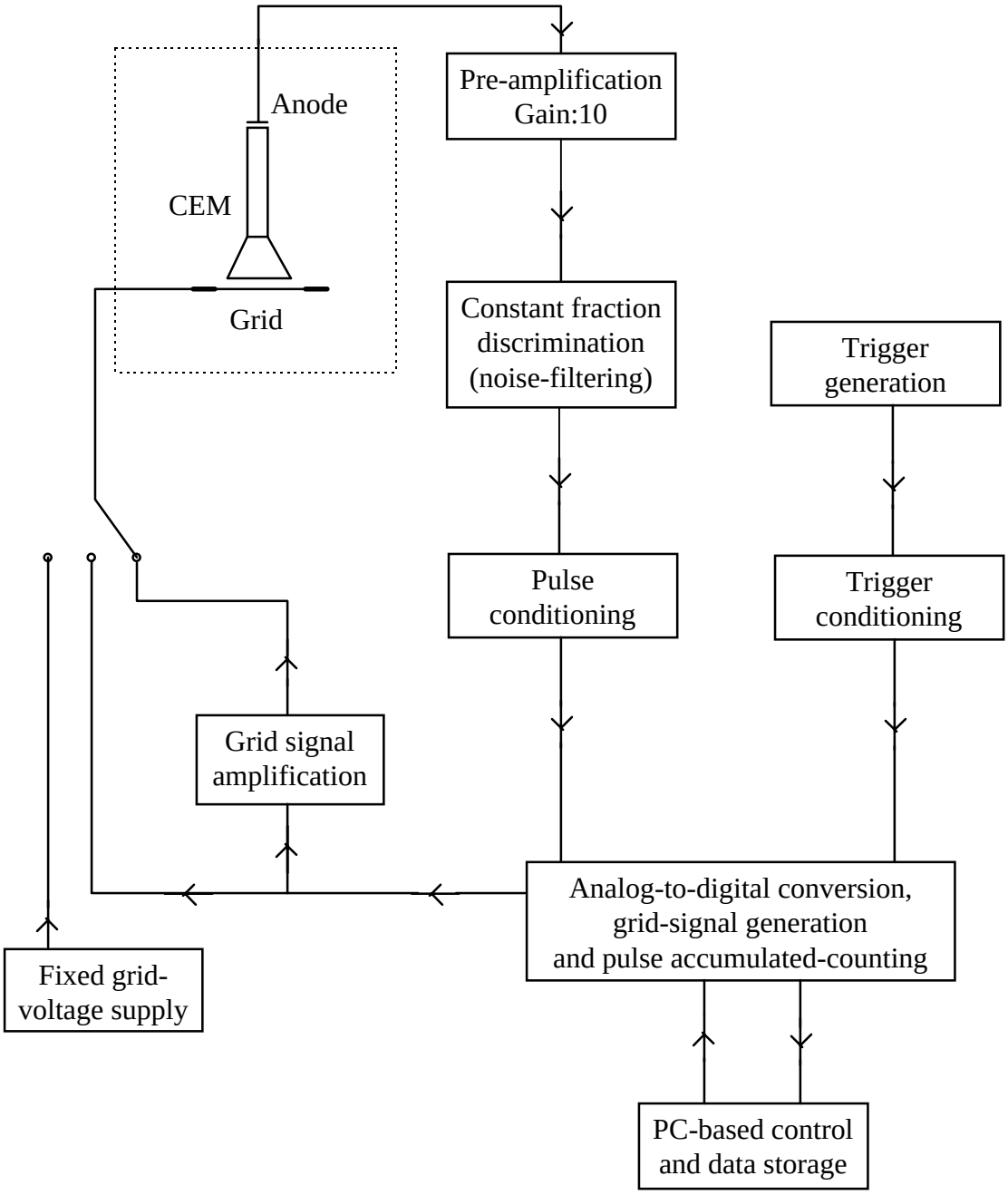

Figure 3.11. Block-diagram of the employed data-acquisition system.

The software to control data acquisition was developed by means of LabView™ on a Microsoft™ Windows95™-platform. In this, the pulse-counting task is performed by accumulation of TTL-signal rising edges in a DAQ-STC™ hardware-counter featured on the data acquisition board. Readings from the accumulating counter and storage of such readings in the computer RAM are performed by the developed software, and they are timed by an external TTL trigger frequency. By design of such software, counter reading neither stops nor interferes with the hardware-counter.

A BK-Precision™ model 3011B function generator is employed to supply the external TTL-trigger in the range of 0.3 Hz to 1KHz. This upper limit was found the highest compatible with reliable data reading and writing. Setting of this external trigger (and, therefore, of a sampling frequency) also defines a so-called data acquisition window. Since no time-history can be resolved within each window, the window length will condition further analysis of data. Therefore, the window length must be chosen smaller than the characteristic length of the studied phenomenon. Chapter 4 describes the experimental work to determine such appropriate data-acquisition frequency for triboemission phenomena.

After each triboemission test is performed, the obtained data can be saved as a standard text file, which is customarily a column of integer values which represent the accumulated-history of counts at the employed sampling-frequency.

3.1.6. Retarded-energy measurement system

As described in previous subsection 3.1.4, a grid was placed between the emitting surfaces and the CEM detector. This grid can be biased with respect to ground reference to perform energy spectroscopy by the method of retarding potentials. In this method, biasing the grid to a defined voltage allows screening of particles according to their kinetic energy: any particle of energy equal to or lower than the set potential will be screened out from reaching the detector and, therefore, from the pulse counting.

Investigating the energy spectrum of burst-type signals (as those expected from triboemission) required some additional data-acquisition techniques. To resolve the fast

changes in the signal, the grid voltage must be swept about the energy range of interest. Also, the sweeping-period should be much smaller than the characteristic decay-time of the signal-bursts. This fast grid-voltage sweeping, which must be also synchronized with data acquisition, was implemented by a software developed on LabView™-Microsoft™ Windows95™-platform.

The software-generated retarding voltage can be controlled in amplitude (in the -10Volt to +10Volt range before amplification), frequency and shape, and is synchronized with the data acquisition. In particular, a stepwise sawtooth grid-voltage can be generated with voltage steps of the same length for a series of discrete integer amplitudes. Figure 3.12 shows the front panel of this LabView™ virtual instrument, with an example of a stepwise sawtooth waveform. By feeding such waveforms to the retarding-grid, emission count-rate can be determined for each discrete voltage-steps to obtain an energy integrated-distribution of the triboemitted charged-particles.

The LabView™ virtual instrument generates the sweeping voltage-signal from the data acquisition board in the zero to ±10V range. Such voltage was fed either directly to the grid for voltage sweeping in such range, or was eventually supplied to a Kepco™ Operational Power Supply model OPS2000B for amplification to a higher range (see Figure 3.11). For this, the amplification-gain was set to 100.

Development of the triboemission instrument constituted an important part of the research work of this dissertation. Testing methodologies and procedures to implement the specific triboemission measurements are reported in the following section of this chapter.

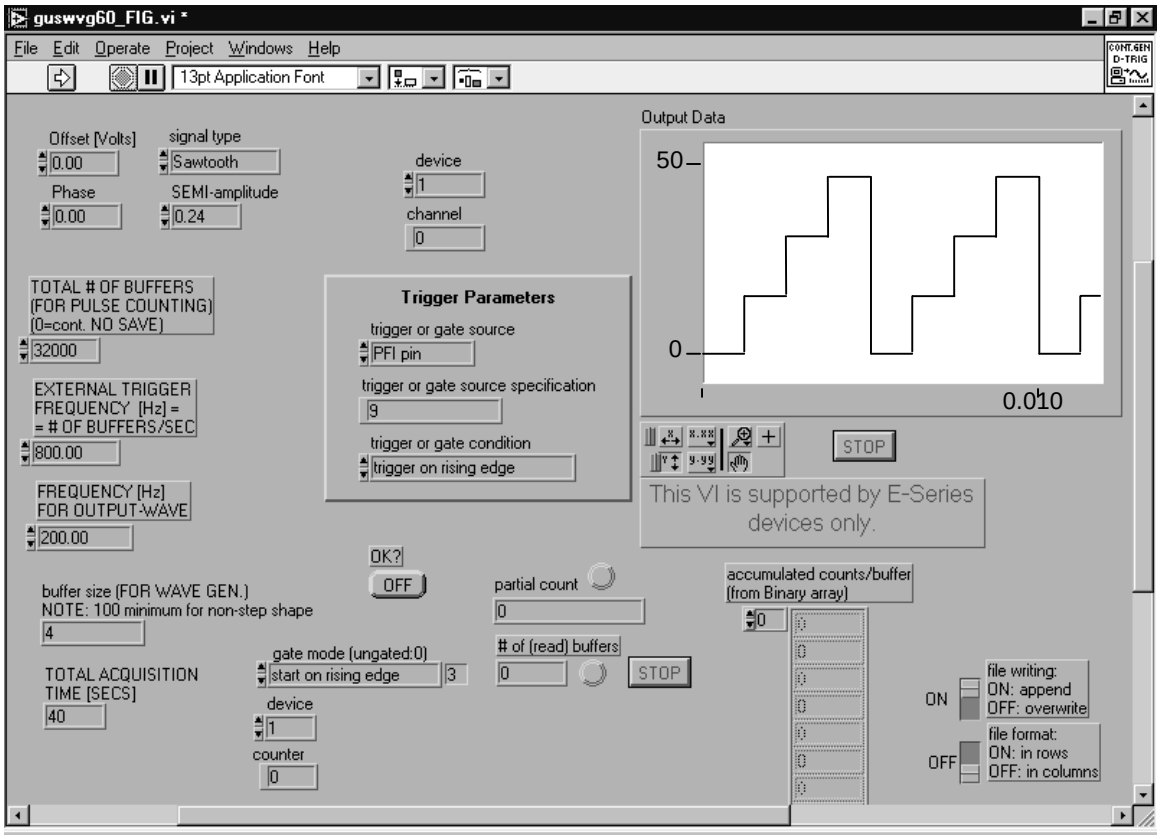

Figure 3.12. Front panel of LabView™ virtual instrument for generation and control of grid voltages, and for pulse counting in CEM outputs.

3.2. Material systems and measurement methodologies

The triboemission instrument presented in previous section 3.1 was primarily designed and developed to measure charge intensity and kinetic energy of both negatively- and positively-charged particles triboemitted from ceramics. This section describes material systems and methodologies employed for such measurements.

3.2.1. Material systems and sliding-contact geometries

This research work on triboemission concerns two types of ceramic-material systems: the diamond pin-on-ceramic (or on, eventually, non-ceramic) and the ceramic-on-same-ceramic systems. The former may be called diamond-on-ceramic system, while the name ceramic-on-ceramic system may apply to the latter.

Diamond-on-ceramic triboemitting systems have been previously considered, though not for all the same ceramics of this work, by Nakayama et al. [84-89] and Dickinson et al. [95-97], as previously reviewed in section 2.3. Important features of the triboemission from the diamond-on-ceramic systems, which were not examined by those researchers, are examined in this research work.

The triboemission from ceramic-on-ceramic systems was not previously investigated, although its fundamental and practical importance is likely greater than that of the diamond-on-ceramic systems.

For the diamond-on-ceramic systems, two related ceramics were employed: alumina and single crystal sapphire (e.g., two different structures of Al_2O_3). A third related metallic material, i.e., aluminum, also was used for the purpose of comparison. The triboemission from ceramic-on-ceramic systems was investigated for alumina-on-alumina.

The contact-geometries used were derived from the classical pin-on-disk. In the case of diamond-on-ceramic, a diamond-pin with a 90 degree-angle-cone tip slid on a disk of the pertaining material. The resultant 0.92cm-diameter wear track was completely inside

the projection of the CEM input-funnel. This assembly is shown in figures 3.11 and 3.13. For the purpose of maximizing the unobstructed solid angle into which the particles are emitted, the diamond pin is not perpendicular to the disk surface, but it is inclined by 30 degrees. Sliding disks were mounted on top of specially designed disk-holders to obtain the disk surface perpendicular to the rotating shaft. Epoxy was used to glue the disks to the holders.

In the case of alumina-on-alumina contact, the pin is a 0.125 inch-diameter alumina ball sliding on the corresponding one-inch-diameter revolving alumina-disk. This assembly, which is shown in Figure 3.14, was obtained from slight modification of the diamond-on-ceramic system. Epoxy was used to glue the alumina ball to a small ball-holder.

The diamond pins were supplied by Bruce Diamond Corp. as standard industrial diamond scribes. Alumina disks (99.5% isostatically-pressed alumina) were supplied by LSP Industrial Ceramics, Inc., with a ground-surface to an average roughness (CLA) of 0.50 to 0.65 micrometers. Sapphire disks (optically flat single-crystal sapphire) were supplied by General Ruby and Sapphire Co. Aluminum disks were machined from commercial rods of SAE 6061 aluminum. Alumina balls (99.5% alumina, grade 25) were supplied by Sapphire Engineering, Inc.

3.2.2. Specimen preparation, and measurement calibration and procedures

The specimens described in previous subsection 3.2.1. were cleaned in ultrasonic baths of acetone and methanol for ten minutes per liquid. The replacement of tested disks and pins required the opening of the vacuum chamber to atmospheric pressure under a flow of dry nitrogen. Resuming the measurement vacuum levels needed a minimum 24-hour pumping time.

Since the CEM gain may decline with use, a check of the CEM-characteristics was carried out before testing each specimen. For this, the output count-rate vs. dynode-to-cathode voltage characteristics was measured. Figure 3.10 shows one of such

Figure 3.13. Triboemission device. View of diamond-pin on alumina-disk geometry.

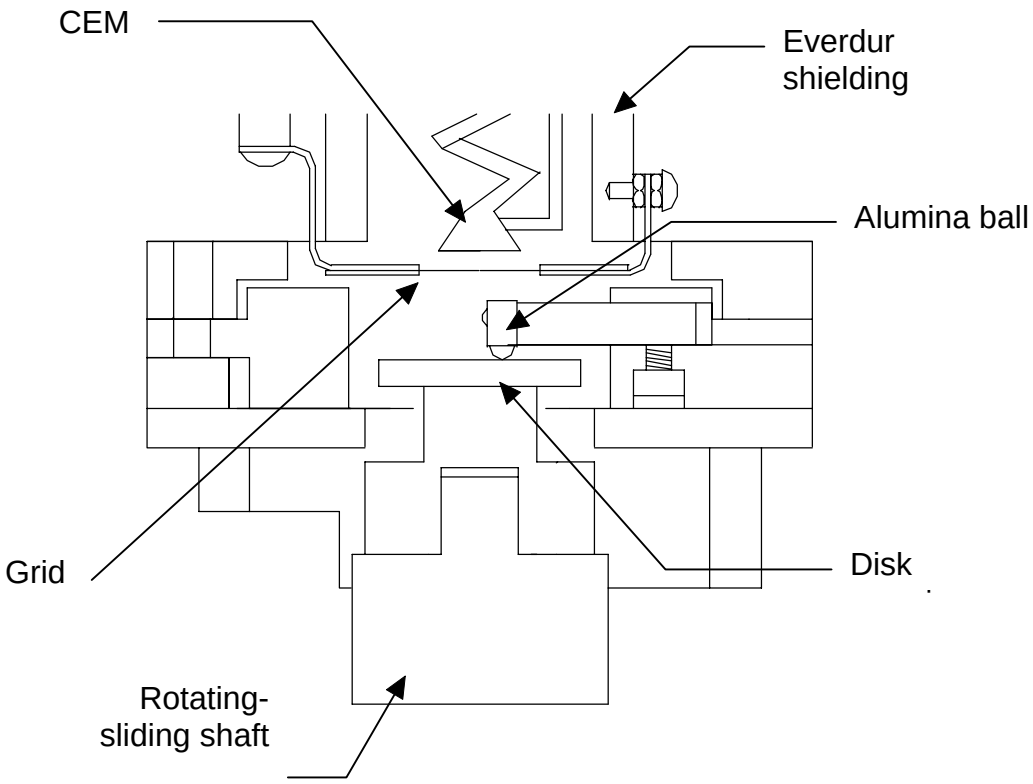

Figure 3.14. Schematics view of the contact-geometry assembly for alumina-ball on revolving alumina-disk.

characteristics for the employed CEM. The input signal to obtain such characteristics was the ion-pump production of high-energy negatively-charged particles (while the vacuum is in the range of 10^{-8} to $2x10^{-8}$ Torr). For this, cathode voltage was usually set to +1,200V.

The data acquisition hardware and software described in previous subsections 3.1.4 and 3.1.5 were employed to record 20-second data (e.g., of accumulated CEM pulse-count) for each of 100V-dynode-to-cathode steps in the range of +1,800V to +3,000V. The average count-rate for each data-record, each of which corresponds to a dynode-to-cathode voltage value, were computed and plotted. As described in subsection 3.1.4, the operation point of the CEM was set at dynode-to-cathode voltage of 50 to 100V above the so-called "knee" of the curve. For all the experimental testing presented in this dissertation, the CEM operation-point was found in the dynode-to-cathode range of 2,250V to 2,450V.

The production of positively-charged particles from the ion-pump (e.g., as detected by the CEM setup) was, however, very low (lower than 1 count/second) at the employed vacuum level and for a -1,500V cathode setting. This low input-signal did not generate any meaningful CEM-characteristic for negative cathode operation. The assumption was made that the same CEM-characteristic applies to both negative and positive cathode settings: the characteristics for positive cathode (e.g., for +1,200V) was employed to determine the dynode-to-cathode operation point in all cases.

As above-suggested, negative-charge particle-production from the ion-pump was not compatible with the negatively-charged particle measurement. For this reason, the ion pump was shut off during such triboemission testing. Although the vacuum slowly deteriorated in the absence of ion pumping, it held lower than $5x10^{-7}$ Torr for periods as long as 8 minutes. Such level of vacuum, together with appropriate grounding and shielding of the triboemission instrument, kept the background-noise lower than 1 count/sec. For positive-ion detection, however, the very low production of positive ions from the ion-pump, allowed pump operation during measurement.

3.2.3. Load, sliding speed and operational testing conditions

In general, load and sliding speed were constant during testing. Applied loads ranged from 2N to 20N among different tests. Applied sliding speeds ranged from 0.12 cm/s to 4.8 cm/s. However, the low values in such ranges were generally employed. These low values hold to negligible levels any frictional heating and generated temperature rise. Therefore, no thermionic emission is produced from the tribological contacts. Such negligible heating does not affect the triboemission measurement.

The new triboemission instrument allows data acquisition, during any single test, for three distinct conditions, by either separating or contacting the tribological surfaces as follows. Typically, data for a initial period of 20 seconds were acquired for the conditions of rotating disk without pin contact. Such data give a rough estimate of the background-noise for the test. By applying the sliding contact (e.g., for the test-load) between the surfaces, data were acquired for the triboemission phenomena itself. Ceasing sliding contact by separating the surfaces, while maintaining data acquisition, resulted in information for the so-called "after-contact" period, e.g., for data pertaining to any post-emission from the activated surfaces.

As described in subsection 3.1.5, setting of the external-trigger sampling-frequency defines a data-acquisition window. Different window-values were set for the triboemission tests, usually as a compromise between the needed time-resolution of data, its file-length, and the further analysis. The following chapter presents experimental results for triboemission intensity and retarded-energy spectra of charged-particles triboemitted from the described material systems. Details of specific testing conditions and procedures are given when they pertain to a particular measurement. Appendix D summarizes the experimental conditions for the examples of triboemission outputs shown in Chapter 4.

CHAPTER 4. EXPERIMENTAL MEASUREMENTS OF TRIBOEMISSION

4.1. Non retarding-grid measurements for diamond-on-alumina sliding contacts.

As described in subsection 3.1.6, charges approaching the CEM are accelerated into its opening by the CEM-cathode voltage. If a grounded grid (or a retarding grid, if set to a voltage different than zero) is placed between the emitting surfaces and the CEM input, only charged-particles being effectively emitted from the sliding surfaces are able to reach the detector (see subsection 3.1.4). This is the case for most of the measurements presented elsewhere in this chapter. However, data obtained without this screening grid may be of interest for the understanding of triboemission.

The preliminary data, in this section only, were acquired for this non-grid condition. Such data gave some initial insight of charged-particle production phenomena from the diamond-on-alumina sliding contacts. The whole production of charged particles, both emitted and electrostatically charged on the rubbing surfaces, however, may be of different intensity than the actual charged-particle triboemission, which is reported in the following sections of this chapter. Detailed information for the load, sliding speed, and contact schedule for the experiments presented in this section is given in Appendix D.

For this non-grid setup and +500V cathode-voltage (i.e., a cathode setting to accelerate negatively-charged particles into the CEM), Figure 4.1 presents CEM output versus time for a diamond-on-alumina sliding contact, during the following contact-schedule: Twenty-second periods of contact (e.g., when the rotating disk was set in contact with the diamond) were alternated with 10-second periods of non-contact (e.g., when disk was set apart from the diamond). The data-acquisition window used was one second. Applied load was 2N and sliding speed was 1.4cm/s. Background-noise data was previously recorded and its average computed as 0.54 counts/second.

Figure 4.1 shows that the CEM-count of negative-charges is burst-type associated with sliding contact. Significant CEM-counting was observed clearly above background

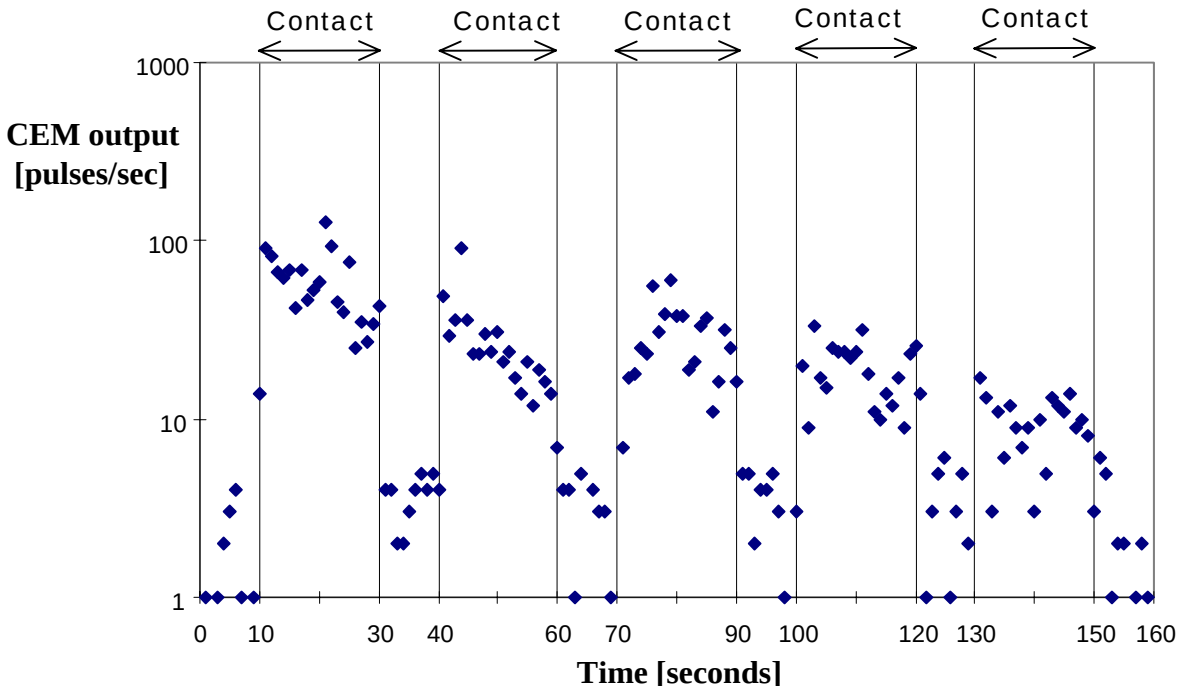

Figure 4.1. Negative-charge CEM-count for diamond-on-alumina sliding contact.
CEM output (in the 1 second data-acquisition window) vs. time.
Non-grid measurement. Cathode: +500V. Load: 2N . Speed: 0.14 cm/s.
Pressure: 1.5×10^{-8} Torr

during sliding-contact periods. The counting dropped when contact ceased (e.g., for the 10-second intermissions of non-contact), although it stayed above background-level. This experiment suggests that CEM-counting for contact-periods decreases for consecutive contact periods. The data also shows that post-contact CEM-counting may be higher than background: this shows a decay of triboemission after contact ceased, with no simultaneous tribological stimulation.

These non-grid tests led to an important experimental finding: when opening the vacuum chamber after such tests, visible alumina-debris was found in the CEM-input. This was clearly related to extraction of electrostatically-charged material-debris from the wear track, which was picked-up by the cathode-voltage. This finding supports the thought that the CEM-count for the non-grid situation does not necessarily reflect particles actually emitted.

CEM-count for the non-grid setup would rather indicate the production of both actually emitted charged-particles and some electrostatically-charged ones, including charges carried by the material-debris, all of which eventually reach the CEM-input. Only the former (e.g., actually emitted particles), however, would have the level of kinetic energy that is of interest in this research.

Another non-grid experiment investigated CEM-counting for the initial three turns of the alumina-disk during diamond scratching. For each turn, the measurement started with a 10-second non-contact period, followed by a 24-second diamond-on-alumina sliding contact. For the 0.12 cm/s sliding speed employed, this contact period corresponded to a single turn of the disk. Contact ceased after that single turn and data was recorded for the remainder of 4 minutes total time. This schedule was repeated to obtain data for the first three-turns of the sliding contact in three different data-records.

Figure 4.2 presents this negative-charge CEM data as accumulated counts versus time for each of the three-first turns of contact, and for the following post-contact measurements. Applied load was 2N. The data-acquisition window used was 100mseconds. Background-noise data was previously recorded and its average computed as 0.28 counts/second.

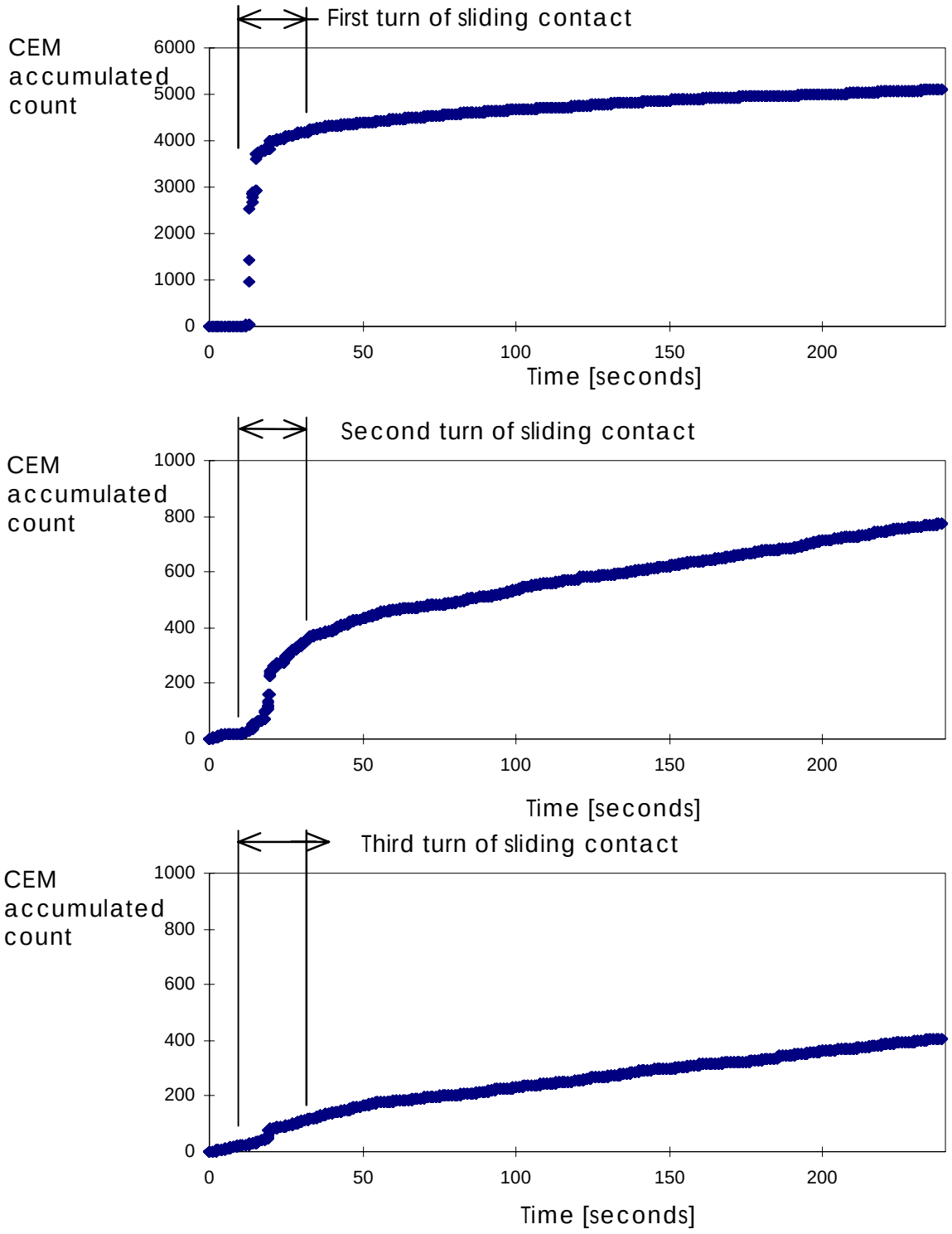

Figure 4.2. Negative-charge CEM accumulated count
for diamond-on-alumina sliding contact.
CEM accumulated output (in the 1 second data acquisition window) vs. time.
Non-grid measurement. Cathode:+500V. Load: 2N. Speed: 0.12 cm/s.
Pressure: 1.5×10^{-8} Torr

Accumulated CEM-count in Figure 4.2 presents three distinct periods associated with the three non-contact/contact/post-contact conditions as described. Slopes of the accumulated-count curves, which correspond to average CEM-counting, are significantly different for each of these periods. Slopes for the initial non-contact periods are negligible, indicating the low background-noise. Slopes for the contact periods, which are significantly higher than background, decrease as consecutive turns of sliding contact are run on the same wear track. Slopes pertaining to the post-contact periods also show a decrease after each consecutive turn, although they are higher than those for background-noise.

The two non-grid measurements shown suggest that time may be an important factor in the production of negative-charges from and on diamond-on-alumina sliding contacts. It was also found, however, that the accumulation of material debris on the detector input reduced CEM-gain during testing. These operational complexities prevented anything more than loose qualitative conclusions from these experiments.

The influence of sliding speed on tribocharge production was briefly explored, although with the above-said limitations of the non-grid measurements. Figures 4.3 and 4.4 respectively show negative- and positive-charge CEM-measurements for variable sliding speed. Top plots of these figures present CEM accumulated counts versus time. Applied load was 2N. A constant sliding-contact acceleration of 0.048 cm/sec^2 was applied during a 100sec-period of contact. Speed was increased between 20 and 120 seconds from the initial speed of 0.12cm/sec to the final of 4.8cm/sec. After that, contact ceased and post-contact data were recorded for additional 25 seconds.

The same data are plotted in the bottom of Figures 4.3 and 4.4 as CEM accumulated counts versus variable sliding speed. The data-acquisition window employed was 100mseconds. Background-noise data was previously recorded and its average computed as 0.94 counts/second for the employed +500V cathode voltage (i.e., for negative charge measurement), and 0.71 counts/second for -1,100V cathode (i.e., for positive charge measurement). The higher absolute value for negative cathode was needed to obtain meaningful results above-background for positive charge.

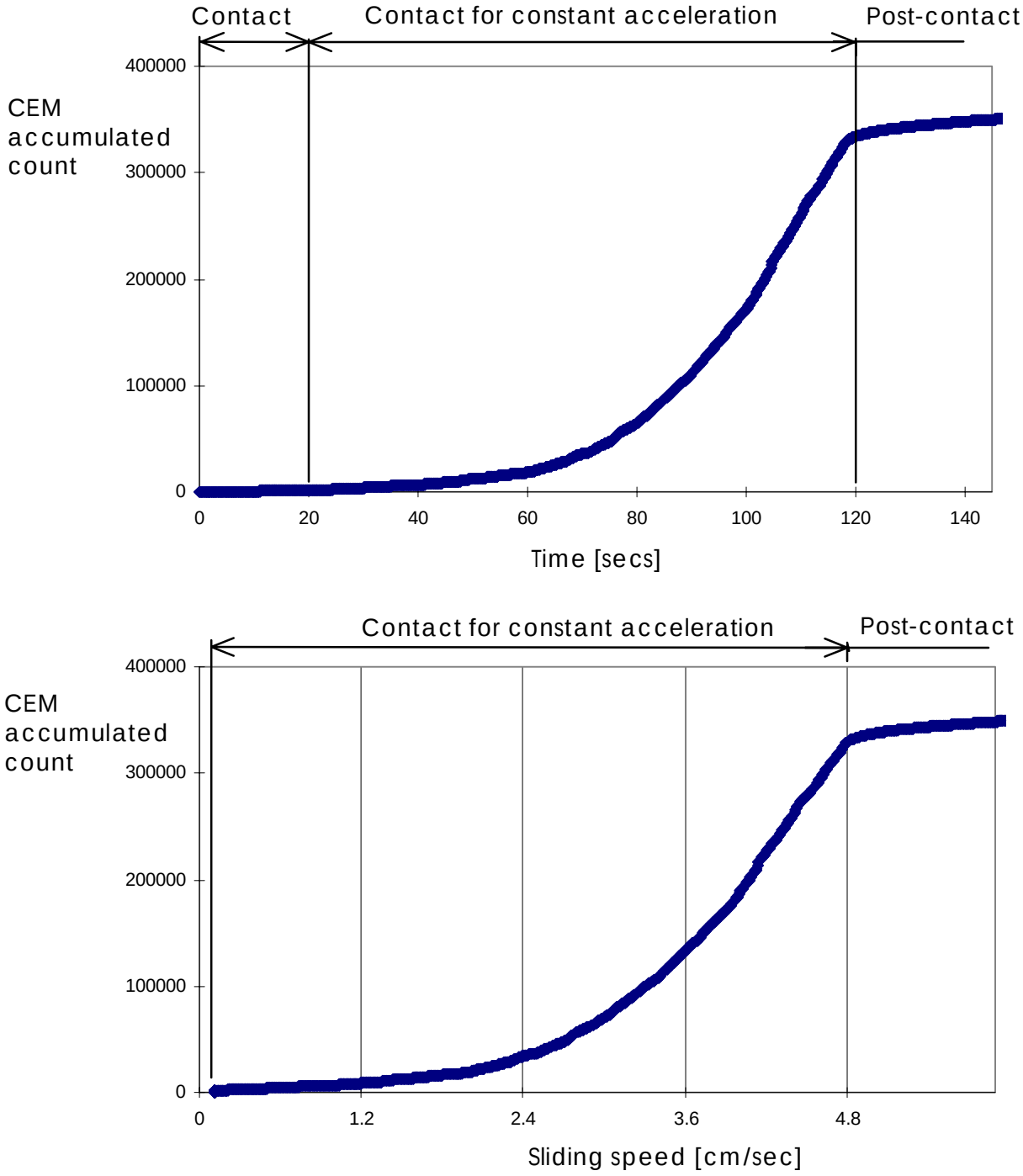

Figure 4.3. Negative-charge CEM-count for diamond-on-alumina sliding contact.

CEM accumulated output vs. time and sliding speed.

Non-grid measurement. Cathode: +500V. Load: 2N.

Acceleration (for sliding speed): 0.048 cm/sec^2. Pressure: 1.5x10^{-8} Torr.

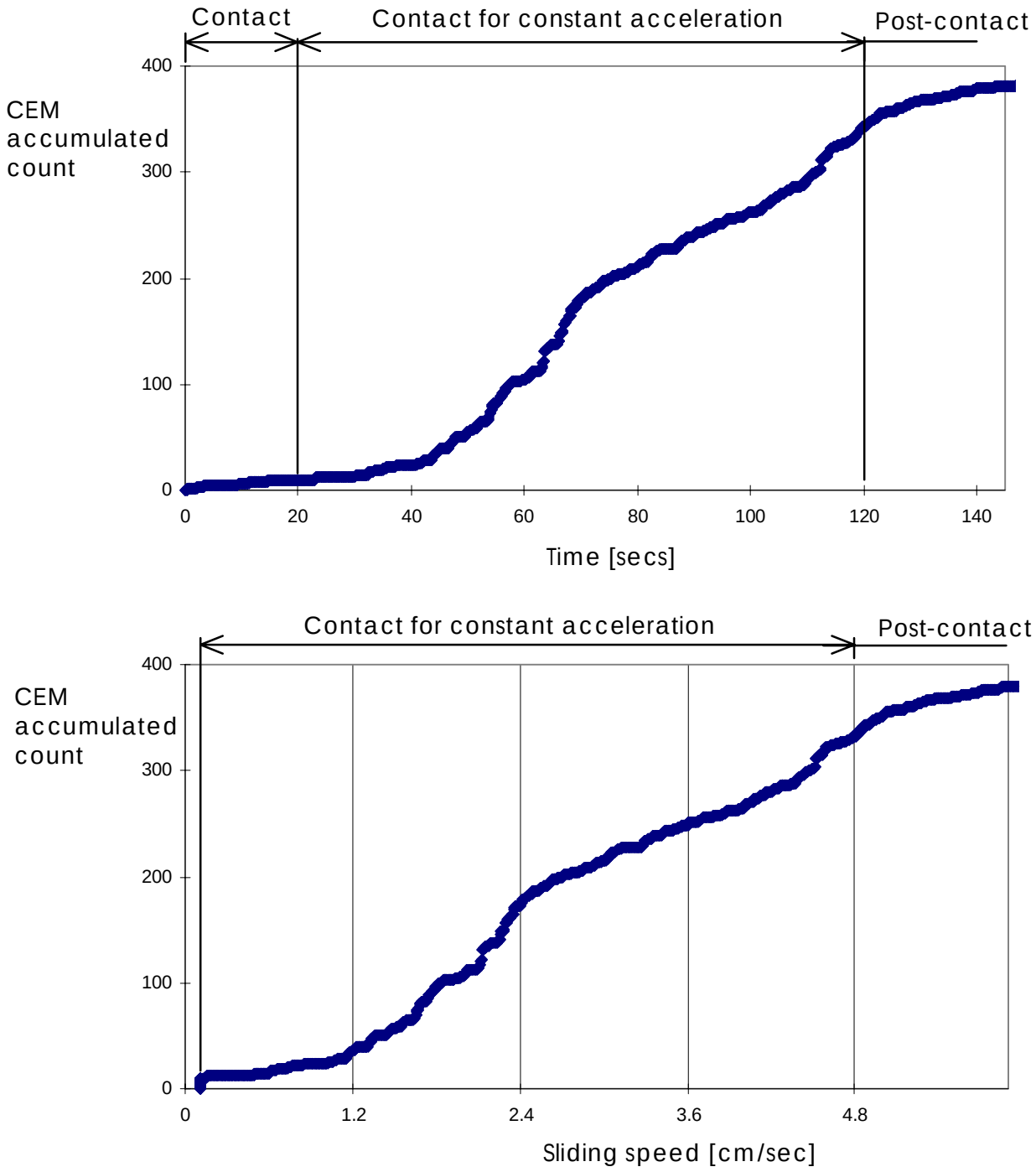

Figure 4.4. Positive-charge CEM-count for diamond-on-alumina sliding contact.

CEM accumulated output vs. time and sliding speed.

Non-grid measurement. Cathode: -1,100V. Load: 2N.

Acceleration (sliding speed): 0.048 cm/sec^2. Pressure: 1.5x10^{-8} Torr.

It is clear from the experiments that a greater CEM-count is obtained for negative-charge than for positive-charge, for the same sliding-contact conditions. The increasing slope of the curves for negative-charge measurements suggests that higher sliding speed would increase the production of negative charges for diamond-on-alumina sliding-contacts. However, the operational complexities of the non-grid experiments prevent any definitive conclusion. A much clearer picture was obtained with the use of a retarding-grid between the detector and the emitting surfaces, as reported in following sections of this chapter.

4.2. Preliminary triboemission measurements for diamond-on-alumina sliding contacts.

This section and the rest of this chapter present measurements of charged-particle intensity from diamond-on-ceramic sliding contacts when a retarding grid is placed between the emitting surfaces and the CEM input. As explained in subsection 3.1.6, only charged-particles being effectively emitted from the sliding surfaces reach the detector (see subsection 3.1.4), if this grid is set to a known potential with respect to frame and ground. Detailed information for the load, sliding speed, and contact schedule for the experiments presented in this section is given in Appendix D.

For a grounded grid (i.e., zero-Volt with respect to reference), triboemission was investigated for the initial three turns of the alumina-disk during diamond scratching. This experiment was conducted for the same material system and operating conditions as the one reported in section 4.1, but for the use of the grounded grid. Figure 4.5 presents such negativey-charged triboemission data as accumulated counts versus time for each turn of contact, and for the respective post-contact measurement.

For each turn, the measurement started with a 10-second non-contact period, followed by a 24-second diamond-on-alumina sliding contact. For the sliding speed of 0.12 cm/second this contact period corresponded to a single turn of the disk. Contact ceased after that turn (by pulling apart the revolving disk from the diamond, and data were recorded to complete 4 minutes of total time. The described schedule was repeated to obtain data for the first three-turns of the sliding contact in three different data-records.

For the measurement of figure 4.5, the applied load was 2N. The data-acquisition window employed was 100mseconds. Cathode voltage was set to +1,200V. Background-noise data was previously recorded and its average computed as 0.08 counts/second.

Accumulated CEM-counts in Figure 4.5 present three distinct periods associated with the three above-described non-contact/contact/post-contact conditions. Slopes of the accumulated-count curve (which correspond, in general, to average CEM-counting) are significantly different for each of these periods. Slopes for the initial non-contact periods are negligible, showing the low background-noise. Slopes for the contact periods, which correspond to triboemission intensity, are significantly higher than background-noise, and they decrease as consecutive turns of sliding contact are run on the same wear track. Slopes for the post-contact periods are smaller than those for sliding-contact, although they show triboemission intensity higher than background-noise.

These data suggest that time may be an important factor in the triboemission of negatively-charged particles from the diamond-on-alumina sliding contacts. It is thought that the decrease of triboemitted-particle production for repeated transit of the diamond on the same wear-track may be related to decreasing wear and surface damage of alumina, and/or to decreasing creation of fresh alumina surfaces.

Figure 4.6 shows the data of Figure 4.5 as counts in the 100msec-window (e.g., as non-accumulated counts) versus time. While accumulated data represent average triboemission-rate, non-accumulated data show instantaneous time features. The measured triboemission is burst-type clearly associated with sliding contact.

After the vacuum-chamber was open, no visible debris was found either on the CEM-input or on the retarding-grid surface. This confirms that debris from the wear track is electrostatically-charged (and picked-up by the cathode voltage in the absence of grid, see section 4.1), and its charge is different than the actually triboemitted charge, which is measured with the grid configuration.

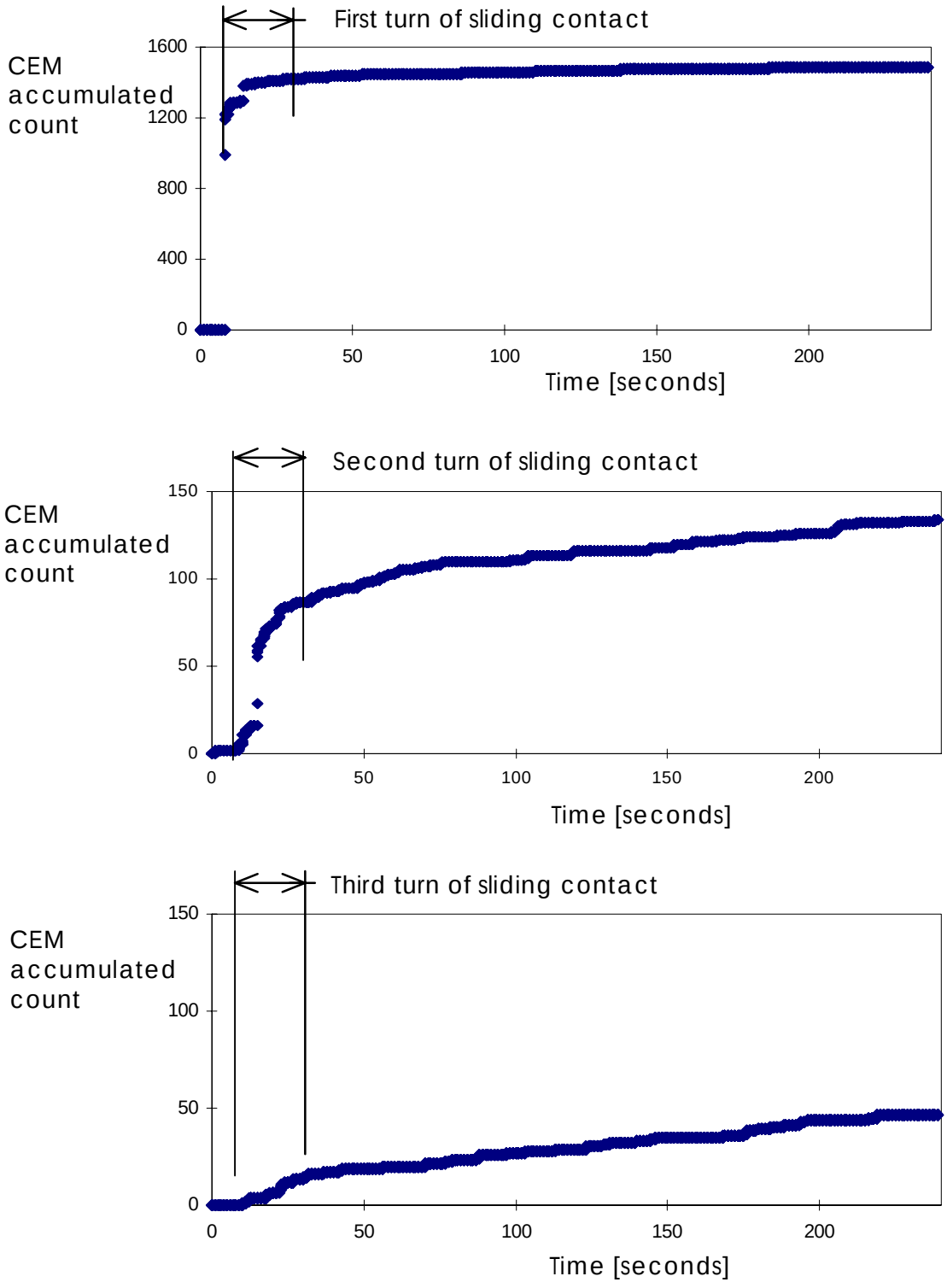

Figure 4.5. Accumulated negatively-charged triboemission
from diamond-on-alumina.
CEM accumulated output (in 0.1 second acquisition window) vs. time.
Grid:0Volt(grounded).
Cathode:+1,200V.Load:2N.Speed:0.12cm/s.Pressure:1.5x10^{-8}Torr.

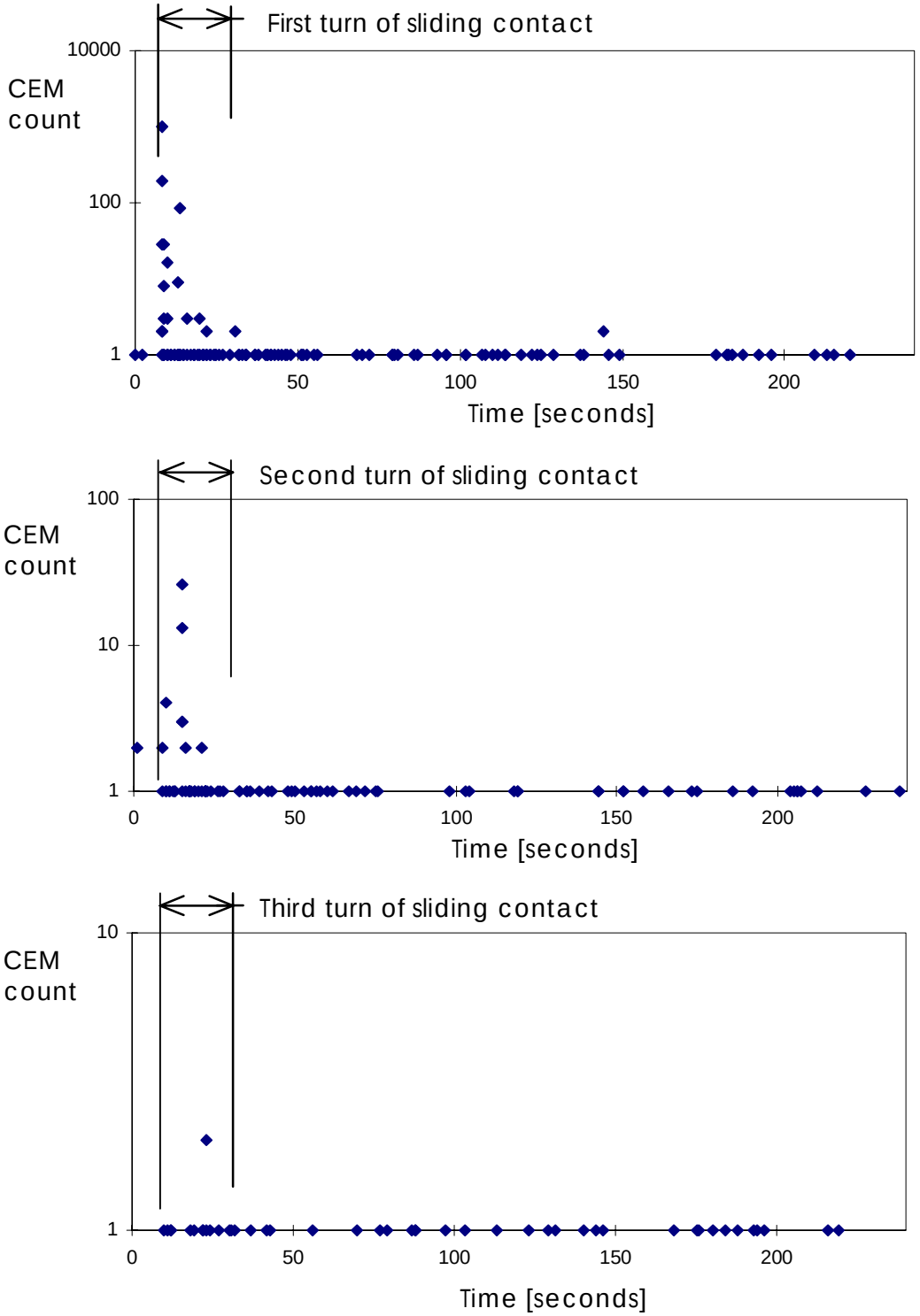

Figure 4.6. Negatively-charged triboemission from diamond-on-alumina. CEM output (in the 0.1 second data-acquisition window) vs. time. Grid:0Volt(ground). Cathode:+1,200V.Load:2N.Speed:0.12cm/s.Press:1.5x10^{-8} Torr.

The measurement of figures 4.5 and 4.6 is compared to the one conducted for the same material system and operating conditions, but for the use of a grounded grid, in section 4.1. The average count obtained for the grid configuration is lower by about one order of magnitude than that for the non-grid configuration measurement. Also, highest bursts of triboemission for the grid-measurements are smaller than those for the non-grid setup. These comparisons suggest that the measured triboemission of actually emitted charged-particles (i.e., with the use of grid) is different than the total production of charges (i.e., including some electrostatic charges in the non-grid configuration). However, only actually emitted particles, which are measured with the grid-setup, would have the kinetic energy that is of interest in this research. Therefore, the use of such retarding-grid was mandatory to perform the measurements of triboemission which follow in this chapter.

The effect of setting a negative retarding-grid voltage (i.e., different than zero) is shown in Figure 4.7. This experiment was carried for all the same material, operating and data acquisition conditions of the experiment reported in Figure 4.5, but for the use of -100V grid voltage.

The comparison of outputs shows that, for negative grid (i.e., for -100Volt grid), both the average count and the highest bursts of measured triboemission are smaller by about one order of magnitude than the pertaining measurements at the zero-volt grid. This comparison indicates that a large fraction of the negatively-charged particles triboemitted from diamond-on-alumina may be comprised of the zero to 100eVolt energy-range. A detailed study of the energy spectrum for this case of triboemission is presented in section 4.4.

The influence of sliding speed on triboemission from diamond-on-alumina was briefly investigated. Figure 4.8 shows, for a test of continuously increasing sliding speed, the negatively-charged triboemission as accumulated counts versus time, and versus sliding speed.

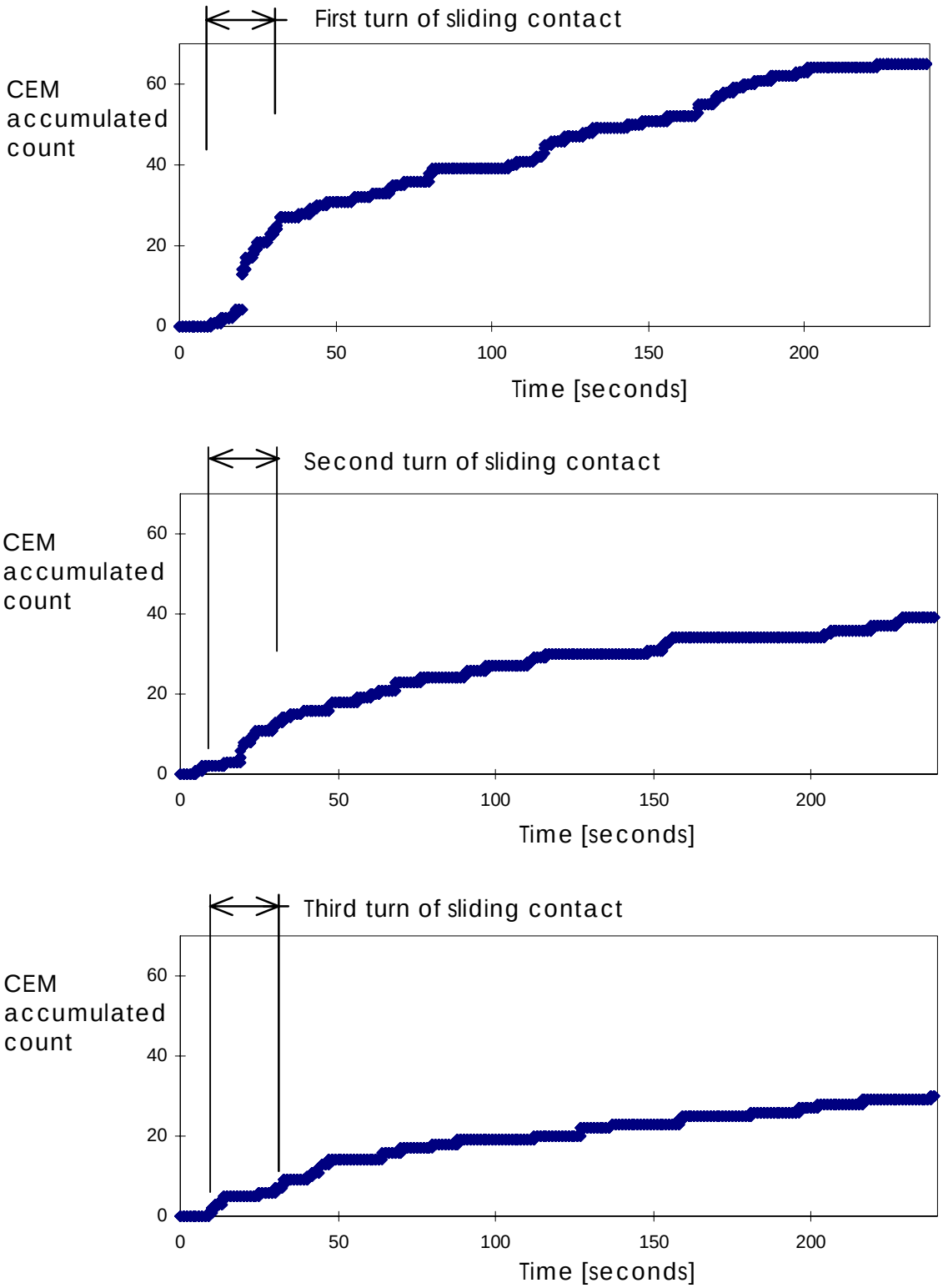

Figure 4.7. Accumulated negatively-charged triboemission from diamond-on-alumina. CEM accumulated output (in the 0.1 second data-acquisition window) vs. time. Grid : -100 Volts. Cathode:+1,200V. Load: 2N . Speed: 0.12 cm/s. Pressure:1.5×10^{-8} Torr.

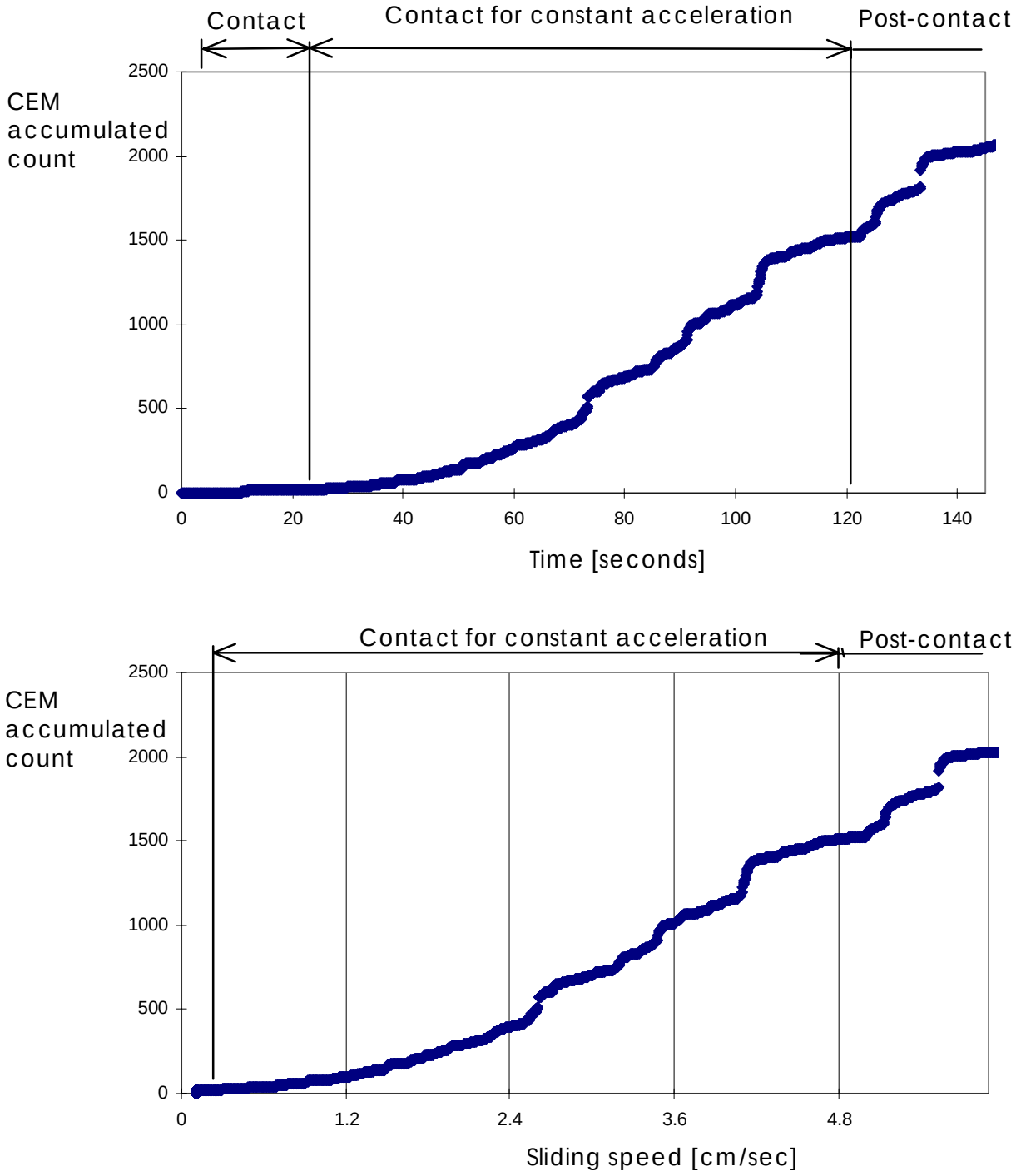

Figure 4.8. Accumulated negatively-charged triboemission from diamond-on-alumina.

CEM accumulated output vs. time and sliding speed.

Grid: 0Volt (grounded). Cathode: +1,200V. Load: 2N.

Acceleration (for sliding speed): 0.048 cm/sec^2. Pressure:1.5x10^{-8} Torr.

In this test, a constant sliding-contact acceleration of 0.048 cm/sec^2 was applied in a 100sec-period of contact. Speed was increased between the 20th and the 120th seconds, from the initial speed of 0.12cm/sec to the final of 4.8cm/sec. After that, contact ceased and post-contact data was recorded for additional 25 seconds. Applied load was 2N.

For the measurement of Figure 4.8, the data-acquisition window used was 100 mseconds. Background-noise data was previously recorded and its average computed as 0.075 counts/second for a cathode voltage of +1,200V. The increasing slope of the curve during contact and increasing speed, suggests that higher sliding speed may increase triboemission of negatively-charged particles from diamond-on-alumina sliding-contacts.

Another experiment was carried for all the same material system, operating and data-acquisition conditions of the above, but for the application of a 10N-load. Figure 4.9 shows, for this experiment at increasing sliding speed, the negatively-charged triboemission as accumulated counts versus time, and versus sliding speed.

The average triboemission in Figure 4.9 for 10N-load is, in general, higher than that for 2N-load. This result would suggest that higher contact load would increase the triboemission of negatively-charged particles from diamond-on-alumina sliding-contacts. The slope of the curve, however, is not increasing for the whole range of tested speeds when 10N-load is applied.

It is possible that complex time-dependence of triboemission shows apparent when this high load is used: The simultaneous and likely interacting effects of load, speed and time, all of which determine wear and surface damage, also affect triboemission intensity. These experimental complexities prevent any general conclusion from this limited experiment. Section 5.1 discusses the reasons a thorough investigation on the effects of these factors (e.g., load, speed, time) was not undertaken in this dissertation research.

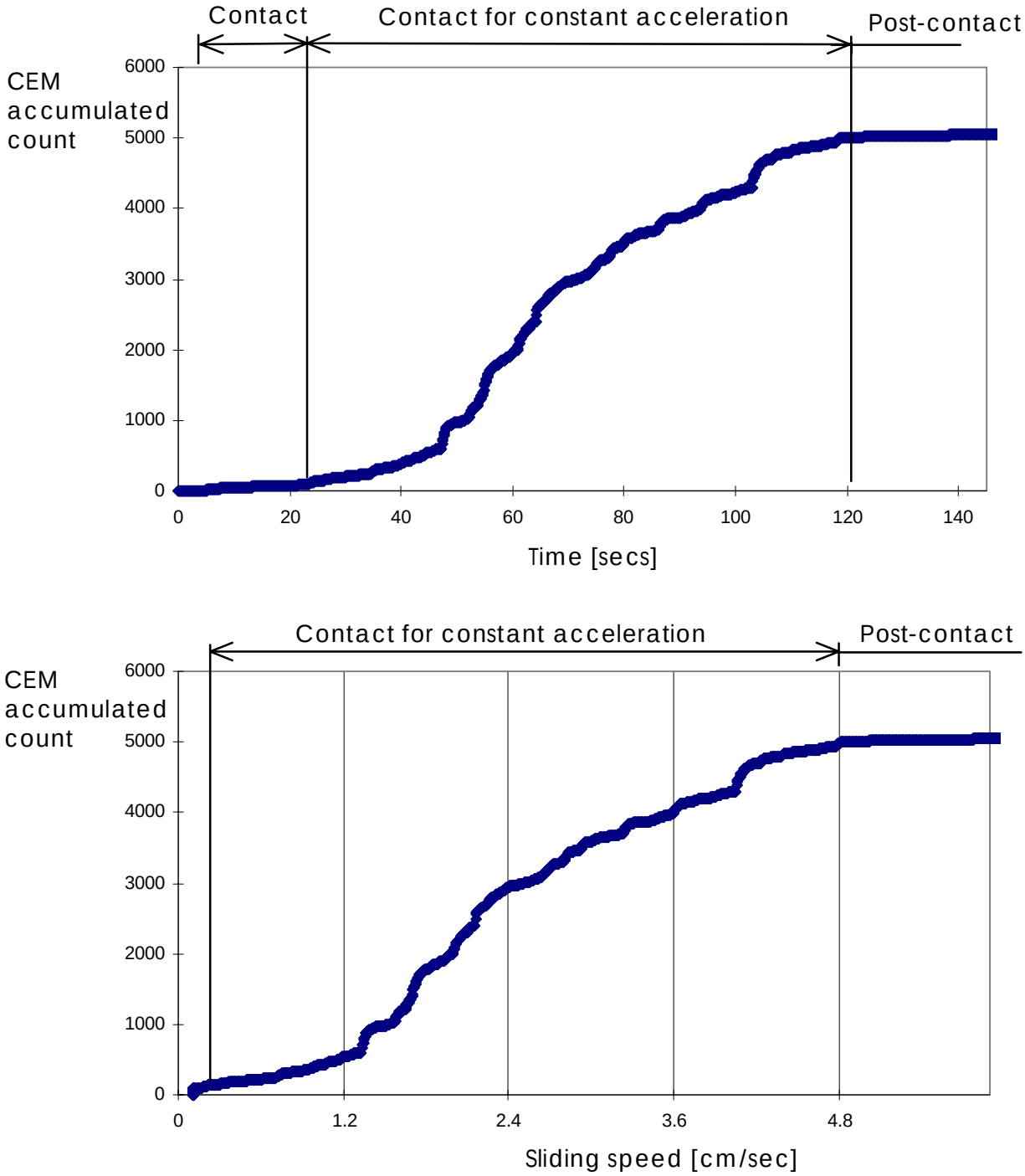

Figure 4.9. Accumulated negatively-charged triboemission from diamond-on-alumina.

CEM accumulated output vs. time and sliding speed.

Grid: 0 Volt (ground). Cathode: +1200V. Load: 10N.

Acceleration (for sliding speed): 0.048 cm/sec^2. Pressure: 1.5x10^{-8} Torr

The preliminary experiments described in this section show that negatively-charged triboemission from diamond-on-alumina is essentially a burst-type intermittent phenomenon. The occurrence of such triboemission bursts was found neither related nor coincident to any change of external or measured variable, but seems to be of random occurrence during contact.

Decaying negatively-charged emission, though of lower level, was also observed after contact ceased. These preliminary experiments helped provide an understanding of basic triboemission features, which was needed for the further measurement development presented in the following section.

4.3. Measurements of charged-particle triboemission from diamond-on-alumina, diamond-on-sapphire, and diamond-on-aluminum sliding contacts.

This section presents and compares measurements of charged-particle triboemission from sliding contacts of diamond on two related ceramics, alumina and sapphire, and from diamond on the related metallic material, e.g., aluminum. Section 3.2.1 reported specifications for the employed materials. A grounded grid was placed between the emitting surfaces and the CEM input to stop particles other than those effectively emitted from reaching the particle-detector, as explained in sections 3.1.5 and 4.2. Detailed information for the load, sliding speed, and contact schedule for the experiments presented in this section is given in Appendix D.

For grounded grid (i.e., for zero-Volt with respect to frame reference) and cathode voltage +1,200V (for negatively-charged particles), the following contact schedule was employed: the measurement started with a 20-second non-contact period, followed by a period of diamond-on-ceramic sliding contact of typically 320second-length. Contact ceased after that period, and data were recorded for total time of typically eight minutes. Applied load was 2N and employed sliding speed was 0.48cm/second. The data-acquisition window employed was 10mseconds. Background-noise in each test was computed as the average emission in the initial 20second non-contact period, being lower than 1 count/second for all tests.

Figures 4.10 and 4.11 show examples of measurements, in the 10msec-window, of negatively-charged triboemission versus time from the sliding contacts of diamond on two different alumina specimens. For the same operating and data acquisition conditions, figures 4.12 and 4.13 show two different measurements of negatively-charged triboemission from sliding contact of diamond on two different sapphire specimens. Negatively-charged triboemission from diamond-on-ceramics is burst-type clearly associated with sliding contact.

Comparison of figures 4.10 to 4.13 suggests that the different crystal structures (i.e., of alumina and sapphire) are not a significant factor in these triboemission measurements. A study of the statistical significance of these results is presented in Appendix C. This study shows that no statistically significant difference was found for the triboemission outputs during the contact of diamond-on-alumina vs. that of diamond-on-sapphire.

Under these conditions of sliding speed and load, the largest bursts of triboemission appear in the first minutes of contact, and the average emission level decreases within the first minutes of sliding. In general, a large spike in the triboemission signal is followed by a sequence of close smaller bursts, the composed signal envelope seems continuous. Figure 4.14 shows a detail of a large burst of triboemission for the diamond-on-sapphire test of Figure 4.13. Triboemission bursts show a characteristic decay-time, which was estimated to be about 100ms per burst.

Maximum levels for the observed largest bursts of diamond-on-ceramic triboemission may differ by two orders of magnitude between different disk-specimens of the same material. The two examples presented for each material-contact pair represent two different types of observed outputs: one type of output features a constant low level of small-burst triboemission, although clearly above background, while the other has some dominant higher-level bursts of triboemission superimposed on the constant lower emission. For the purposes of analysis and discussion in following Chapter 5, the former is called “constant-level” type of triboemission output, while the latter is called the “large-burst” type.

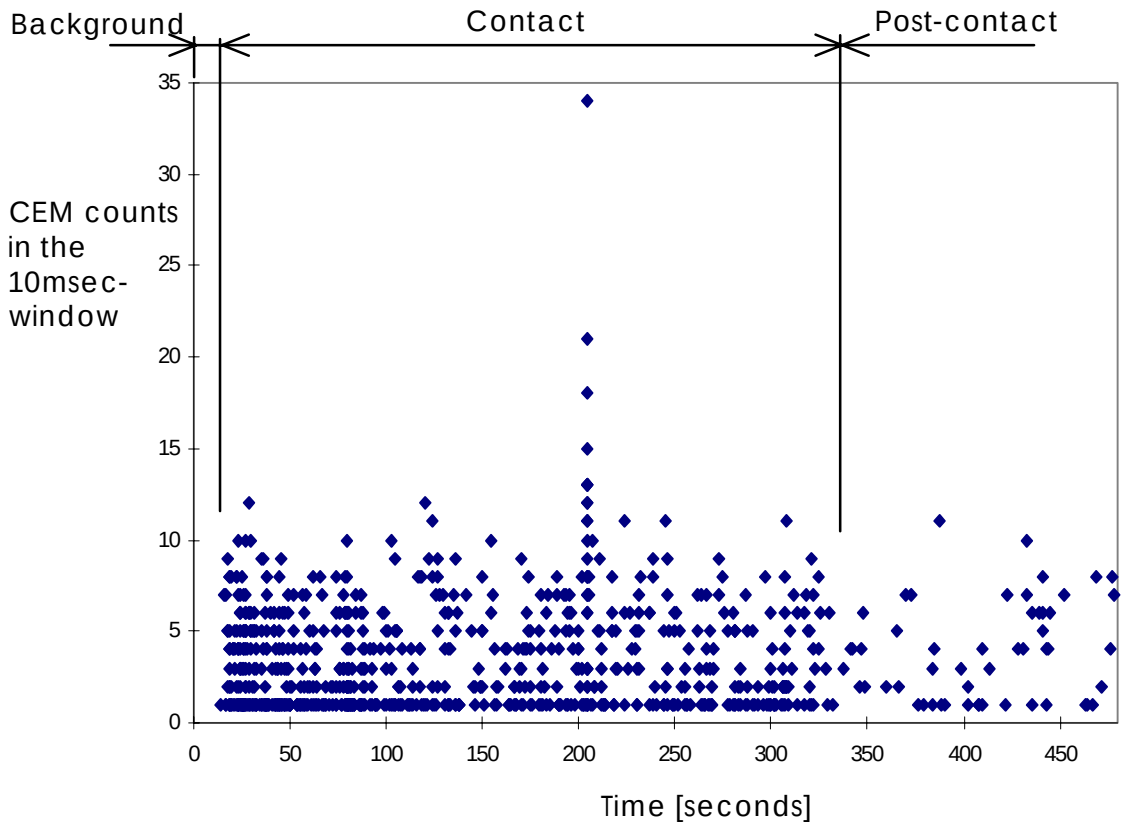

Figure 4.10. “Constant-level” negatively-charged triboemission for diamond-on-alumina sliding contact. CEM output versus time

Grid: 0Volt (ground). Cathode: +1,200V. Load: 2N. Sliding speed: 0.48cm/s.

Pressure: 1.5 x 10^{-8} Torr

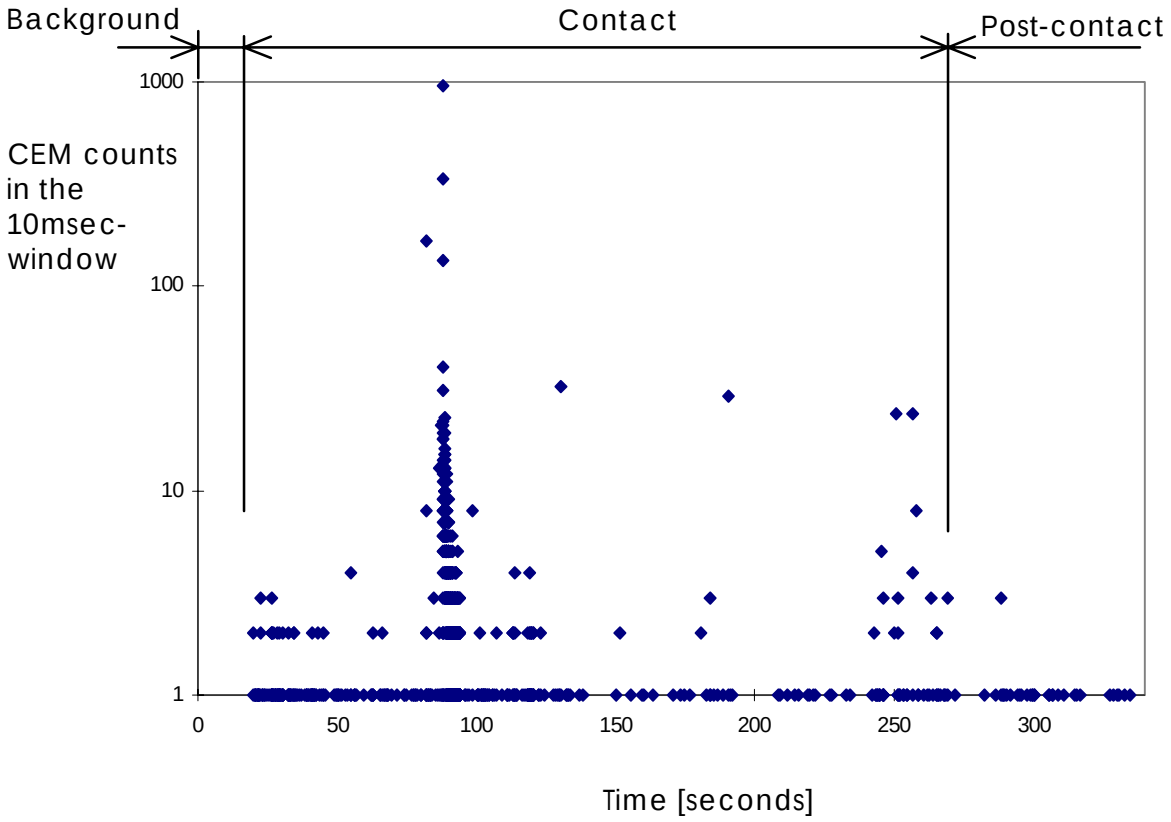

Figure 4.11. “Large-burst” negatively-charged triboemission from diamond-on-alumina sliding contact. CEM output versus time output.
Grid: 0Volt (ground). Cathode: +1,200V. Load: 2N. Sliding speed: 0.48cm/s .
Pressure: 1.5 x 10^{-8} Torr

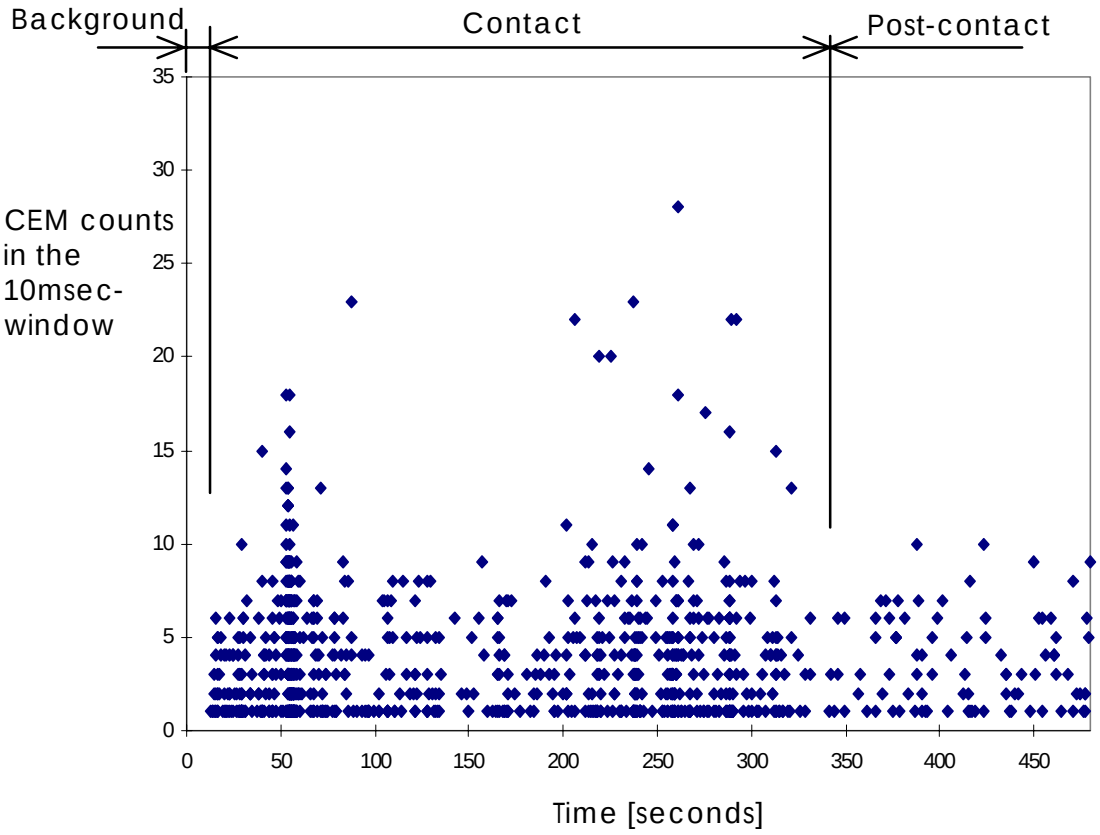

Figure 4.12. “Constant-level” negatively-charged triboemission for diamond-on-sapphire sliding contact. CEM output versus time.

Grid: 0Volt (ground). Cathode: +1,200V. Load: 2N. Sliding speed: 0.48cm/s .

Pressure: 1.5 x 10^{-8} Torr

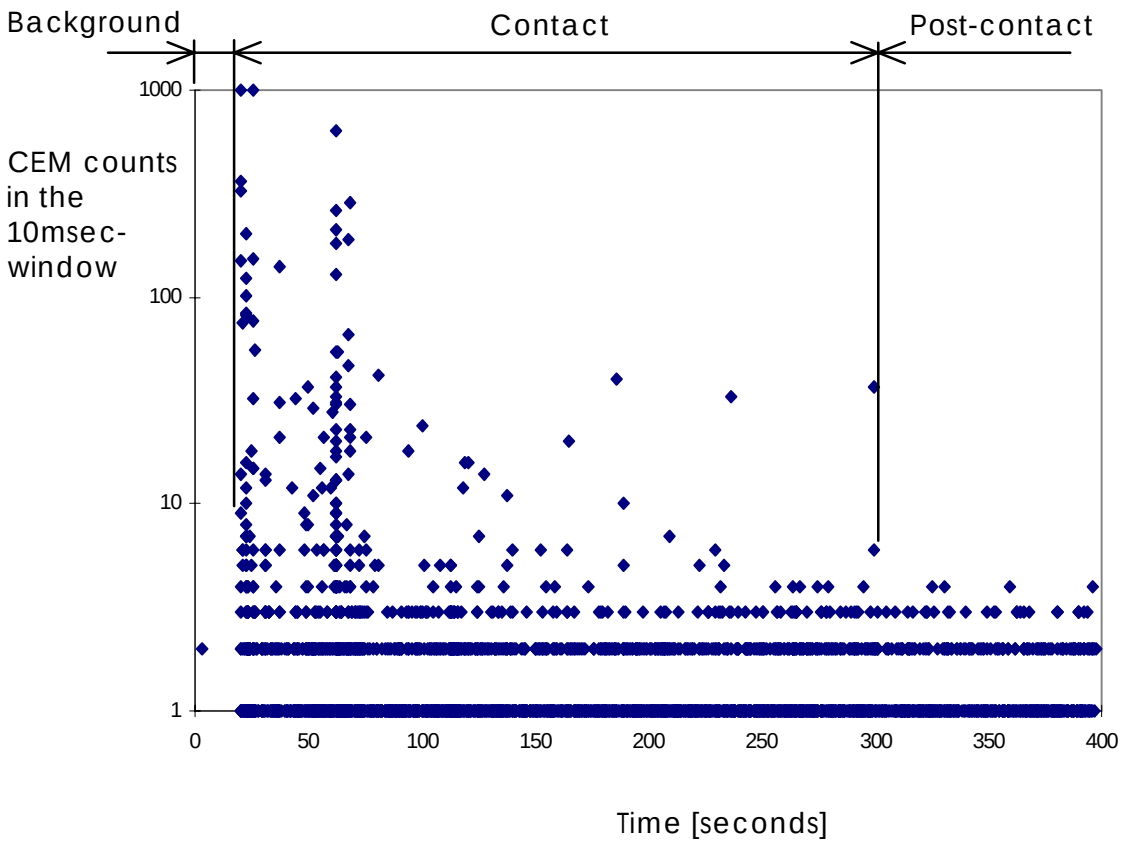

Figure 4.13. “Large-burst” negatively-charged triboemission for diamond-on-sapphire sliding contact. CEM output versus time.
Grid: 0Volt (ground). Cathode: +1,200V. Load: 2N. Sliding speed: 0.48cm/s .
Pressure: 1.5 x 10^{-8} Torr

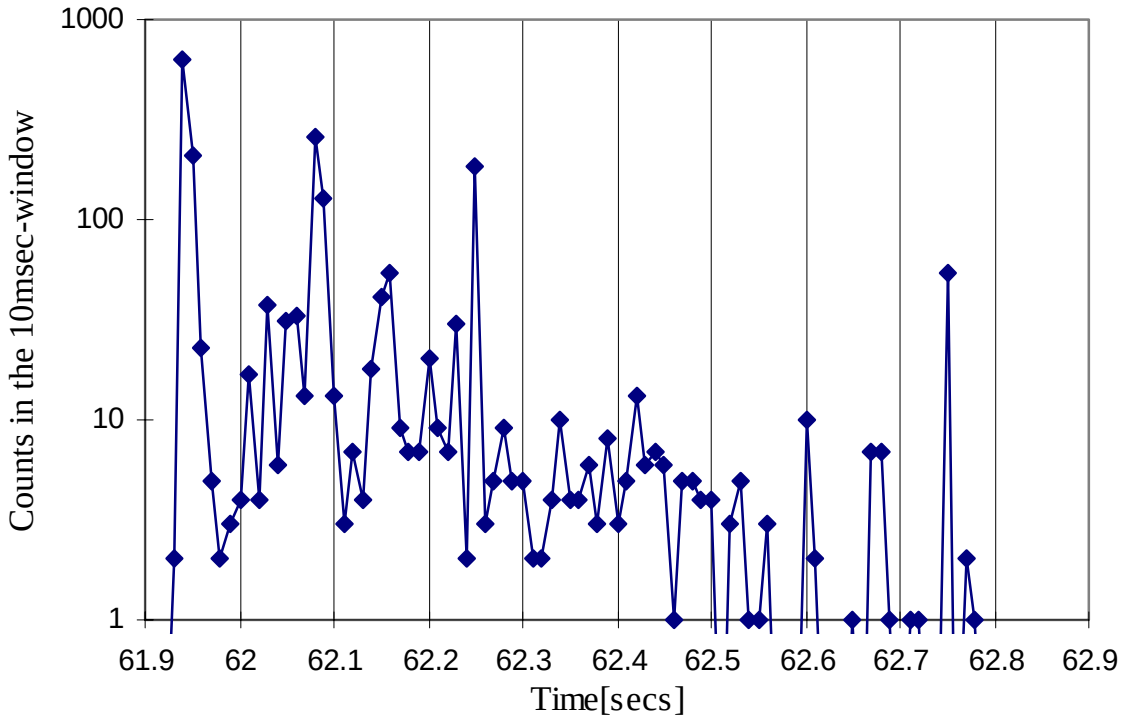

Figure 4.14. Large burst of triboemission for diamond-on-sapphire test of Figure 4.13.

No operation, material, or surface feature variable was identified that could relate to such differences in triboemission outputs. As discussed in Chapter 5, Dickinson et al. [95] suggested they may be related to stick-slip in the plowing or sliding process. However, the low speed employed for the is not compatible with stick-slip regimes. Post-contact decaying emission of low level, although higher than background-noise, is also observed after contact ceased. Table 4.1, at the end of this section, summarizes the average of measured negatively-charged triboemission for these experiments.

Figure 4.15 shows a measurement in the 10msec-window of the negatively-charged triboemission versus time from a diamond-on-aluminum sliding contact. Negatively-charged emission from aluminum is very low when compared to that from diamond-on-alumina and diamond-on-sapphire for the same sliding conditions. Only small sporadic bursts (of about 7 counts in the 10msec window) rose above the lower background-noise in the first minute of contact. No post-contact emission was observed from this material system.

In this experiment of Figure 4.15, the wear track and aluminum debris revealed that the contact proceeded as a cutting process of the aluminum by the diamond, different from the plowing and sliding for diamond-on-ceramics. Such observations were carried out by an optical macroscope. These results suggest the weaker emission from aluminum is not related to the scratching of the metal substrate, but rather that it originates from wear of a thin surface oxide-layer. Therefore, triboemission from diamond-on-aluminum would be a marginal case of those for diamond scratching on aluminum-oxides (e.g., of diamond-on-alumina and diamond-on-sapphire).

Positively-charged emission from diamond-on-alumina, diamond-on-sapphire and diamond-on-aluminum contacts also was investigated. For grounded grid (i.e., zero-Volt with respect to reference) and cathode voltage -1,500V, the same contact schedule and data-acquisition parameters were employed as those for negative-charge measurements.

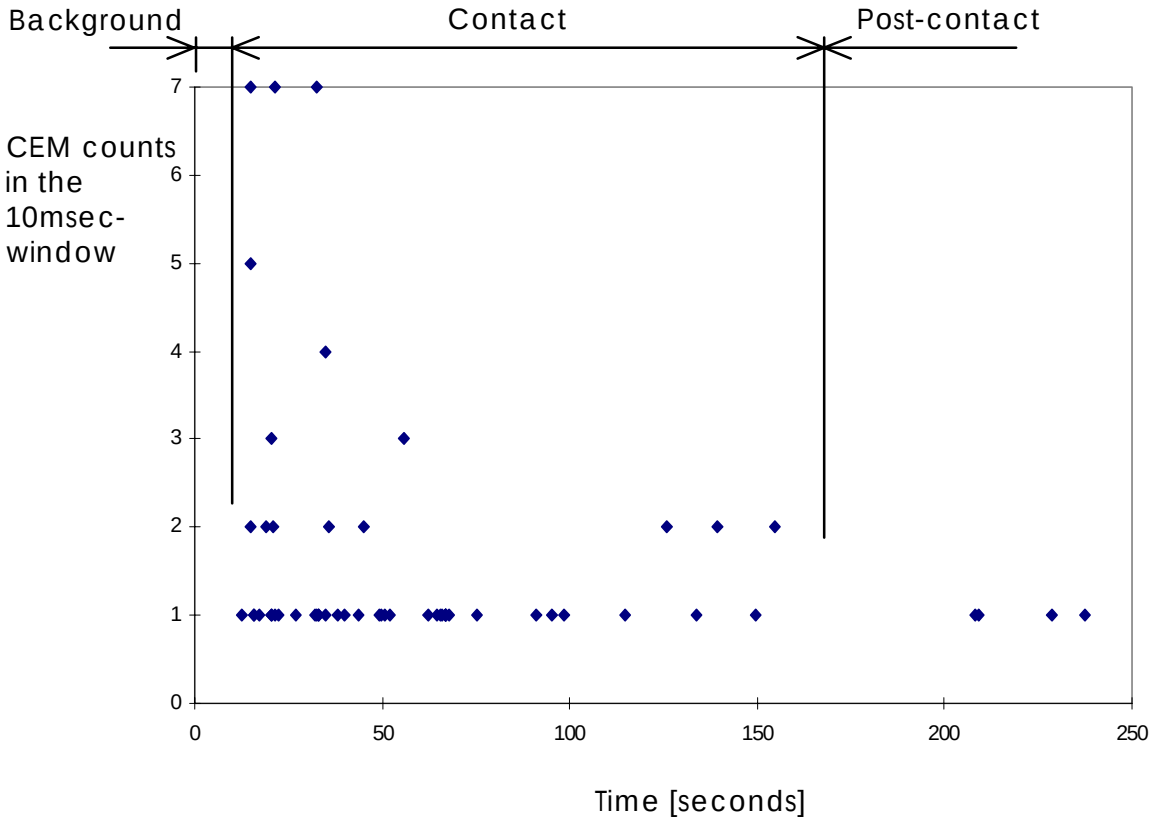

Figure 4.15. Negatively-charged triboemission from diamond-on-aluminum.
CEM output versus time.
Grid: 0Volt (ground). Cathode: +1,200V. Load: 2N. Sliding speed: 0.48cm/s.
Pressure: 1.5 x 10^{-8} Torr.

Figure 4.16 shows a measurement of positively-charged triboemission from diamond-on-alumina. In this case only, applied load was 10N and the sliding speed was 0.96cm/s. Figure 4.17 shows a measurement of positively-charged triboemission from a diamond-on-sapphire sliding contact. Applied load was 2N and the sliding speed was 0.48cm/s. Table 4.1 summarizes the results for negatively-charged and positively-charged triboemission from diamond on ceramics (and from diamond on aluminum).

Table 4.1. Measured average triboemission rates from diamond-on-ceramics.
(For two specimens per each material system).

Sliding-contact material system	Average triboemission rates during contact (in counts/sec)			
	Negative-charge			Positive-charge
	(*)	(**)	(***)	(*)
Diamond-on-alumina	8.5 to 13	61	2,307	~ 0.5
Diamond-on-sapphire	11 to 36	140	4,196	~ 0.4
Diamond-on-aluminum	< 0.4	1.25	14	None

(*) Triboemission rate during 320 sec contact tests.

(**) Maximum triboemission rate for one minute around largest burst of emission.

(***) Maximum triboemission rate for one second around largest burst of emission.

Figures 4.16 and 4.17 show that low positively-charged triboemission, although above background-noise, is observed from diamond-on-alumina and diamond-on-sapphire sliding contacts. Relatively higher contact loads and/or sliding speeds were needed to measure this positively-charged triboemission.

It is possible that this positive-ion emission did not originate from the contacting surfaces, but was produced by triboemitted electrons interacting with gas molecules immediately above the wear track. No positively-charged triboemission was observed from diamond-on-aluminum.

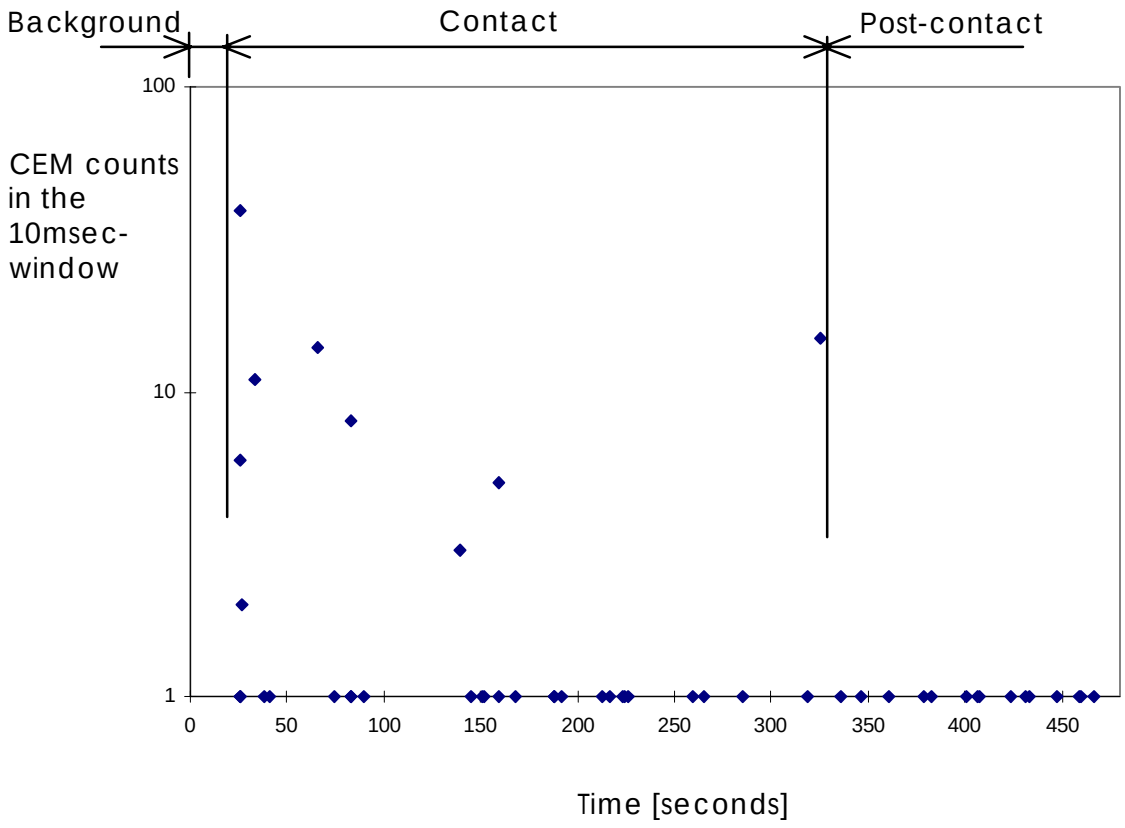

Figure 4.16. Positively-charged triboemission from diamond-on-alumina.
CEM output versus time.
Grid: 0Volt (ground). Cathode: -1,500V. Load: 10N. Sliding speed: 0.96cm/s.
Pressure: 1.5 x 10^{-8} Torr.

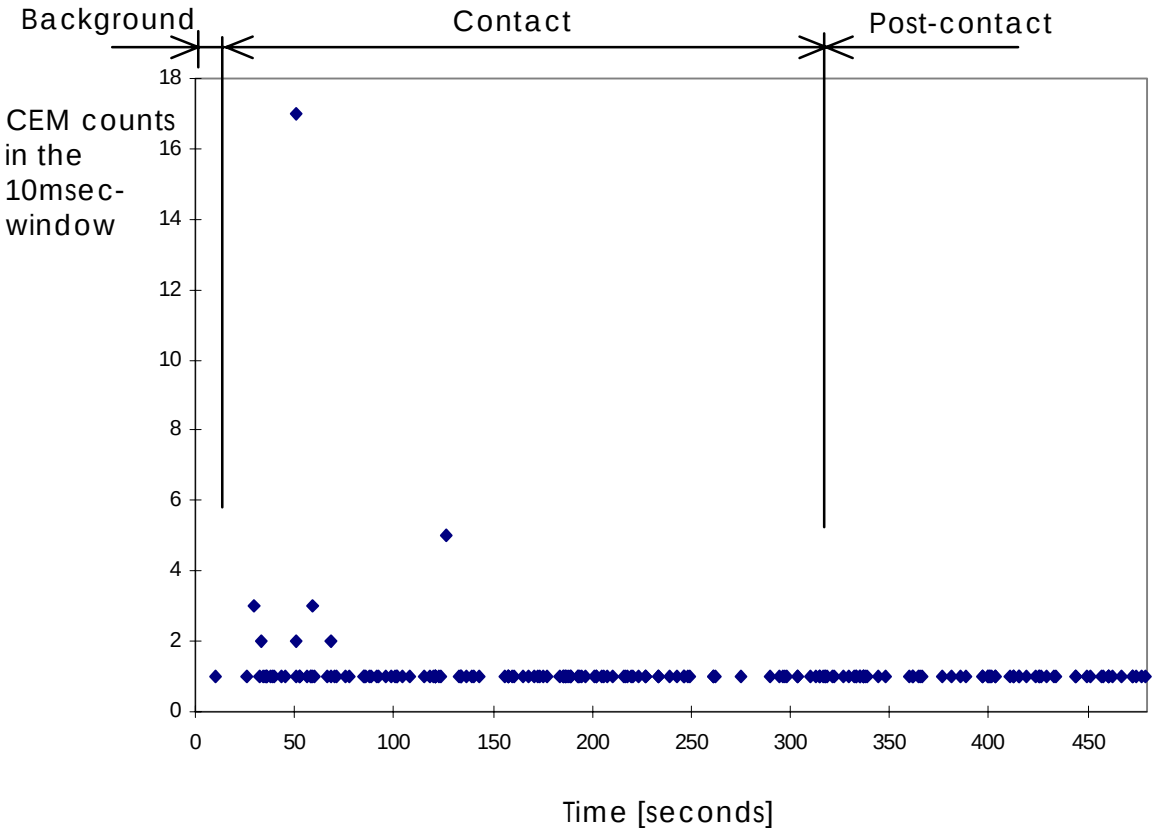

Figure 4.17. Positively-charged triboemission for diamond-on-sapphire.
CEM output versus time.
Grid: 0Volt (ground). Cathode: -1,500V. Load: 2N. Sliding speed: 0.48cm/s.
Pressure: 1 x 10^{-8} Torr

A study on the statistical significance of the results in this section (e.g., of the statistical significance of triboemission outputs during contact vs. CEM count during non contact for the material systems investigated) is presented in Appendix C. This study shows that average negatively-charged triboemission during contact was significantly above background noise for the diamond-on-alumina, diamond-on-sapphire and diamond-on-aluminum systems.

However, this study in Appendix C found no statistical difference for the average positively-charged triboemission during contact (i.e., vs. background noise during non-contact) for these three material systems investigated. It is possible that samples larger than the ones employed are needed to show statistical significance in these cases.

The experimental results presented in this section suggest that triboemission is mainly an electron-emission phenomenon. Negatively-charged triboemission from diamond-on-ceramics is constituted by a constant emission of low-level small-bursts, although higher than background, with eventually superimposed higher-level bursts of emission. In this, levels of the largest triboemission-spikes may differ by two orders of magnitude between different specimens of the same material system. Constant low-level triboemission, however, may not be different between ceramic specimens.

Occurrence of triboemission bursts seems to be random, and their magnitude to diminish in time. Decaying negatively-charged triboemission from ceramics occurs after the contact ceased. Although both weak negatively-charged emission from aluminum and weak positively-charged emission from ceramics are observed, they would be just marginal effects of the dominant electron-triboemission phenomena. Results in this section are discussed in Chapter 5. Section 5.2 proposes a description of the random-burst triboemission outputs in the frequency domain of representation.

4.4. Retarded-energy measurements of triboemission from diamond-on-alumina and diamond-on-sapphire sliding contacts.

As described in section 4.2, the triboemission instrument features a retarding-grid, which can be biased by a controlled voltage, between the emitting surfaces and the CEM detector. This allows one to perform energy spectroscopy measurements by the method of retarding potentials.

In the method of retarding potentials, biasing the grid by a defined voltage allows screening of particles according to their kinetic energy: any particle of energy equal or lower than (and of the same polarity of) the set potential is screened out from reaching the CEM detector. By this method the retarded-energy spectra can be measured of the triboemission from different material-contact systems. Grid potential-values, in Volts, can be translated to minimum energy of the single-charge particle, in eVolts (i.e., the energy of an electron overcoming a -1V grid is equal or higher than 1 eVolt).

To resolve the fast burst-type changes in the triboemission output, the retarding-grid voltage was swept about the energy range of interest. Grid-voltage sweeping was synchronized with data acquisition. Stepwise sawtooth grid-voltage waveforms were employed (See subsection 3.1.6 and Figure 3.10). Such bias-waveforms were constituted of same-length voltage steps for discrete integer voltage-values. The sweeping-rate employed was 1.25 mseconds per voltage-step. This voltage step-length was well below the characteristic decay-time of the triboemission signal bursts. The triboemission count-rate can be computed for each of these discrete voltage-steps to obtain an energy integrated distribution of the triboemitted charged-particles.

An uneven sequence of discrete negative-voltage biases (e.g., zero, -1, -2, -3, -4, -8, -12, -16, -32 and -48 Volts) was investigated, which enhanced the measurement resolution in the lower-voltage end of the bias range. Each of these bias-values screens out particles of energy equal or lower than the set potentials. Because of software requirements and to manage the storage of large amounts of data, the above grid-voltage sequence was run as three different sub-sequences as follows: [0, -1, -2, -3] Volts, [0, -4, -8, -12] Volts, and [0, -16, -32, -48] Volts.

Only one of these sub-sequences was swept in each of the repeated measurements from each ceramic sample, according to schedules presented in this section and Appendix B. The zero-bias as reference in these three sub-sequences allowed their combination in a single retarded-energy spectrum for each material system tested.

Repeated measurements were obtained from each of a number of replicated samples, as described in this section and Appendix B. For this exploratory study, the assumption was made that the retarded energy spectra were not affected by load and speed in the ranges employed. Because triboemission was observed to decrease as sliding occurred under the same load and speed (See section 4.3), both applied load and speed were increased as repeated measurements were taken from the same ceramic sample. Those increases roughly kept triboemission at high-enough levels for the intended measurements.

Low to medium load and low sliding speed about the ranges employed in section 4.3 (e.g., 2N to 40N and 0.15 cm/second to 0.96cm/second) were applied for the measurements. Appendix B shows examples of the employed schedules to apply for the repeated measurements the different load and speed values, and the grid-bias sub-sequences.

The retarded-energy spectra were measured of negatively-charged triboemission from diamond-on-alumina and diamond-on-sapphire. The specimen sample-sizes were six and three respectively for these two material systems.

A database was acquired for each material-system as follows: Repeated 40second-records were obtained for each ceramic specimen. The first 20 seconds in each record were of reference background-noise, and the following 20 seconds corresponded to triboemission data for the pertaining sub-sequence of grid-bias, as per the schedules of Appendix B. Twelve such repeated measurements were acquired from each diamond-on-alumina sample, and 36 repeated measurements were acquired from each diamond-on-sapphire sample.

Once the database for the energy-range of interest was acquired, the average and standard deviation of the triboemission-rate were computed (considering both specimen replication and repeated measurements) for each voltage level. This average triboemission-rate for each voltage level constitutes an estimation of the fraction of particles triboemitted with energy higher than the grid setting, the total triboemission being given by the average rate for zero-Volt grid. The average triboemission rates for the investigated grid-bias in the range of zero to -48Volts were plotted as a single retarded-energy spectrum for each material system tested.

Figures 4.18 and 4.19 show these measures of the retarding-energy spectra for negatively-charged triboemission from diamond-on-alumina and diamond-on-sapphire respectively. As previously explained, the abscissas can be alternatively read in units of negative grid voltage (e.g., in Volts) or particle minimum-energy (e.g., in eVolts). Appendix B includes a summary of numerical data from these results.

Both spectra show decaying rates of negatively-charged triboemission for greater minimum energy of the triboemitted particles. In particular, these energy distributions suggest that important fractions of negatively-charged particles are triboemitted in the zero to about 5eV energy-range, with a decaying tail extending beyond the highest retarding potential, i.e., -48 Volts, employed for the measurement. The importance of this information will be discussed in Chapter 5.

It is possible that particle triboemission in the zero to about 5eV energy-range may be enhanced by some secondary-electron emission from interactions of higher-energy particles in the region surrounding the wear track. However, the measurements carried out in this research are not able to sort out these secondary electrons - if they are present - from the low-energy triboemitted electrons. Higher-energy emission may result from patches of electrostatic charge on the surface, as suggested by Dickinson et al. [96]. The overall effect of triboemission and these added interactions is shown in the measured retarding-energy spectra. These retarded-energy distributions for triboemitted electrons are discussed in Chapter 5 with a focus on the role of such particles in tribochemical reactions.

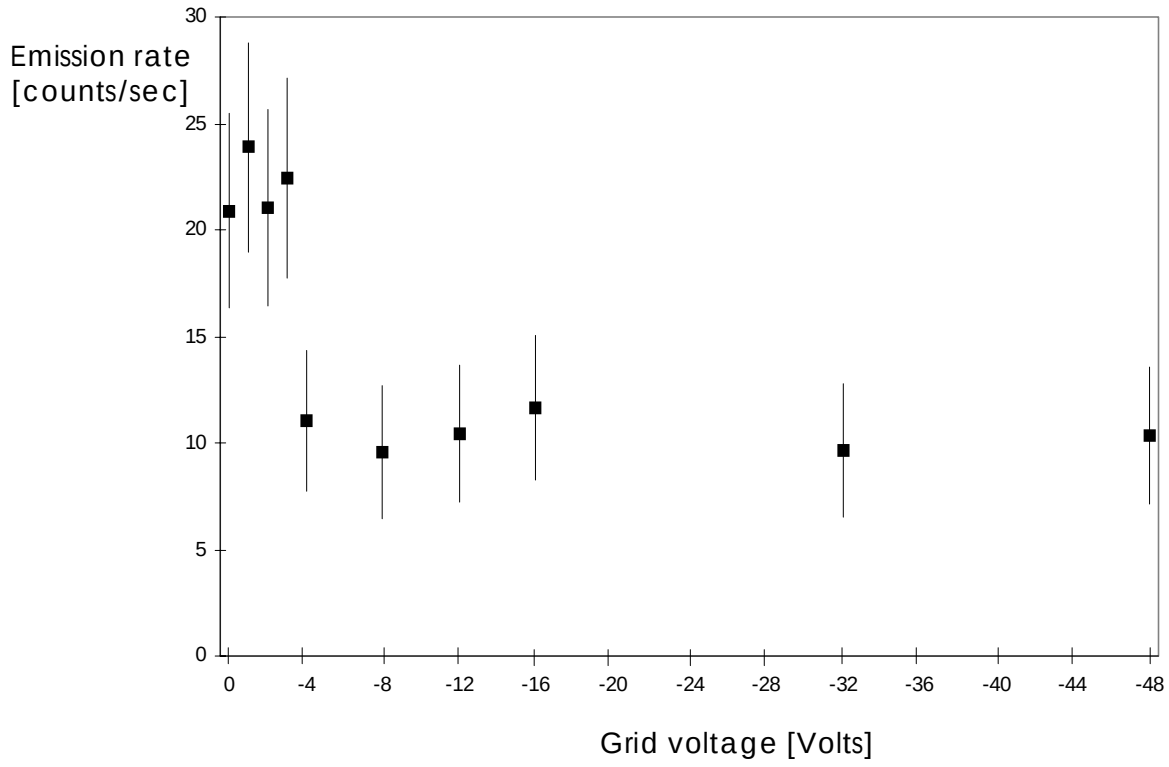

Figure 4.18. Retarded-energy spectrum for negatively-charged triboemission from diamond-on-alumina sliding contacts.
Average and ± standard deviation of rate of emission versus grid voltage.

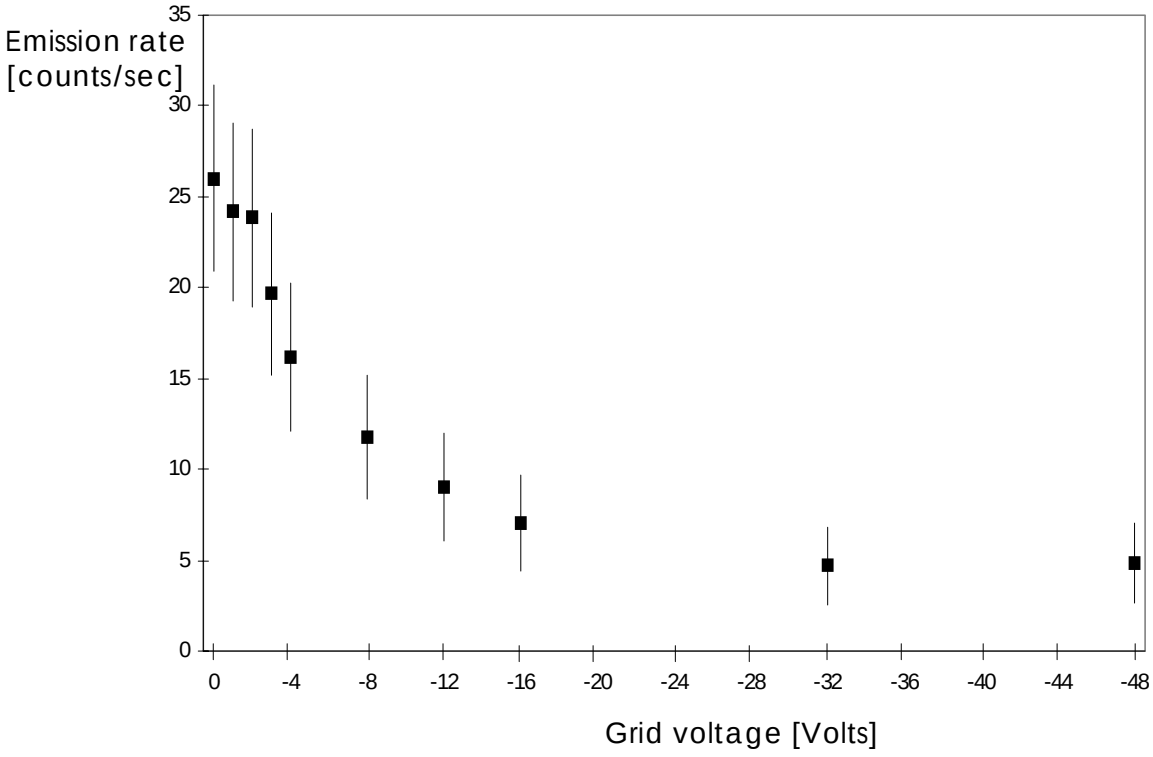

Figure 4.19. Retarded-energy spectrum for negatively-charged triboemission from diamond-on-sapphire sliding contacts.
Average and ± standard deviation of rate of emission versus grid voltage.

Measurement of energy-spectra by the new triboemission instrument constitutes an important part of the research work in this dissertation. Energy spectra of the positively-charged triboemission from diamond-on-alumina and diamond-on-sapphire were not measured, because of the low-level positive-ion emission from these sliding pairs (see section 4.3). Likewise, energy spectra for the low triboemission from diamond-on-aluminum were not determined.

It is thought, however, that weak positive-ion triboemission from ceramics results from ionization of gas species by the dominant triboemitted electrons. On this assumption, positive-ion energy spectrum would be of marginal interest to the purpose of this research. The weak negatively-charged triboemission from diamond-on-aluminum would be just an example of emission from the surface aluminum-oxide layer, and its energy-distribution would be of little interest in this research.

4.5. Measurements of charged-particle triboemission from alumina-on-alumina sliding contacts.

This section presents measurements of charged-particles triboemitted from the sliding contact of an alumina ball on a rotating alumina disk. The contact geometry was shown in figure 3.12, and the employed materials were described in subsection 3.2.1. These measurements are compared to those for diamond-on-ceramics, i.e., for diamond-on-alumina and diamond-on-sapphire, which were presented in section 4.3.

For these measurements of triboemission from ceramic-on-ceramic, detection and data acquisition setups were the same as used for diamond-on-ceramics: a grounded grid (i.e., for zero-Volt with respect to frame reference) was placed between the emitting surfaces and the CEM (see subsection 3.1.4). Detailed information for the load, sliding speed, and contact schedule for the experiments presented in this section is given in Appendix D.

Figure 4.20 presents a typical CEM measurement of negatively-charged particles from alumina-on-alumina, for +1,200V cathode voltage.

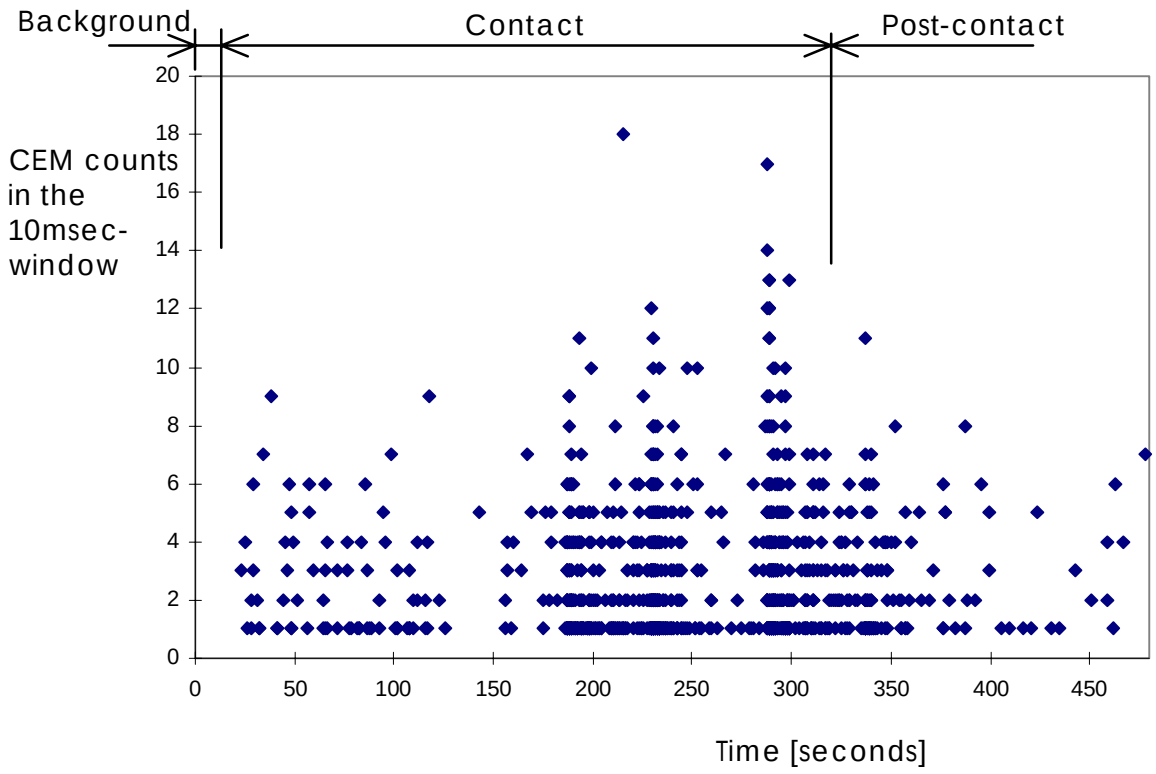

Figure 4.20. Negatively-charged triboemission for “first-minutes” of alumina-on-alumina sliding contact. CEM output versus time.

Grid: 0Volt (ground). Cathode: +1,200V. Load: 2N. Sliding speed: 0.48cm/s .

Pressure: 1.5 x 10^{-8} Torr

The following contact schedule was employed for Figure 4.20: the measurement started with a 20-second non-contact period, followed by a period of alumina-on-alumina sliding contact of 320second. Contact ceased after that period, and data were recorded for total time of eight minutes. The applied load was 2N and the sliding speed was 0.14cm/second. The data-acquisition window was 10mseconds. Background-noise was computed as the average emission for the initial 20second non-contact period, being lower than 1 count/second .

The measured negatively-charged triboemission from alumina-on-alumina is burst-type clearly associated with sliding contact. Post-contact emission also was observed at levels lower than that of contact, although higher than that of background-noise. There is an important difference, however, with respect to similar measurements in diamond-on-ceramics: the largest bursts of triboemission do not show at the beginning of contact, nor in the first minute of sliding, at least for the speed and load used: Such large peak occurred when the same load and speed schedule was repeated for the ball and disk specimens (i.e., when contact was resumed on the same wear track). For the purpose of resuming high-vacuum level needed for measurement, a 4 minute-intermission was scheduled between these two measurements.

Figure 4.21 shows the effect of resuming sliding contact on the same wear track after the test of Figure 4.20: triboemission of negatively-charged particles reached larger emission bursts and higher average emission rate than those for the initial run. Therefore, the highest level of emission was observed only after 5 minutes of sliding contact on the same alumina-on-alumina system. These results suggest a different time dependence from that for diamond-on-alumina, at least for the occurrence of the largest peaks.

Figures 4.20 and 4.21 show that average triboemission levels as high as 20 counts/sec (for average emission rate) can be sustained for as long as 5 minutes from these alumina-on-alumina systems. These results suggest that alumina-on-alumina contacts can produce negatively-charged triboemission at levels similar to those from of diamond-on-ceramics, but for longer periods of time. The following test showed that levels of triboemission may be, however, much higher.

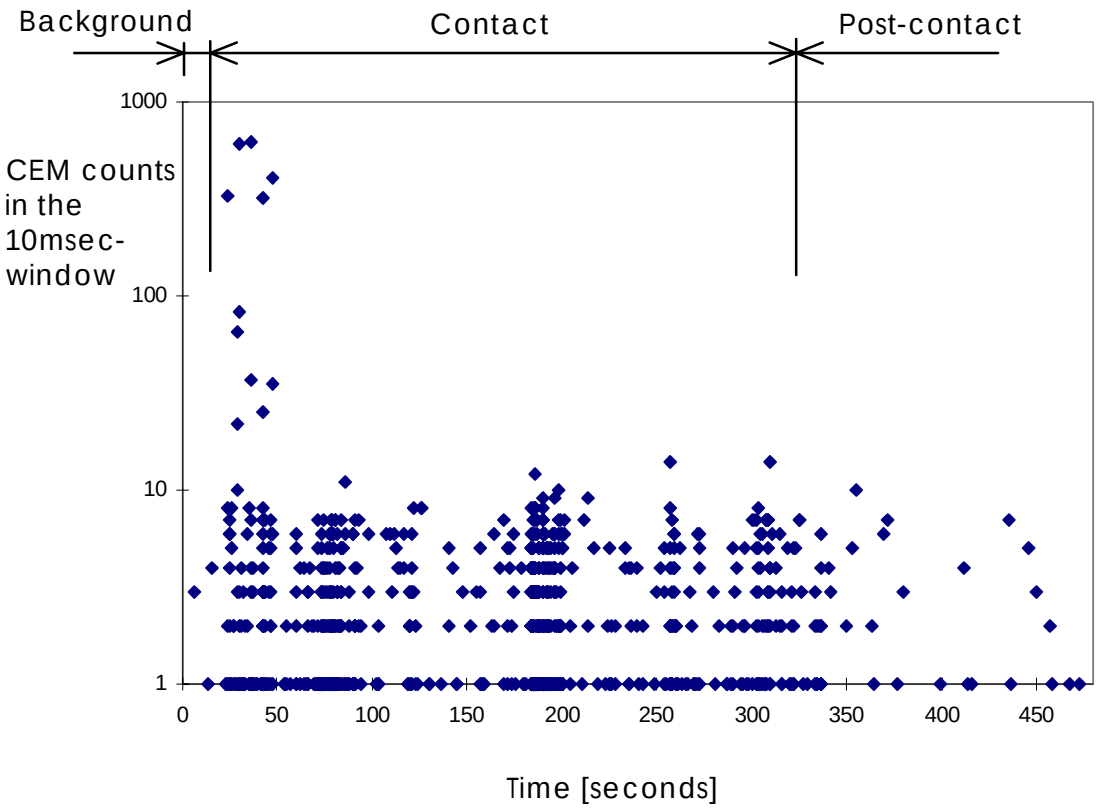

Figure 4.21. Negatively-charged triboemission for “second run on same wear track” of alumina-on-alumina sliding contact. CEM output versus time.
Grid: 0Volt (ground). Cathode: +1,200V. Load: 2N. Sliding speed: 0.48cm/s .
Pressure: 1 x 10^{-8} Torr

Figure 4.22 shows two consecutive measurements of negatively-charged triboemission from the same alumina-on-alumina wear track. The following contact schedule was employed: the measurement started with a 20-second non-contact period, followed by a 45 second-period of sliding contact. After contact ceased, data were recorded for 95 seconds. A second measurement for the same schedule was taken from the alumina-on-alumina contact pair, with a 4 minute intermission between them. This intermission was needed for the purposes of resuming high-vacuum levels and storage of data. Applied load was 2N and the employed sliding speed was 0.14cm/second. The data-acquisition window was set at 10mseconds. Background-noise was lower than 1 count/second.

In Figure 4.22, while the largest burst of triboemission for the first 45second contact-period was 85 counts (in the 10mseconds-window), the largest burst for the following contact-period was as high as 603 counts in the same window. This particularly large burst also initiated sustained high-level post-contact emission after contact ceased.

Figure 4.23 shows the measurement of triboemission during contact (also presented in Figure 4.22) and the post-contact emission for 445 seconds after the contact ceased. The gaps of data acquisition in Figure 4.23 were needed to save acquired data at the employed data-acquisition rate.

A study of the statistical significance of the results in this section (e.g., of the statistical significance of triboemission outputs during contact vs. CEM count during non contact for alumina-on-alumina system) is presented in Appendix C. This study shows that average negatively-charged triboemission during contact was significantly above background noise for this material system.

These experiments show that negatively-charged triboemission from alumina-on-alumina is burst-type, clearly associated with sliding contact. There are important differences, however, with respect to similar measurements in diamond-on-ceramics: in the case of alumina-on-alumina, there is a considerable lag between the application of sliding contact, and the occurrence of the largest bursts of triboemission, at least for the speed and load used.

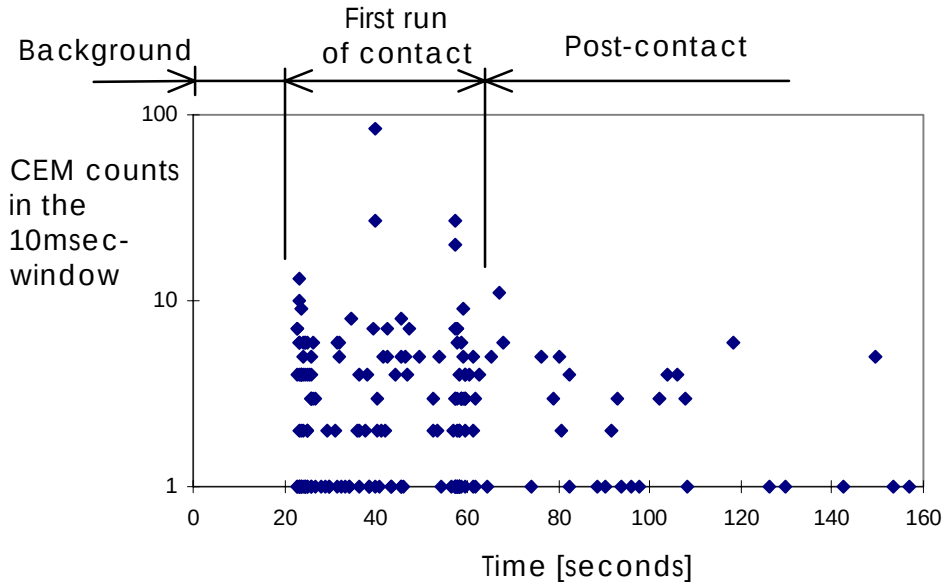

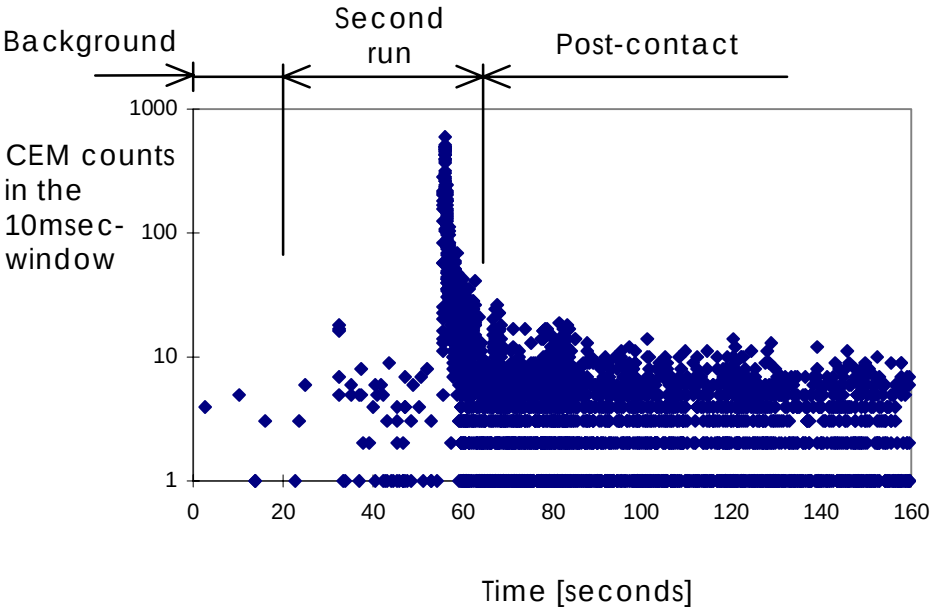

Figure 4.22. Negatively-charged triboemission for two consecutive runs on same wear track of alumina-on-alumina sliding contact. CEM output versus time.
Grid: 0Volt (ground). Cathode: +1,200V. Load: 2N. Sliding speed: 0.14cm/s .
Pressure: 1.5 x 10^{-8} Torr.

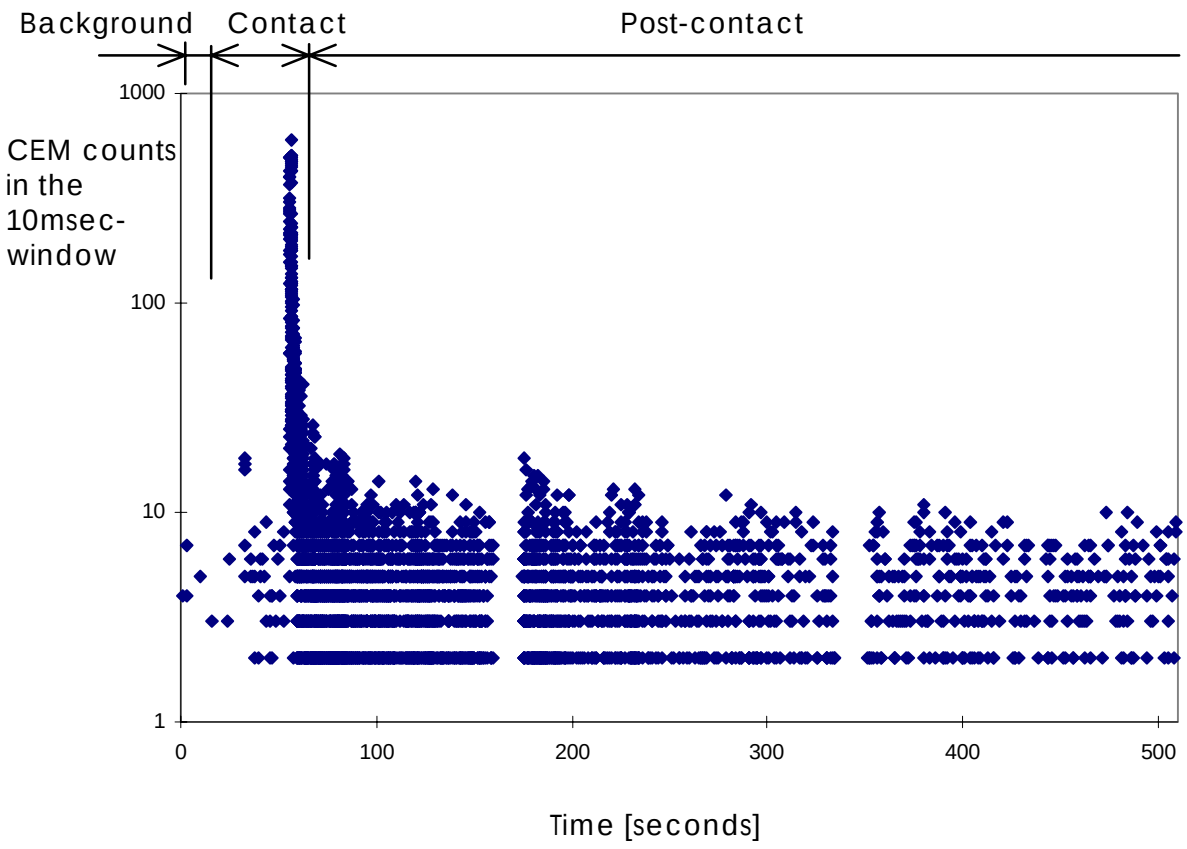

Figure 4.23. Negatively-charged triboemission for “large burst and after contact” of alumina-on-alumina sliding contact. CEM output versus time.
Grid: 0Volt (ground). Cathode: +1,200V. Load: 2N. Sliding speed: 0.14cm/s .
Pressure: 1.5 x 10^{-8} Torr

After the large peaks occur, alumina-on-alumina contacts may produce negatively-charged triboemission at higher levels than those of diamond-on-ceramics, and for longer periods of time. In this, the levels of largest triboemission bursts greatly differ between different specimens of the same alumina-on-alumina system. Occurrence of triboemission bursts seems to be random and their magnitude may diminish in time. Sustained high levels of negatively-charged triboemission occur after the contact ceased for the alumina-on-alumina system.

Positively-charged emission from alumina-on-alumina sliding contacts also was investigated. Figures 4.24 and 4.25 show two tests for positively-charged triboemission from alumina-on-alumina. For the purpose of comparison to triboemission from diamond-on-ceramics, tests of Figures 4.24 and 4.25 employed the grounded grid (i.e., zero-Volt with respect to reference), -1,500V cathode voltage, and same contact schedule and data-acquisition parameters than for those for positive-charge measurements (i.e., those of figures 4.16 and 4.17 in section 4.3 for diamond-on-alumina (2N load) and diamond-on-sapphire (20N load) respectively. The sliding speed was 0.48cm/s for both tests.

Figures 4.24 and 4.25 show that low positively-charged triboemission, barely above background-noise, is observed from alumina-on-alumina sliding contacts. Even for contact loads and speeds relatively higher than those of negative-charge measurement, the observed positive-ion triboemission was low. The statistical study in Appendix C found no significant difference for the average positively-charged triboemission during contact (i.e., vs. background noise during non-contact) for alumina-on-alumina.

As in the case of positive-ion emission from diamond-on-ceramics (see section 4.3), it is possible that the positive-charge triboemission did not originate from the contacting surfaces, but resulted from triboemitted-electron interaction with gas molecules immediately above the wear track.

Table 4.2 summarizes these results of positively- and negatively-charged particle triboemission from alumina-on-alumina systems.

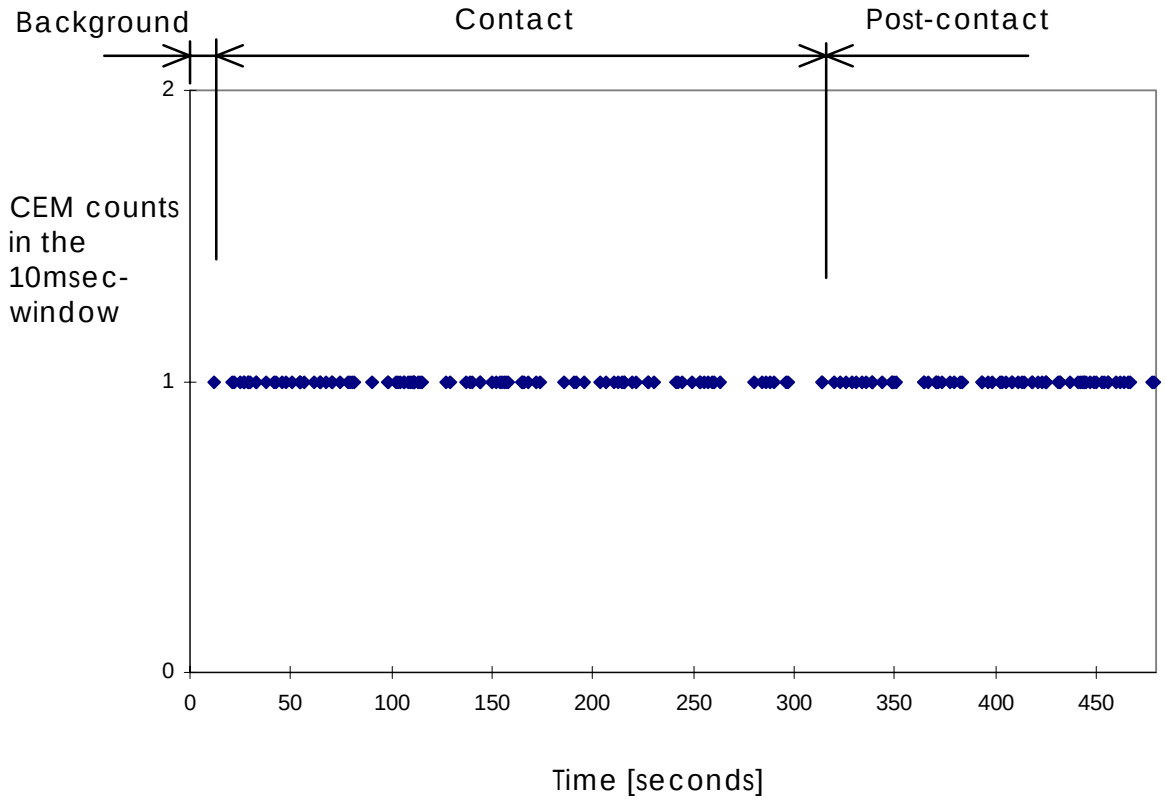

Figure 4.24. Positively-charged triboemission for alumina-on-alumina sliding contact.
CEM output versus time
Grid: 0Volt (ground). Cathode: -1,500V. Load: 2N. Sliding speed: 0.48cm/s.
Pressure: 1 x 10^{-8} Torr

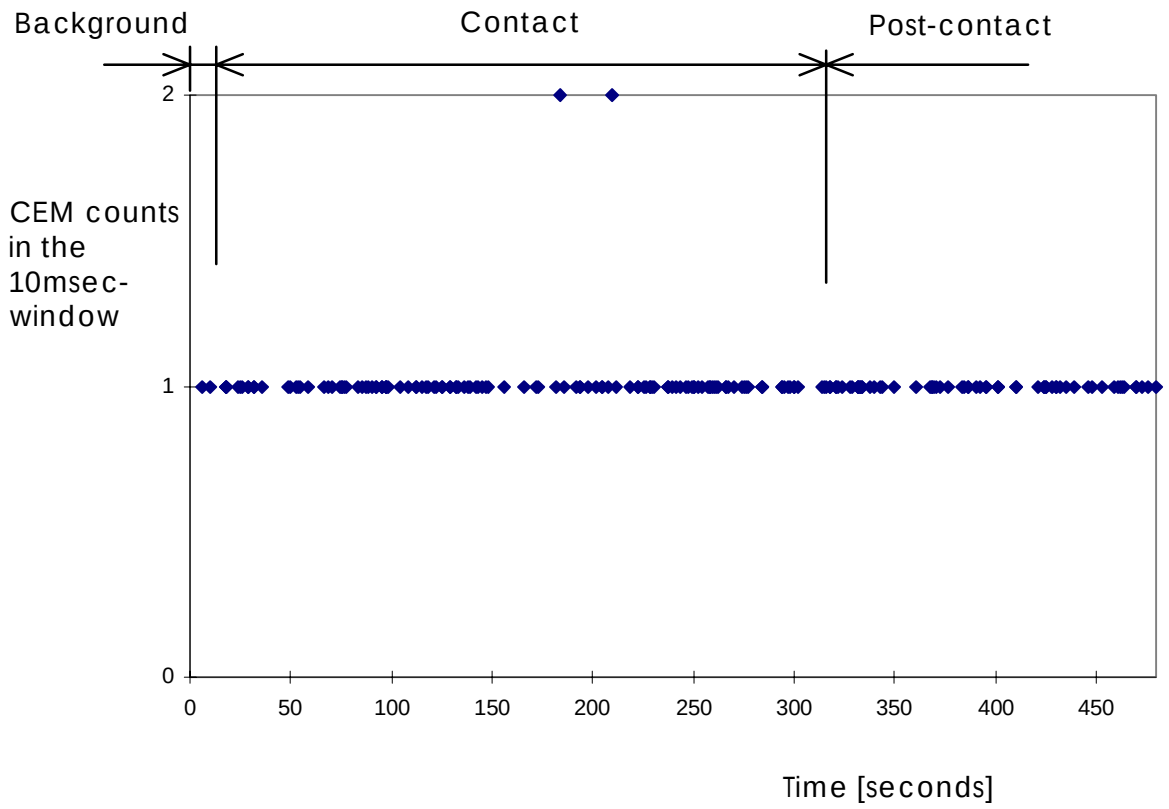

Figure 4.25. Positively-charged triboemission for alumina-on-alumina sliding contact.

CEM output versus time

Grid: 0Volt (ground). Cathode: -1,500V. Load: 20N. Sliding speed: 0.48cm/s .

Pressure: 1 x 10^{-8} Torr

Table 4.2. Measured average triboemission rates for the presented tests of sliding contact of alumina ball on alumina disk (For three ball-and-disk specimen sets).

Average triboemission rates during contact (in counts/sec)			
Negative-charge			Positive-charge
(*)	(**)	(***)	(*)
15.9 to 710	38,417	1.21×10^6	~0.4

(*) Triboemission rate during 320 sec contact tests.

(**) Maximum triboemission rate for one minute around largest burst of emission.

(***) Maximum triboemission rate for one second around largest burst of emission.

It is apparent from these measurements for alumina-on-alumina sliding pairs, that triboemission from this material system is mainly composed of triboemitted electrons. As in the triboemission from diamond-on-ceramics, electrons are emitted in bursts of seemingly random occurrence. The start of the largest bursts of triboemission may take, however, a significantly longer period of contact for the alumina-on-alumina system, and triboemission levels may be sustained for longer periods, with respect to those for diamond-on-ceramics, at least for the loads and sliding speeds used. It is believed that both the different contact conditions (i.e., of severe plowing for the diamond with respect to light penetration and sliding for the alumina ball), and the different material systems may have an effect on such observed differences in triboemission.

CHAPTER 5. DISCUSSION AND ANALYSIS OF TRIBOEMISSION MEASUREMENTS

The main purpose of the research reported in this dissertation was to design, construct and develop a new triboemission instrument for the experimental measurement of charged-particles triboemitted from ceramics. These low-energy particles are believed to be important in tribochemical reactions and, in particular, in the tribopolymerization of addition-type monomers. During and after instrument development, measurements were carried out of charged-particles triboemitted from several ceramic systems. In this chapter, the triboemission measurements of Chapter 4 are discussed and analyzed with a focus on the possible reaction-initiating role of triboparticles. A frequency domain description of such triboemission data is proposed and discussed.

5.1. Discussion of the triboemission measurements

Initial CEM-count measurements for a non retarding-grid configuration showed that a variety of eventually produced charges (both emitted and electrostatic charges) may be extracted from diamond-on-alumina sliding contacts by the CEM-cathode voltage. It was shown that electrostatically-charged particles, even charged wear debris, may be collected by such cathode-voltage in this condition. In particular, it was found that alumina wear-debris was electrostatically-charged, because it was attracted by the cathode voltage, and accumulated in the CEM input.

An important measurement development derived from such initial experiments: to measure charged-particles actually triboemitted, a grid was placed between the emitting surfaces and the CEM input, and it was referenced to a known voltage. This screening grid stops particles of energy lower than the set voltage before they reach the CEM: charged-particles with the minimum energy to pass through the grounded grid are actually triboemitted from the sliding contact, and are thus of primary interest in this research work.

Preliminary testing, for which the retarding-grid was grounded, showed that negatively-charged triboemission is clearly associated with sliding contact of diamond-on-alumina. The measurements of charged-particles triboemitted from diamond-on-ceramics early revealed some basic features: triboemission from ceramics is essentially a burst-type intermittent phenomenon.

Further measurements later showed that triboemission was mainly composed of low-energy electrons. These preliminary measurements also suggested that time, load and speed may be important factors in the triboemission of negatively-charged particles. These operating conditions, which are connected to wear, may affect the triboemission level: higher load and/or higher sliding speed seem to increase the triboemission of negatively-charged particles. However, no final conclusions on the effects of such factors can be derived from these limited measurements.

It is believed also that complex interactions between load, speed and time are determining factors in triboemission. In this, the decrease with time of triboemitted-particle production, which in the experiments showed for the repeated transit of the diamond on the same wear-track, may be connected to decreasing wear and surface damage, and/or to decreasing creation of fresh surfaces.

Further characterization of the burst-type triboemission phenomena was needed before testing for the effects of these factors and their interactions: burst-type triboemission requires an identification of adequate quantitative outputs to describe such seemingly random phenomena. After such outputs (called responses in the design of experiments terminology) were identified, experimental testing for the factors of interest could be eventually planned and carried out. In this, section 5.2 presents a frequency-domain analysis of the triboemission data. Such analysis will allow a better understanding of the triboemission phenomena.

Negatively-charged triboemission was observed from both diamond-on-alumina and diamond-on-sapphire under the same conditions of low load and low sliding speed. The different crystalline structures of these two Al-oxides do not appear to be a significant factor in triboemission.

A study of the statistical significance of these results is presented in Appendix C. This study found statistically significant differences for the negatively-charged triboemission outputs during contact vs. CEM-count during no-contact (i.e., vs. background noise) for the diamond-on-alumina and diamond-on-sapphire systems. However, no statistically significant difference was found for the comparison of triboemission outputs during contact of these two systems.

In general, these comparative tests showed initial large-burst emission, which decreased within the first two minutes of sliding, at least for the employed load and sliding speed. This decay of the triboemission intensity suggests strong time dependency, which may be connected to the decrease in time of wear, and/or to a decreasing rate of fresh surface creation.

Dickinson et al. [95] observed large bursts of negatively-charged triboemission from MgO scratched by a diamond (See section 2.3). The triboemission bursts in their measurements were larger than those for diamond-on-ceramic contacts in this dissertation research. It is possible that the effects of electrostatic charge on the surface (e.g., patches of positive surface charge), which can accelerate electrons after emission, may account for such difference.

Post-contact negatively-charged triboemission of low level, although higher than background, was measured to decay after the contact ceased of the diamond on the ceramics. No large bursts were observed, however, after contact. It is thought that the surface conditions under which electrons are triboemitted evolve for minutes after the contact and sliding ceased, with no need for simultaneous tribological excitation.

Negatively-charged triboemission is observed from alumina-on-alumina sliding systems, showing that triboemission is produced from ceramic-on-ceramic tribological wear conditions. These results also show that neither different material (as in the case of diamond-on-ceramics) nor the severe plowing of diamond scratching are needed for charged-triboemission to occur. As in the case of diamond-on-alumina, triboemission from alumina-on-alumina is burst-type, clearly associated with sliding contact.

The study of Appendix C found statistically significant differences for the negatively-charged triboemission outputs during contact vs. CEM-count during no-contact (i.e., vs. background noise) for this alumina-on-alumina system. Sustained post-contact emission also was observed from this material system, although at an intensity lower than that during contact.

Maximum levels of triboemission for the observed largest bursts may differ by two orders of magnitude between different specimens of the same ceramic systems. In general, large bursts of negatively-charged triboemission may appear superimposed to a constant lower level of smaller-burst emission. This constant level, being higher than background-noise, does not vary significantly between different specimens of the tested ceramic systems. Also, the characteristic decay-time of the triboemission bursts is of about 100mseconds. Research work by Dickinson et al. [95,96], on triboemission from MgO, found the same decay time.

For the occurrence of the largest bursts of negatively-charged triboemission from alumina-on-alumina, an important difference is observed with respect to diamond-on-ceramic triboemission. The largest bursts of triboemission from the former do not show at the beginning of contact, nor in the first minute of sliding, at least for the speed and load used: there is a considerable lag, for the alumina-on-alumina contact pair, between the application of sliding contact and the occurrence of the largest bursts of triboemission. These results suggest a different time dependence than that for diamond-on-alumina, at least for the occurrence of the largest peaks.

These particularly large bursts also initiate sustained high-level post-contact emission after contact ceased of the alumina ball on the alumina disk. After such large peaks occur, alumina-on-alumina contacts may produce negatively-charged triboemission at higher intensity than that of diamond-on-ceramics, and for longer periods of time. It is possible that different wear conditions result from the different contacts (i.e., diamond versus alumina ball) and material systems (i.e., hard-on-softer material for diamond -on-ceramics versus same hardness material for alumina-on-alumina). Therefore, different wear behavior may account for the observed differences in triboemission.

The occurrence of triboemission bursts was found neither related nor coincident to any external or measured variable, or any surface feature, but seems to be of random occurrence. It is believed that large-burst occurrence relates to stick-slip behavior. The role of stick-slip in the plowing process by diamond, which would prompt large triboemission-bursts, was previously suggested by Dickinson et al. [96]. It is also thought that triboemission originates, at microscopic scale, from surface changes: in general, new surface is created during dry-contact of diamond-on-ceramic and ceramic-on-ceramic. There is strong evidence from previous research, which was reviewed on section 2.2, that fresh-surface presents a diminished value of work function, by which exoemission would proceed.

For the low loads and low sliding speeds used, the largest bursts of negatively-charged triboemission from ceramics may show sporadically within the first minutes of contact. The constant low-level of small-burst emission, however, is sustained for longer periods of time (e.g., for contact periods of several minutes), and it seems to be an important component of the triboemission phenomenon. It is thought that both this constant triboemission level and the large superimposed bursts relate to the same origin (e.g., surface microfracture and/or fresh surface creation), although for different wear rate. Large bursts may relate to stick-slip behavior, while low constant-level triboemission may originate from more continuous-sliding wear.

Surface creation during ceramic dry-contact may result from both surface plastic-deformation and fracture. In particular, wear of alumina presents two consecutives regimes, which are called mild (i.e., of negligible wear at the beginning of sliding) and severe stages of wear. Cho et al. [128], in ball-on-flat wear tests, showed that the alumina mild-regime proceeded by plastic deformation and with the occurrence of fine surface scratches, which can be described in terms of microscopic contact asperities. The severe stage of alumina wear which follows was clearly related to the occurrence of surface microfracture. They also found that the transition between the two regimes was characterized by prior subsurface intergranular cracking. These two regimes of wear behavior are also apparent in other ceramics, e.g., in Si_3N_4 and SiC [129].

It is believed that, in the triboemission tests carried out with severe plowing of diamond-on-ceramics, the mild regime at the beginning of sliding is negligible. Therefore, initial large bursts of electron triboemission would occur during severe wear, i.e., during surface microfracture. In such case, however, the measurements of triboemission from alumina-on-alumina contacts suggest that the mild regime of wear exists at the start of contact for a short period: for such mild wear, low intensity triboemission may occur.

In the case of alumina-on-alumina, the large bursts of triboemission which follows after a few minutes of sliding contact – at least for the load and speed used – seem to relate to the severe regime of wear. It is not clear if the transition between the two regimes (i.e., the subsurface intergranular cracking) may have any role on the occurrence of triboemission.

The connections between triboemission and surface modifications during ceramic wear indicate that surface microfracture plays a role on electron triboemission. Following section 5.2 makes further connections between the results of a frequency domain analysis of the triboemission data and surface modifications of the tribological contact. It also makes comparisons with the phenomena of fractoemission, which is known to originate from surface microfracture.

Fresh surface creation, however, should not be ruled out as source and/or condition for triboemission, since surface fracture ultimately implies creation of fresh material. Microfracture during tribological contact proceeds not only by surface cracking but also by grain and particle pullout, both mechanisms that create new surface.

Low intensity of positively-charged triboemission was observed from diamond-on-alumina, diamond-on-sapphire, and alumina-on-alumina contacts. These positively-charged particles were observed only when relatively higher contact loads and/or sliding speeds were applied. It is thought that no positive ions are actually emitted from the sliding surfaces, but triboemitted electrons ionize gas species in the surrounding of the wear track. The same phenomenon might take place to produce some negative ions: these negative ions would be, however, a negligible fraction of the negatively-charged emission reaching the detector, which is eventually measured.

The employed detection system did not allowed separate measurements for electrons than for negative ions. No post-contact positive-ion emission was observed after contact ceased from the investigated diamond-on-ceramic and alumina-on-alumina material systems.

A study of the statistical significance of these results is presented in Appendix C. This study found no statistically significant differences for the positively-charged triboemission outputs during contact vs. CEM counts during non-contact (i.e., background noise) for the diamond-on-alumina, diamond-on-sapphire, diamond-on-aluminum, and alumina-on-alumina systems. Since the measured differences between positively-charged contact outputs vs. non-contact situation were small, it is possible that samples larger than the ones employed may be needed to reveal any statistical significance.

Low intensity of negatively-charged triboemission was measured from diamond-on-aluminum sliding contact. The measured negatively-charged emission is very low when compared to that for the same sliding conditions from diamond-on-alumina and diamond-on-sapphire. Just some small bursts (of about 10 counts in the 10msec window) sporadically rise above the lower background-noise. However, a study of this result in Appendix C (e.g., of the statistical significance of negatively-charged triboemission outputs during contact vs. CEM count during no-contact for diamond-on-aluminum) found a statistically significant difference. No post-contact emission was observed from this material system. This result strongly suggests the weaker emission from aluminum is not related to the scratching of the metal substrate, but rather originates from wear of the surface oxide-layer.

Triboemission from diamond-on-aluminum is a marginal case of diamond scratching of aluminum-oxides (e.g., of alumina and sapphire). No positive-ion emission was measured from diamond-on-aluminum system: its weak electron-emission would not produce positive-ionization of gas species. Therefore, both negatively-charged triboemission from aluminum and positively-charged from the ceramics are marginal effects of the dominant exoelectron triboemission.

The retarded-energy spectra were measured of negatively-charged triboemission from diamond-on-alumina and diamond-on-sapphire. Both spectra extend for minimum energy levels higher than the test maximum-level, 48 eVolts. They show decaying rates of negatively-charged triboemission for increasing minimum energy of the triboemitted particles.

These energy distributions suggest that an important fraction of the total negatively-charged particle triboemission is produced in the zero to 5eVolts energy-range, with a decaying tail extending to higher-energy triboemission. It is believed that the triboemission yield in the zero to 5eVolts range may be enhanced by secondary electron emission from interactions in the region surrounding the wear track. Also, some higher-energy emission can result from patches of electrostatic charge on the surface: electrostatic potential may increase kinetic energy of particles immediately after emission [96]. The effects of both triboemitted particles and these added interactions are shown in the measured retarding-energy spectra.

Energy spectra of positively-charged triboemission from diamond-on-alumina and diamond-on-sapphire were not measured. The low-level emission of positively-charged particles make difficult any meaningful measurement by the technique employed. On the assumption that weak positively-charged emission would result from ionization of gas species by the triboemitted electrons, the positive-ion energy spectrum is of marginal interest to the purpose of this research.

Because of the low level of negatively-charged triboemission from diamond-on-aluminum, no energy-measurement was carried out for such output. However, the weak electron triboemission from aluminum is an example of emission from surface aluminum-oxide layers, and its energy-distribution is no part of this research.

The experiments in this dissertation show that indeed low-energy electrons are emitted from alumina and sapphire surfaces under rubbing contact, the essential first step in the hypothesis of tribopolymerization of certain addition-type monomers presented by Furey and Kajdas [28,31,37]. In liquid phase experiments, using minor concentrations of anionic-polymerization-type vinyl monomers in hexadecane, significant wear reduction

was found for alumina sliding-contacts. Cationic-type vinyl monomers were not effective, at least in the liquid phase studies.

The findings of this dissertation research, that low-energy exoelectrons are significantly triboemitted from alumina under wear conditions, while positively-charged emission is negligible, confirms Furey and Kajdas' line of thought. However, vapor phase studies show that the picture is not so simple [30] (see section 2.1.2). Recent work by Kempinski et al. [130] show that other factors besides triboemission (e.g., adequate monomer concentration) are needed for tribopolymerization to work. Some of the experimental results in this dissertation were also presented in [131, 132].

5.2. Frequency analysis of triboemission data

5.2.1. Frequency representation of triboemission data

Triboemission data for the diamond-on-ceramic and ceramic-on-ceramic measurement was presented in sections 4.2 to 4.5, for the time domain description. The time domain plot is the simplest representation of triboemission data, and it depends on the chosen window-length. This description showed that low-energy electron triboemission was clearly related to the sliding contact of ceramics and that triboemission bursts occur at random. However, the time-domain description does not reveal a characteristic pattern of triboemission, which is apparent in the frequency domain of representation.

This section presents an analysis of the random-burst triboemission outputs in the frequency domain. As described in section 4.3, triboemission data for each test was originally acquired as a record of 32,000 bins of 10msec-length (i.e., for a 10msecond-window during 320 seconds of sliding contact). Each such record is a log of the number of detected particles during contact, which are called "events" for the purposes of this section, in each of the acquired 10msecond-bins. In this, analyzed data pertain to sliding contact (and not to post-contact).

To transform such triboemission-data into the frequency domain, a tally is computed of the frequency the number x of events occurs for the chosen window (Where x goes from zero events in the window to the largest observed number of events in such window). This transformed data is a description for frequencies of occurrence of the number x of events (in the total number of acquired bins).

Figure 5.1 shows a plot of this frequency domain description of data for one example of the negatively-charged triboemission from diamond-on-alumina: this example corresponds to the contact period in time-domain data of Figure 4.10 in section 4.3. It is apparent that such frequency-domain description depends on the chosen window. In this, data can be presented for any window longer than the acquisition one, by a "consolidation of data": during post-processing, data can be simply grouped in bins longer than the acquisition window. The longer bin and window must be an integer multiple of the acquisition ones. For the purposes of this section, the same data is consolidated in the 40msecond-, 100msecond- and 250msecond-windows, from the data acquisition window of 10mseconds.

Normalization of the frequency-domain data is made by dividing the frequencies of occurrence, as above computed, by the total number of acquired bins in the record (e.g., by 32,000). This normalization means just a scale-change for the frequencies of occurrence, and the normalized values can be understood as experimental estimations of the probabilities of occurrence for x events in the window. Figure 5.2 shows this normalized frequency-domain description for the example in Figure 5.1, for the triboemission from diamond-on-alumina.

The acquired triboemission data include, however, a component of background-noise. As described in previous section 4.3, a record of background-noise data was also acquired, for reference purposes, in each triboemission experiment. A post-processing procedure, which is described as follows, was employed to subtract such background noise from the triboemission data. In this, the probability of occurrence for the background-noise can be assumed to be a classic Poisson probability-distribution. This is a reasonable assumption that means the underlying random process for background occurrence would be a classic Poisson process.

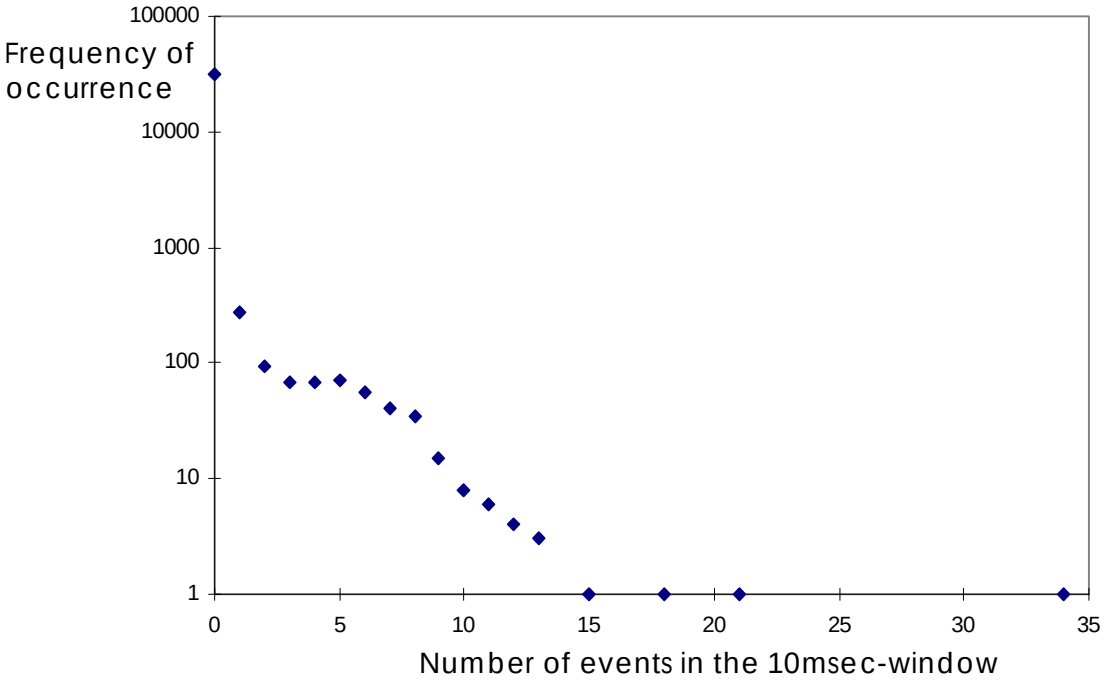

Figure 5.1. Frequency-domain description of triboemission data from Fig 4.10. Negatively-charged triboemission from diamond-on-alumina.

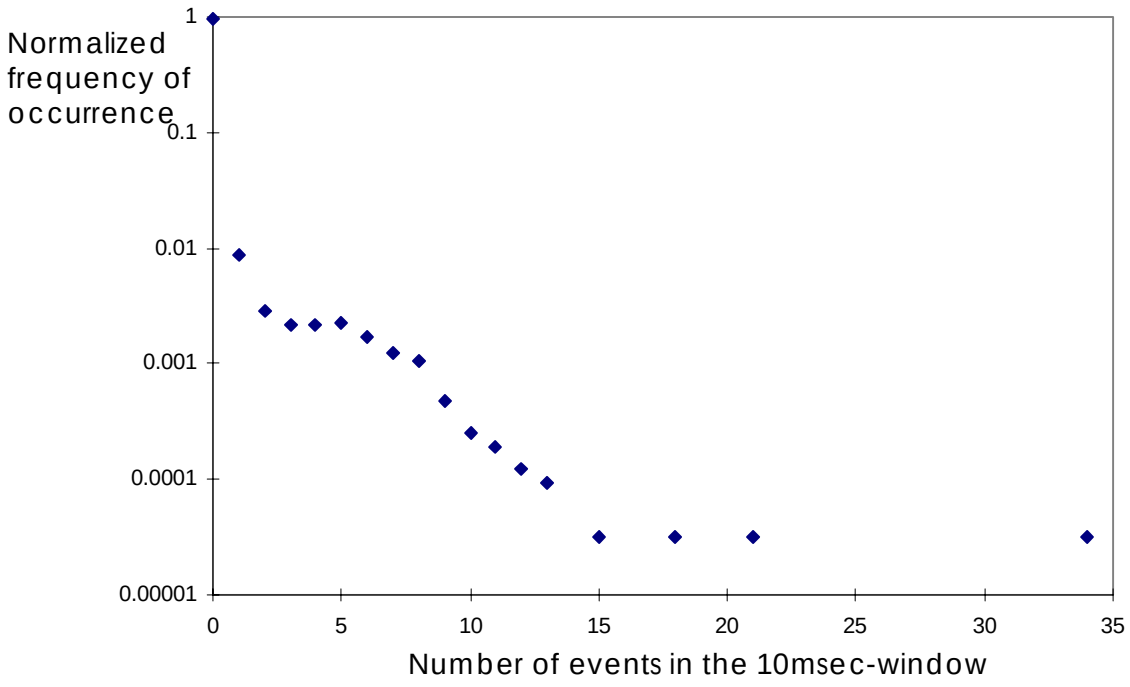

Figure 5.2. Normalized-frequency domain description of triboemission data from Figure 4.10. Negatively-charged triboemission from diamond-on-alumina.

Properties of the classic Poisson process, which describes a variety of random phenomena, can be found in references [133,134] and Appendix A.

Under such assumption, the pertaining Poisson probability density p(b) for the occurrence of b background-events is expressed:

$$p(b) = \frac{(\lambda_b t)\ e^{-(\lambda_b t)}}{b!} = p(b, \lambda_b t) \qquad (5.1)$$

where: b is the predicted number of background-events in the bin,

λ_b is the average rate of occurrence for background (in events per time-window length) , and

t is the time-window length (e.g., the bin length) for which the probability is computed.

For the purposes of this section the average rate of background-noise, which was computed from the reference of background-noise in each data record (see section 4.3), is a reasonable estimate of the rate λ_b . For these references of background-noise in the data analyzed in this section, this average rate was computed to be 0.7counts/sec.

On the above-said assumptions, this probability density of background-noise can be subtracted from the experimental estimations of the probabilities of occurrence for the acquired data; an example of the latter was previously shown in Figure 5.2. Figures 5.3 to 5.6 present the results from such subtraction of background noise, in the frequency domain, for four cases of negatively-charged triboemission from diamond-on-ceramics.

These cases were previously presented for the time domain in Figures 4.10 to 4.13 of section 4.3. Therefore, Figures 5.3 to 5.6 show the experimental estimations of the probabilities of occurrence for the acquired triboemission data minus the background noise.

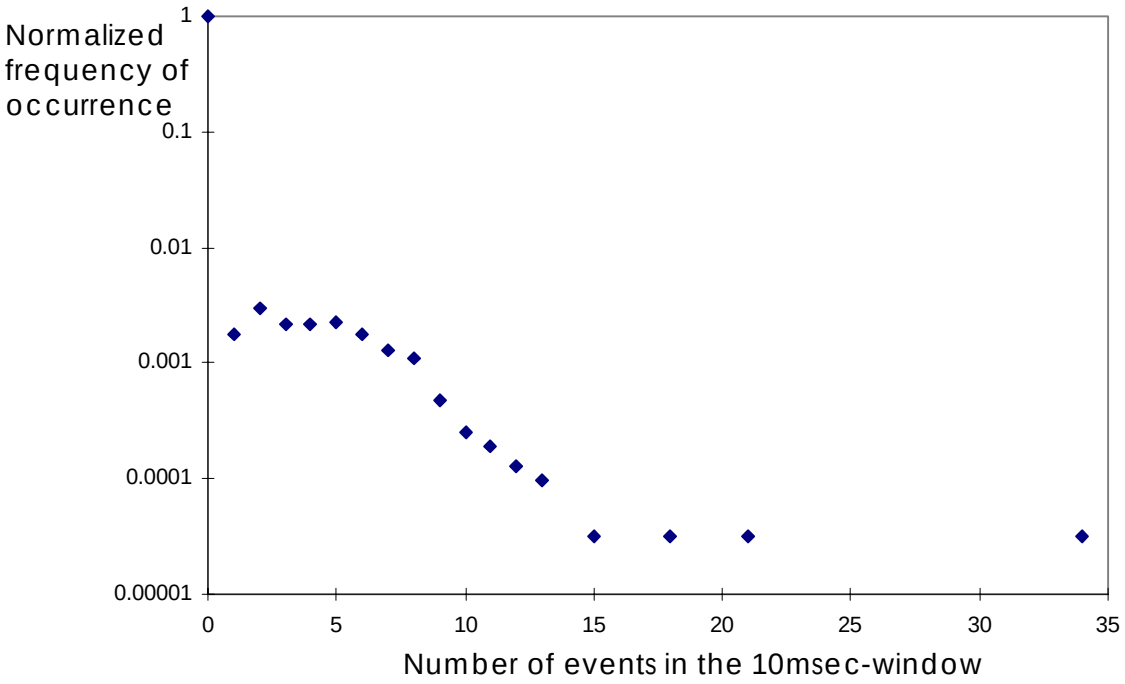

Figure 5.3. Normalized-frequency domain description of the triboemission data from Figure 4.10 minus background (Background rate: 0.7 counts/sec). Diamond-on-alumina, constant level output.

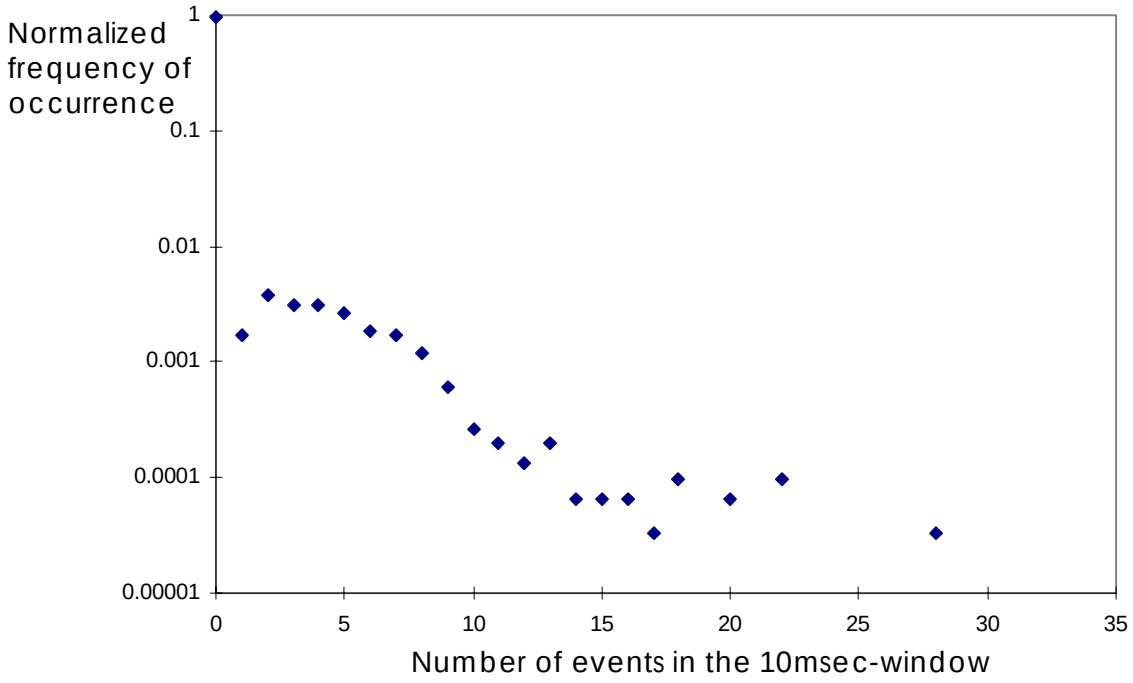

Figure 5.4. Normalized-frequency domain description of the triboemission data from Figure 4.11 minus background (Background rate: 0.7 counts/sec). Diamond-on-sapphire, constant level output.

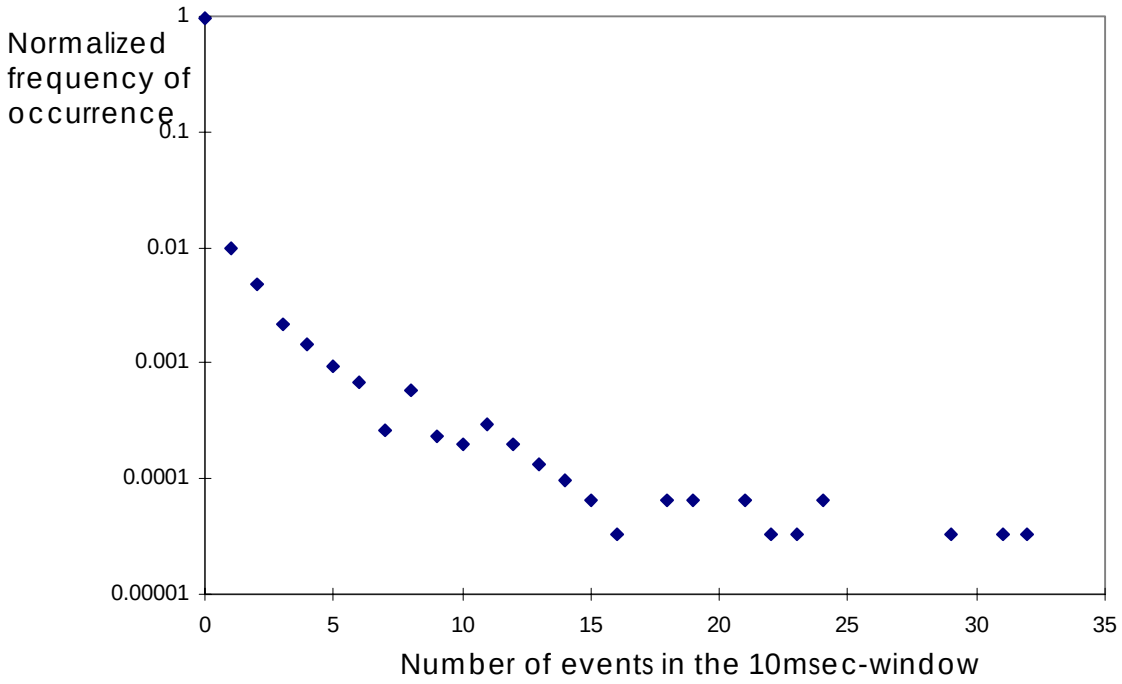

Figure 5.5. Normalized-frequency domain description of the triboemission data from Figure 4.12 minus background (Background rate: 0.7 counts/sec). Diamond-on-alumina, large bursts output.

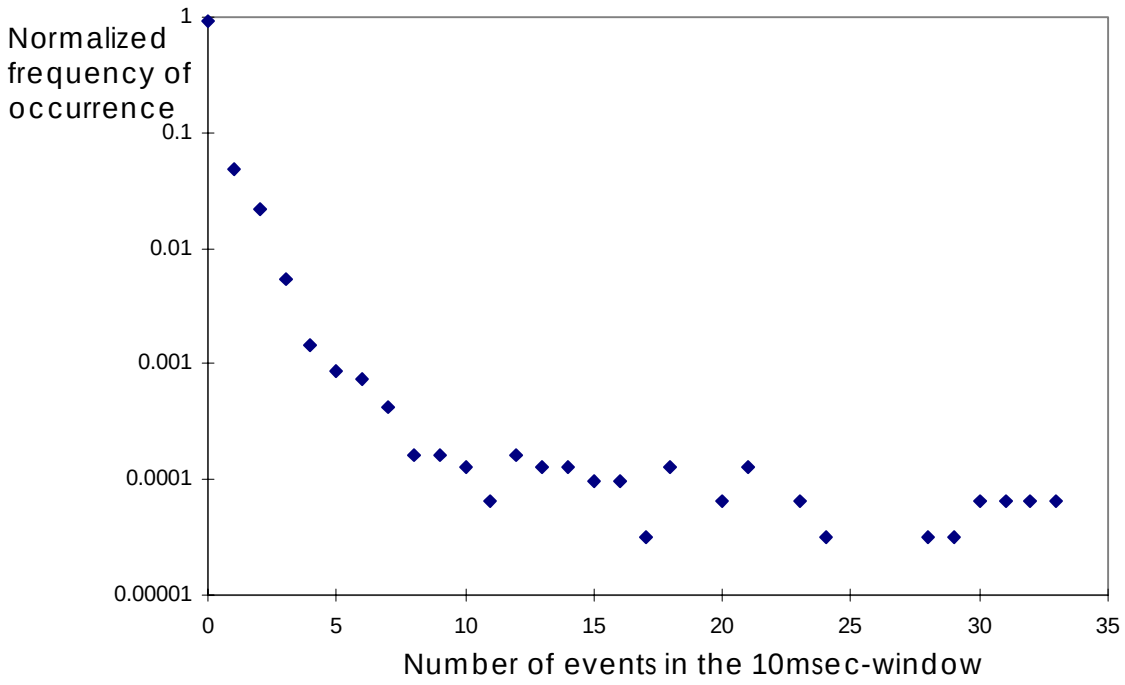

Figure 5.6. Normalized-frequency domain description of the triboemission data from Figure 4.13 minus background (Background rate: 0.7 counts/sec). Diamond-on-sapphire, large bursts output.

The frequency domain representation of Figures 5.3 to 5.6 reveals a characteristic pattern for triboemission data, which is made particularly apparent by employing a logarithmic scale for the probability of occurrence. Although such pattern may change for a different window-length of presentation, a similar pattern exists for all analyzed triboemission data if they are shown in the same window-length.

This strongly suggests that a general type of probability distribution of events (i.e., of particle triboemission occurrence) may describe all the acquired triboemission data. Some differences in pattern may be noticed for the so-called “constant-level” cases of triboemission, in Figures 5.3 and 5.4, when compared to the “large-burst” cases, in Figures 5.5 and 5.6. However, a general pattern is consistent within each case.

The frequency domain plots of figures 5.3 to 5.6 suggested that triboemission data might be described by classic probability distributions, the Poisson distribution among them. Formulae 5.1 also describes the classic Poisson probability density in such cases, if λ_b is understood as the predicted number of events in the bin (hereafter called λ_t for the classic Poisson). Attempts were made to fit the classic Poisson distribution to the analyzed triboemission data. However, no adequate fit was obtained.

Figures 5.7 to 5.10 show examples of those unsuccessful attempts in the four cases of figures 5.3 to 5.6. The criteria for such attempts employed for λ_t an “average” triboemission rate, from dividing for each triboemission record the total number of events (minus background, as previously presented) by the pertaining total time. Other criteria were also used, e.g., λ_t was adjusted in each case for the minimization of the squares of the differences between the experimental and the Poisson distribution probabilities.

Figures 5.11 to 5.13 show an example of unsuccessful attempt of fit with the latter criteria. Although a reasonable fit may be obtained in, for instance, the 100msecond-window, such fit is poor when tried for the same data in different window-lengths (in the 40msecond- and 250msecond-window in the example). The classic Poisson distribution was in no case able to follow the pattern of triboemission data.

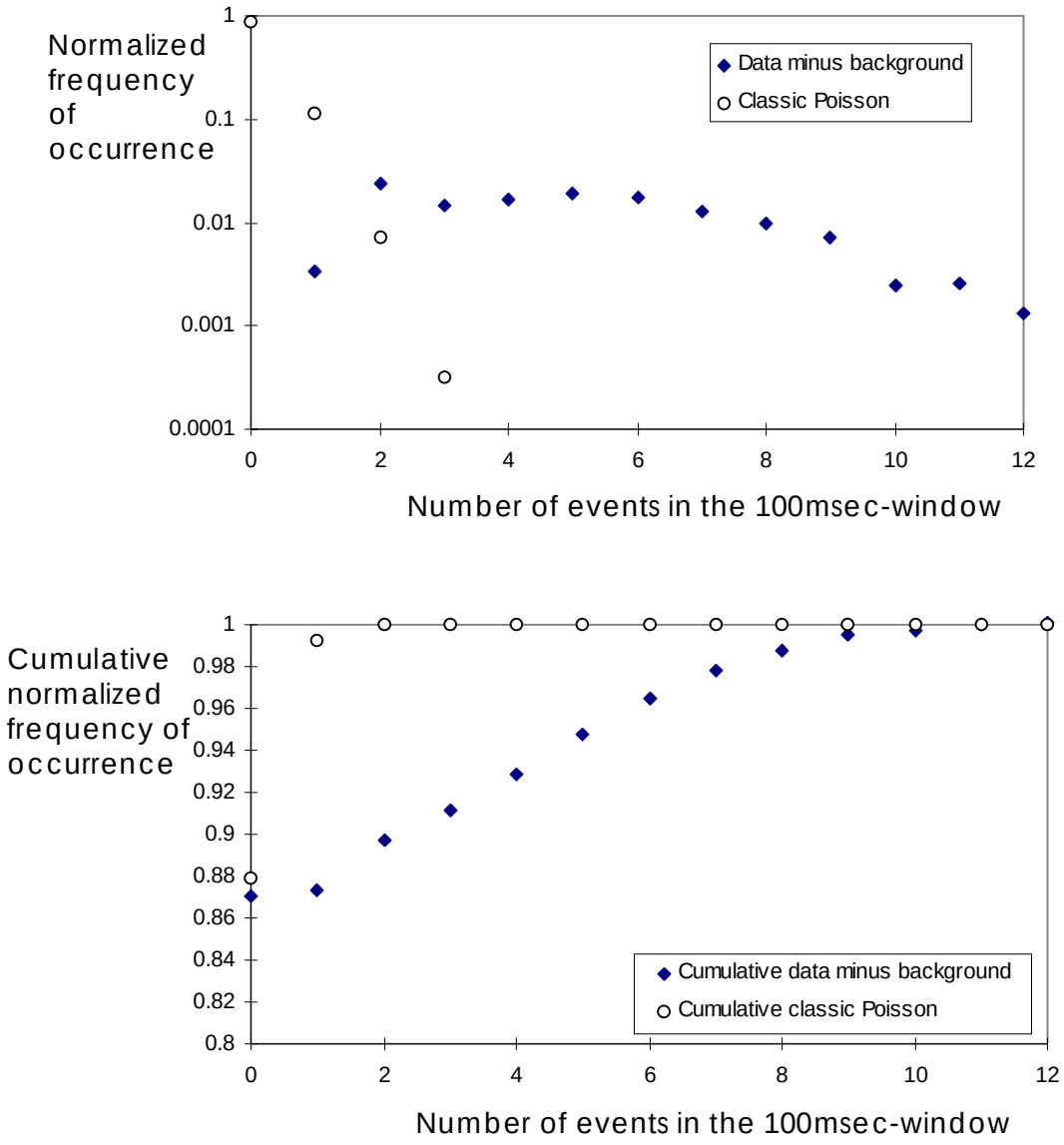

Figure 5.7. Experimental frequencies of occurrence from Figure 5.3 and classic Poisson distribution probabilities (Average rate above background: 0.13 counts/100msec). Diamond-on-alumina, constant level output.

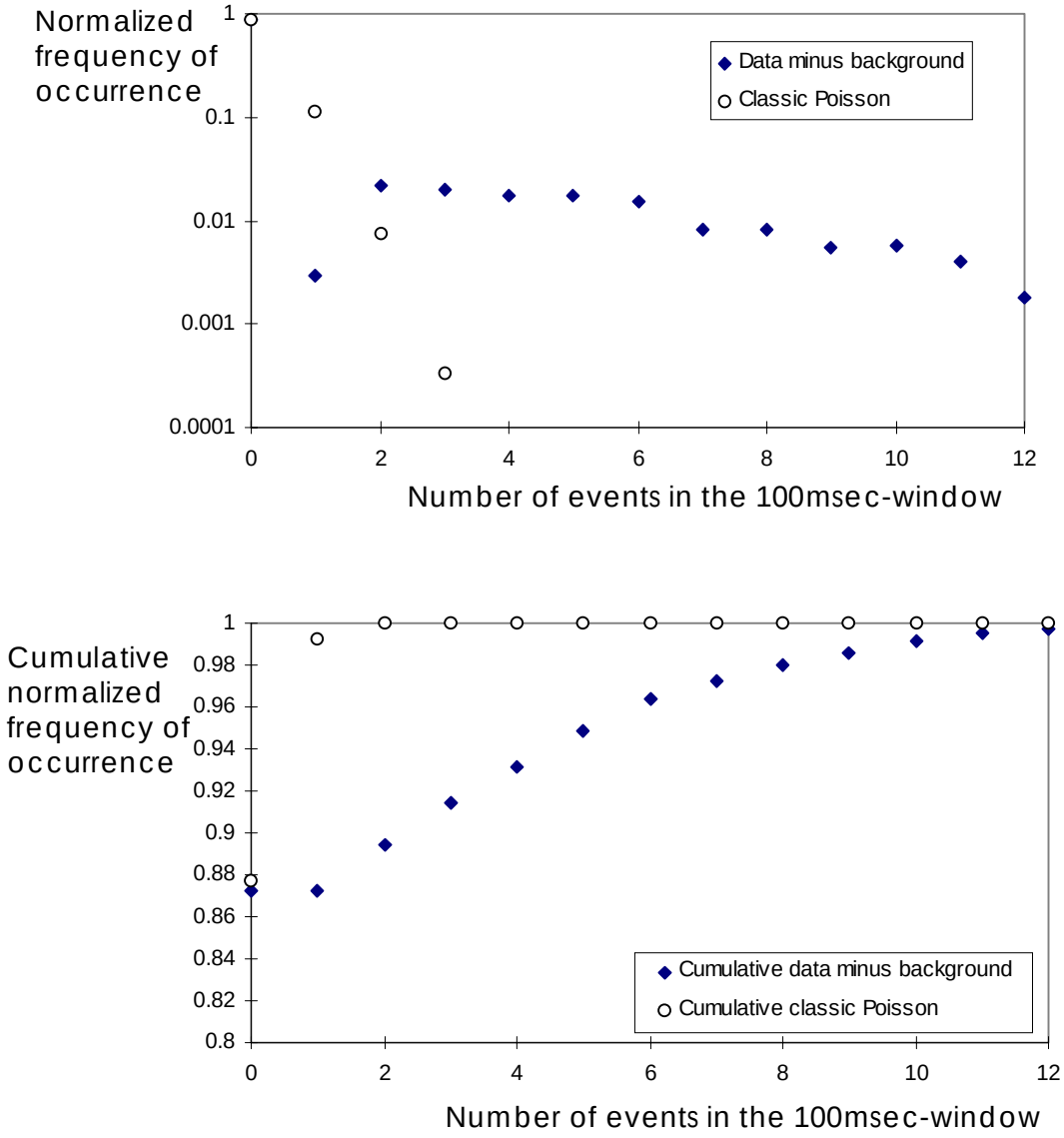

Figure 5.8. Experimental frequencies of occurrence from Figure 5.4 and classic Poisson distribution probabilities (Average rate above background: 0.13 counts/100msec). Diamond-on-sapphire, constant level output.

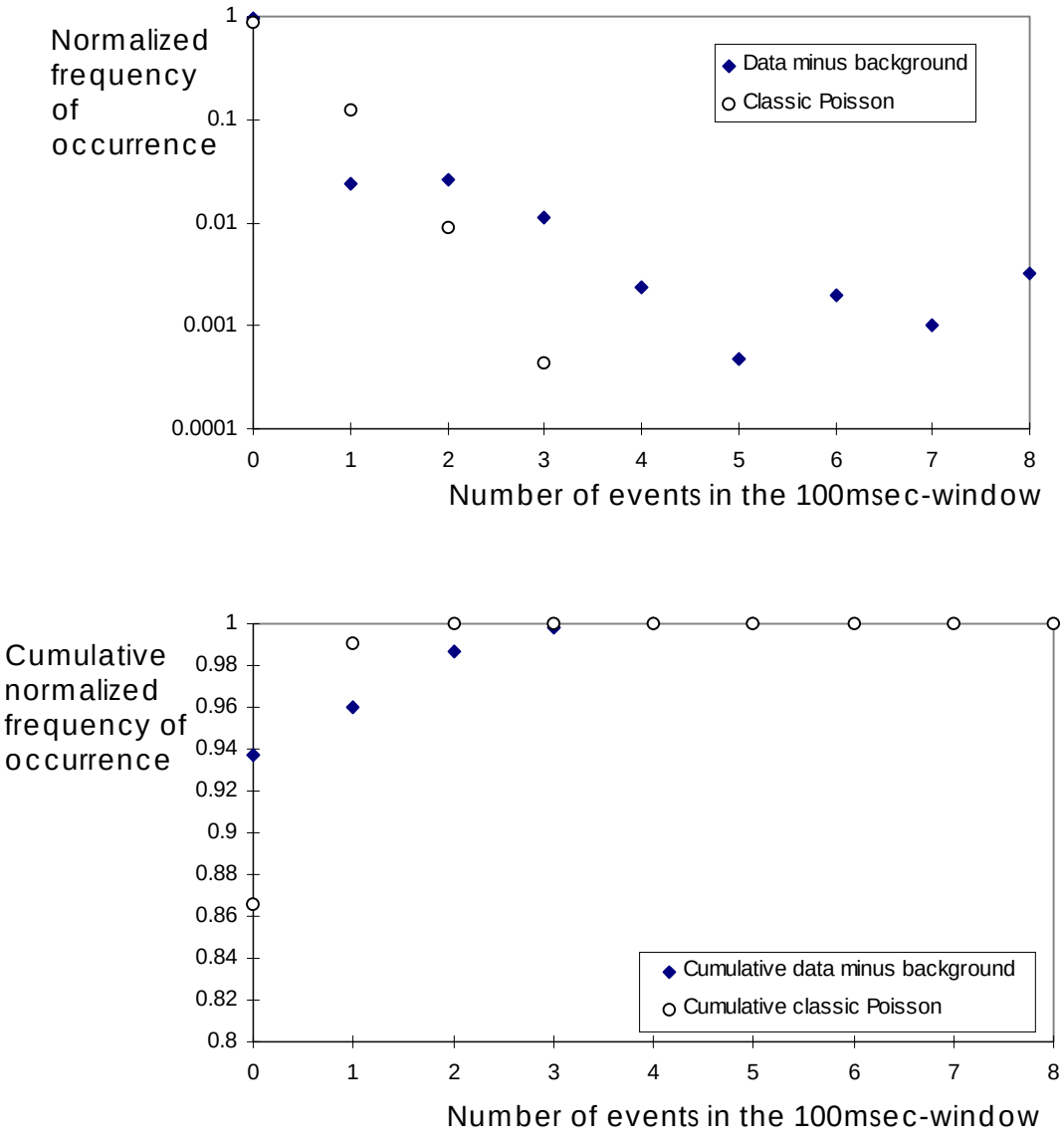

Figure 5.9. Experimental frequencies of occurrence from Figure 5.5 and classic Poisson distribution probabilities (Average rate above background: 0.14 counts/100msec). Diamond-on-alumina, large burst output.

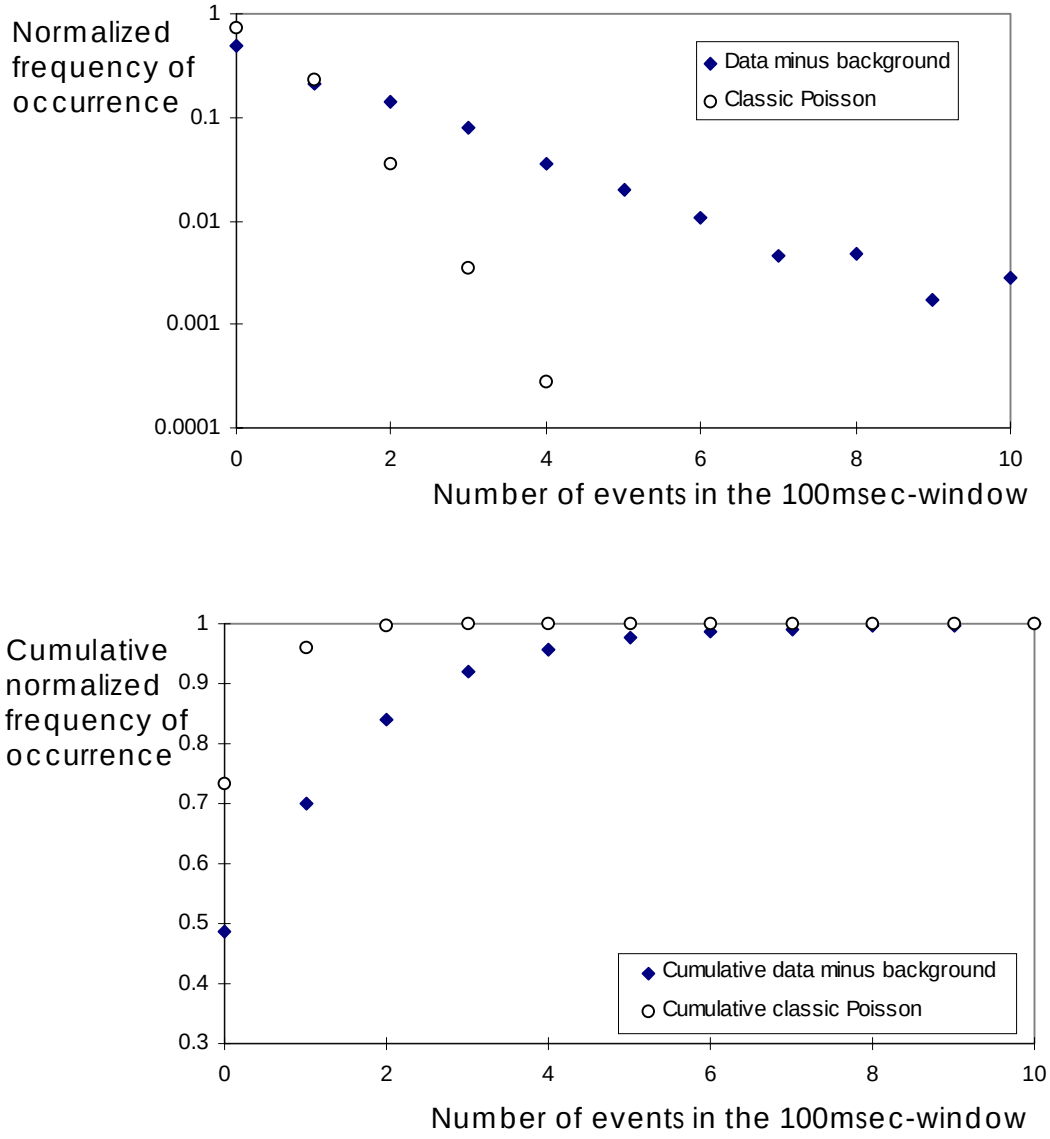

Figure 5.10.Experimental frequencies of occurrence from Figure 5.6 and classic Poisson distribution probabilities (Average rate above background: 0.31 counts/100msec). Diamond-on-sapphire, large burst output.

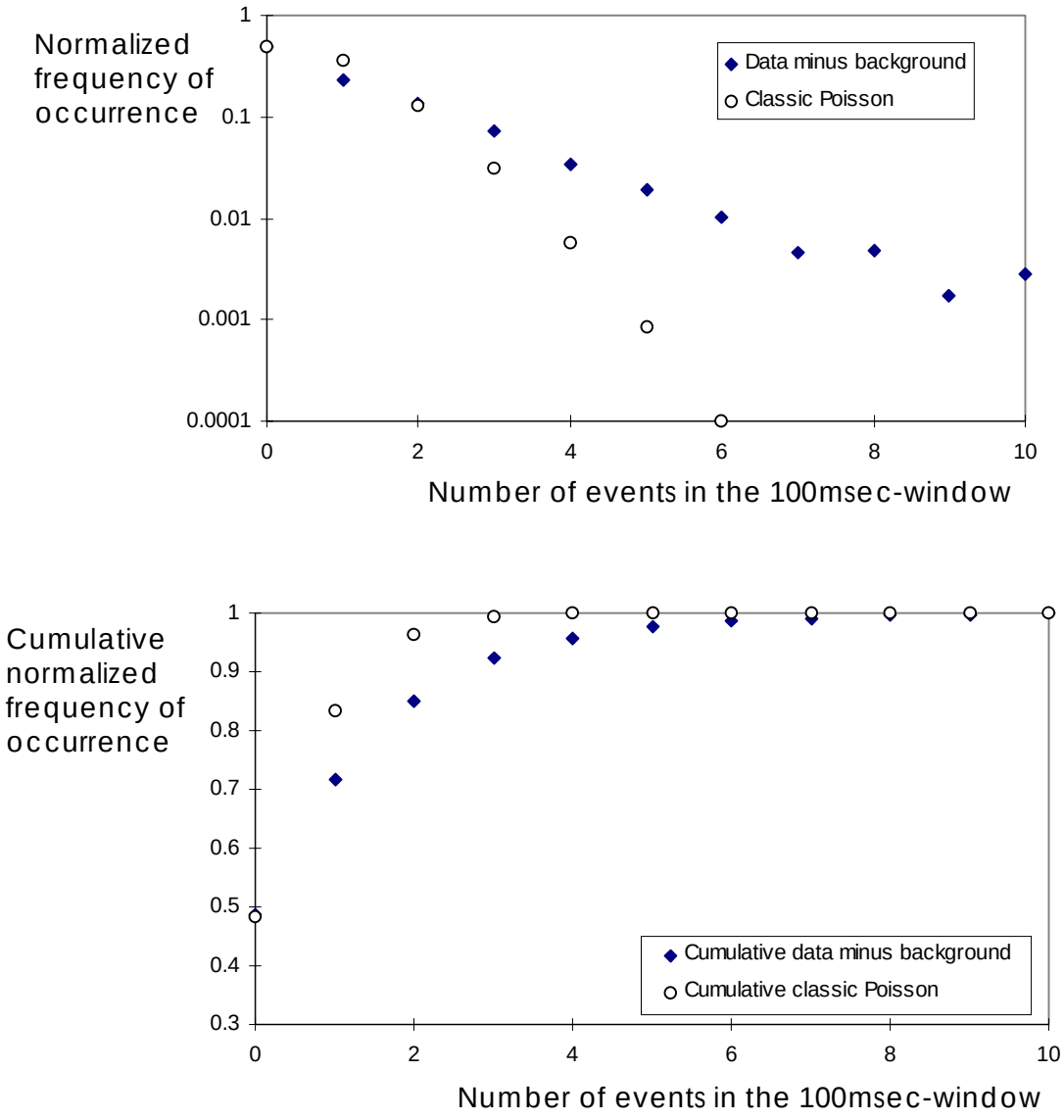

Figure 5.11.Experimental frequencies of occurrence from Figure 5.6 and classic Poisson distribution probabilities for "adjusted λ_t " in the 100msec-window.
Diamond-on-sapphire, large burst output.

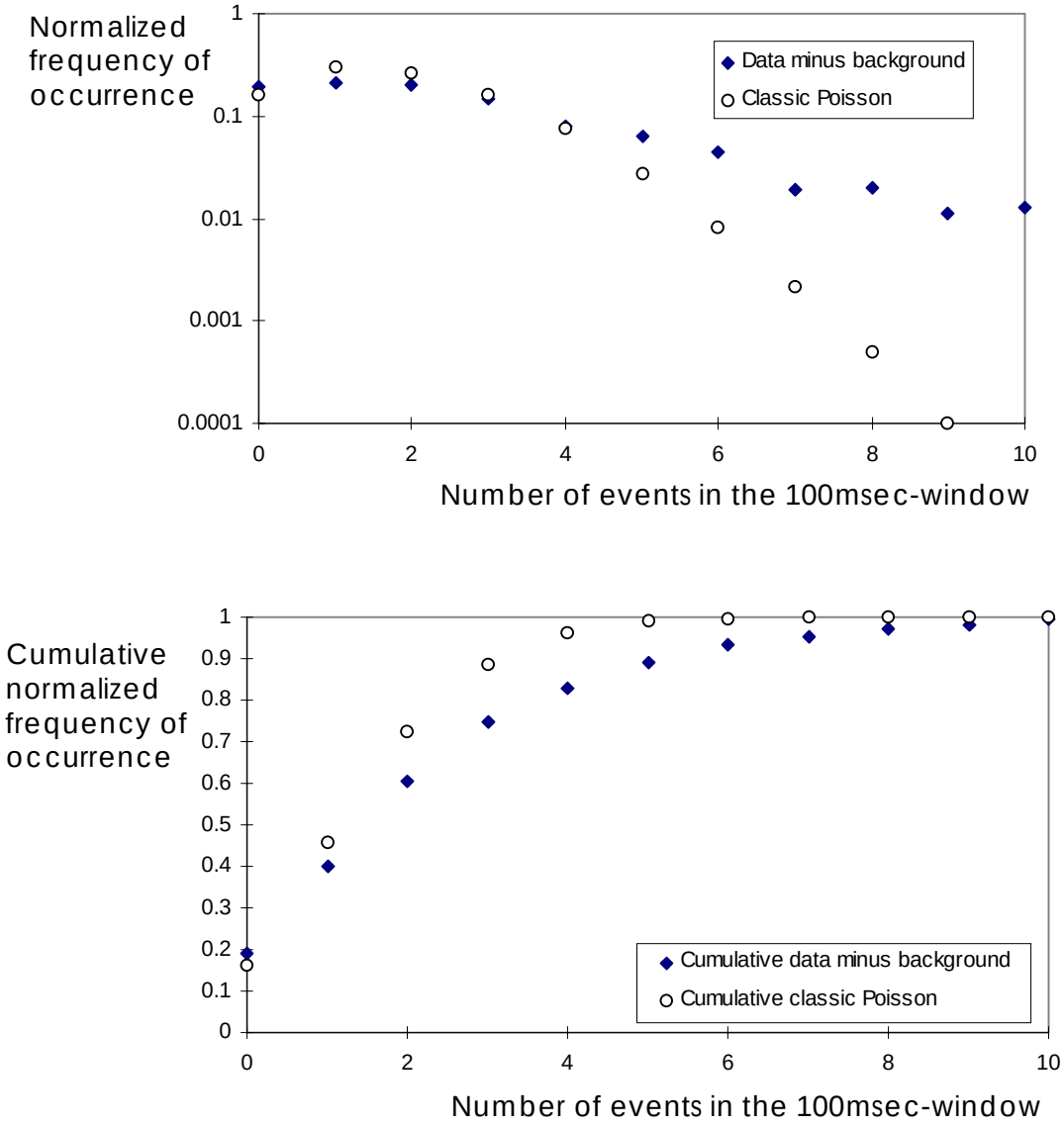

Figure 5.12.Experimental frequencies of occurrence from Figure 5.6 and classic Poisson distribution probabilities for "adjusted λ_t " in the 40msec-window.
Diamond-on-sapphire, large burst output.

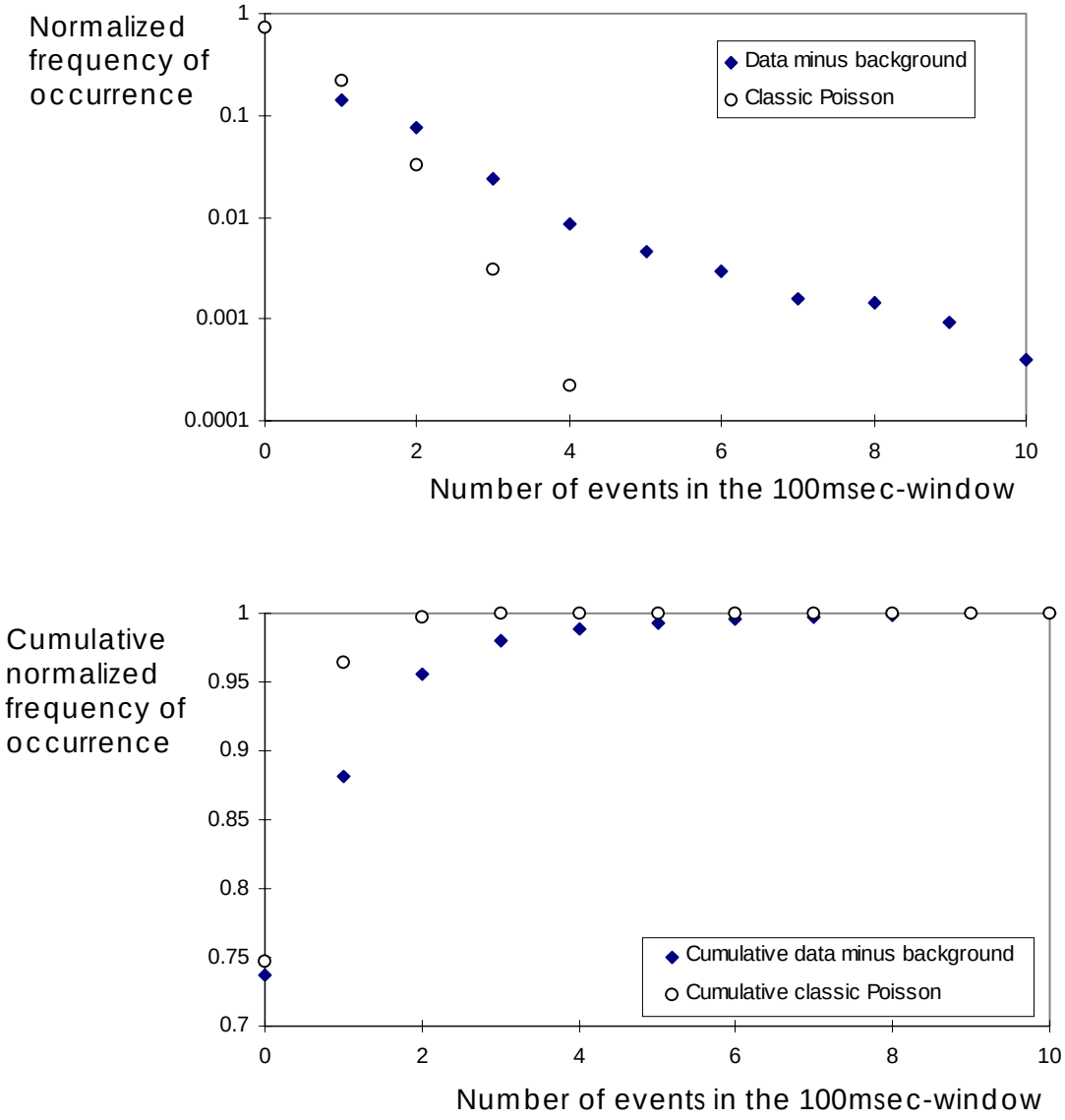

Figure 5.13.Experimental frequencies of occurrence from Figure 5.6 and classic Poisson distribution probabilities for "adjusted λ_t " in the 250msec-window.
Diamond-on-sapphire, large burst output.

In general, while a low value of the average rate of occurrence (λ_b in formulae 5.1) allowed a partial fit to the probability of zero-event, a much higher value would be needed for the probability of a larger number of events in the bin. Similar unsuccessful attempts were made to fit an exponential distribution [133] to the triboemission data. None of such distributions passed statistical testing for "goodness-of-fit."

It was clear that neither Poisson nor exponential distributions, which are single parameter descriptions, can explain the complexities of triboemission data. It was concluded, however, that a new distribution, which was developed from the Poisson's, may describe the triboemission pattern. The following subsection introduces such a probability distribution.

5.2.2. "Convoluted Poisson" probability distribution to describe triboemission data

A new probability distribution is designed and proposed to describe the experimental triboemission data in the frequency domain. Such probability distribution for the occurrence of n events (e.g., for the occurrence of n triboemitted particles) in a bin of chosen length is named "Convoluted Poisson", and it is based in the following assumptions:

(i) "Primary events" occur as described by a classic Poisson probability-distribution for a constant rate of event-occurrence per window-length λ_p. From this assumption, the pertaining Poisson probability density p(y) (i.e., the probability of occurrence of y primary events in the bin) is expressed as:

$$p(y) = \frac{(\lambda_P t)\ e^{-(\lambda_P t)}}{y!} = p(y, \lambda_P t) = p_y \qquad (5.2)$$

where: λ_p is the constant rate of event-occurrence per window-length (in events per time-window length),
t is the window-length (e.g., the bin length) of representation, and
y is the predicted number of primary events in the bin.

(ii) “Secondary events” occur as described by a Poisson probability-distribution for a constant rate of event occurrence <u>per primary-event</u> λ_s . From this assumption, the pertaining Poisson probability density s(z) (i.e., the probability of occurrence of z secondary events in the bin) is expressed as:

$$s(z) = \frac{(\lambda_S y)\ e^{-(\lambda_S y)}}{z!} = s(z, \lambda_S y) = s_{z,y} \qquad (5.3)$$

where: λ_s is the constant rate of event occurrence <u>per primary-event,</u>

y is the predicted number of primary events in the bin, and

z is the predicted number of secondary events in the bin.

By the above definition, the probability for secondary event occurrence in a bin depends on the primary-event occurrence in such bin.

(iii) The total number n of predicted events is the sum of the predicted primary and secondary events:

$$n = y + z \qquad (5.4)$$

On the above three assumptions, the probability density [p × s (n)] of the total number n of events for the “Convoluted Poisson” distribution can be expressed as:

$$[p \times s(n)] = \sum_{j=1}^{n} p_j\ s(n-j, \lambda_S j) \qquad (5.5)$$

Appendix A presents a detailed development of the above formulation. Also, the cumulative probability [P $\times$ S (n)] for this “Convoluted Poisson” distribution is simply:

$$[P \times S(n)] = \sum_{k=0}^{n} [\, p \times q(k) \,] \qquad (5.6)$$

The above definition of the "Convoluted Poisson" probability distribution also gives formula for the distribution mean and standard deviation, from numerically generated data (see Appendix A), as follows:

$$\text{mean}[\, p \times s(n)] = (\lambda_P t)(1 + \lambda_S) \qquad (5.7)$$

$$\text{variance}[\, p \times s(n)] = (\lambda_P t)(\lambda_S + (1 + \lambda_S)^2) \qquad (5.8)$$

It is apparent from the above two formula, that both mean and variance of the “Convoluted Poisson” can be substantially larger than those of the original classic Poisson distribution (in such case both mean and variance are equal to λ_b in equation 5.1). The presented formulation of “Convoluted Poisson” was implemented in Microsoft™ Excel™ for the purposes of fitting to experimental triboemission data and testing of such fits, as presented in the following subsection.

5.2.3. Testing of proposed “Convoluted Poisson” distribution for triboemission data.

This subsection presents the testing of the hypothesis that the “Convoluted Poisson” probability distribution reasonably describes the experimental estimation of the probability of occurrence minus the background noise for triboemission data. For each of the four cases of Figures 5.3 to 5.6, which were described in subsection 5.2.1, the proposed distribution was fitted to the experimental data in frequency domain. To adjust the two parameters of the “convoluted Poisson” distribution (i.e., λ_p and λ_s), the criterion was employed of minimizing the Chi-square statistics [133] computed from the two sets of probabilities (i.e., for experimental data and for the proposed distribution) in the

100msec-window. Since the characteristic decay-time of observed triboemission bursts is of about 100msec (See section 4.3), this window-length was assumed adequate to this fit.

The four examples of triboemission data in section 4.3 were investigated for this fit. They comprise two different types of output for each of the two material systems (i.e., diamond-on-alumina and diamond–on-sapphire): one type of output, called “constant-level” type, features a constant lower-level of small-burst emission, while the other, called “large burst” type, has superimposed a higher-level of triboemission bursts (See Figures 4.10 and 4.13 in section 4.3).

For each of these four examples in the 100msec-window, the probabilities from the proposed "Convoluted Poisson" distribution were computed for the best fit to the experimental probabilities of occurrence, according to the criterion of minimizing the Chi-square statistics. Both probability density and pertaining cumulative probability were computed.

The Chi-square goodness-of-fit test [133] was used to evaluate the fit. The computation of Chi-square, which is employed for both fit and goodness-of-fit testing, requires that the frequency of occurrence for the number x of events must be at least five events in all the considered bins [133]. For the analyzed triboemission data, this minimum frequency of occurrence is consistently obtained in the range of zero to about 12 events (See Figure 5.1). Such minimum is not usually reached, however, for a number of events higher than 12. Therefore, the fit procedure was limited to that range of number of events (i.e., to the range of zero-event to twelve-event cutoff). Data in this fitted range include, however, a minimum 91% of the acquired bins (e.g., of the total acquisition time).

Values of the two adjusted parameters λ_P and λ_S , and the mean (as per formula 5.7) for the proposed distribution are shown in following Table 5.1. Also, an “average triboemission-rate” (Average (*) column in Table 5.1) can also be obtained from the below-cutoff data in each case, by just computing the total number of comprised events over the effective acquisition time (i.e., total acquisition time minus non comprised bins).

Table 5.1. Values of λ_P, λ_S , and mean (as per formula 5.7) from adjustment of "Convoluted Poisson" distribution to triboemission data.

Diamond on	Large burst	λ_P	λ_S	Mean	Average (*) triboemission-rate
Alumina	NO	1.40	3.7	6.58	6.49
Sapphire	NO	1.28	3.5	5.76	6.79
Alumina	YES	0.56	1.2	1.23	1.19
Sapphire	YES	6.80	0.48	10.06	11.03

(*) As computed from "below cut-off data" after subtracting background noise of 0.7 counts/sec

The comparison of such average from the triboemission data and the mean of the "Convoluted-Poisson" in Table 5.1 shows that the proposed distribution can closely predict the rate of triboemission, at least for the data comprised below-cutoff.

Figures 5.14 to 5.17 show the plots for experimental probabilities from the triboemission data, and for computed probabilities in the proposed "Convoluted Poisson" distribution, for the four investigated cases in the 100msec-window. Both probability density and pertaining cumulative probability are shown in each figure.

Since the fit of the proposed distribution to experimental data should be independent of window-length, the goodness-of-fit testing was carried out for the same data in three different windows of representation (e.g., in the 40msecond- and 250msecond-windows, in addition to the 100msecond-window of reference). For this, no adjustment of the parameters λ_P and λ_S was made, but the values for the 100msecond window were employed in the three windows investigated. Figure 5.18 shows a plot that summarizes the Chi-square confidence levels obtained for the four tested cases in these three windows.

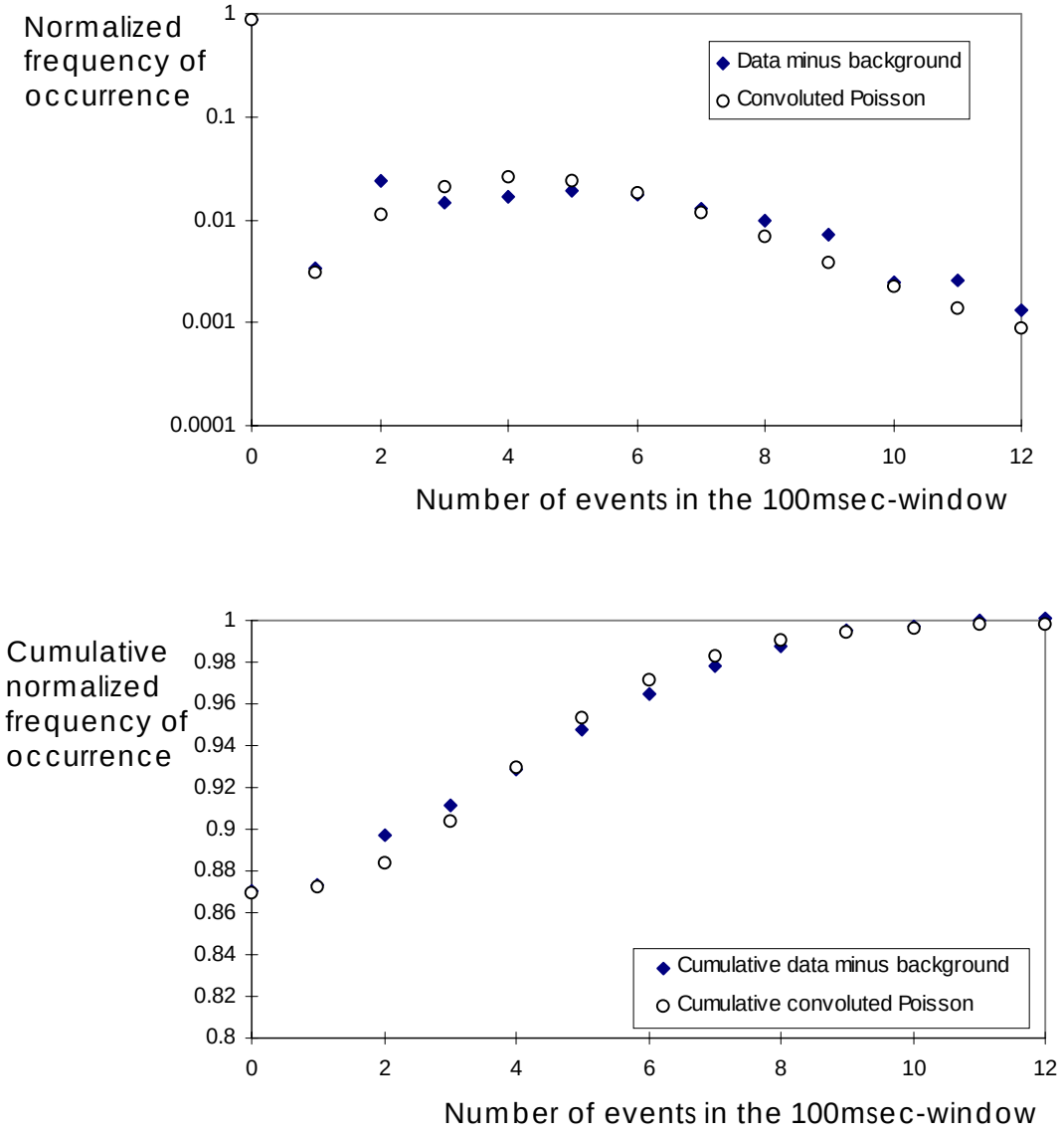

Figure 5.14. Experimental frequencies of occurrence from Figure 5.3 and "Convoluted Poisson" probabilities in the 100msec-window. Diamond-on-alumina, constant level output.

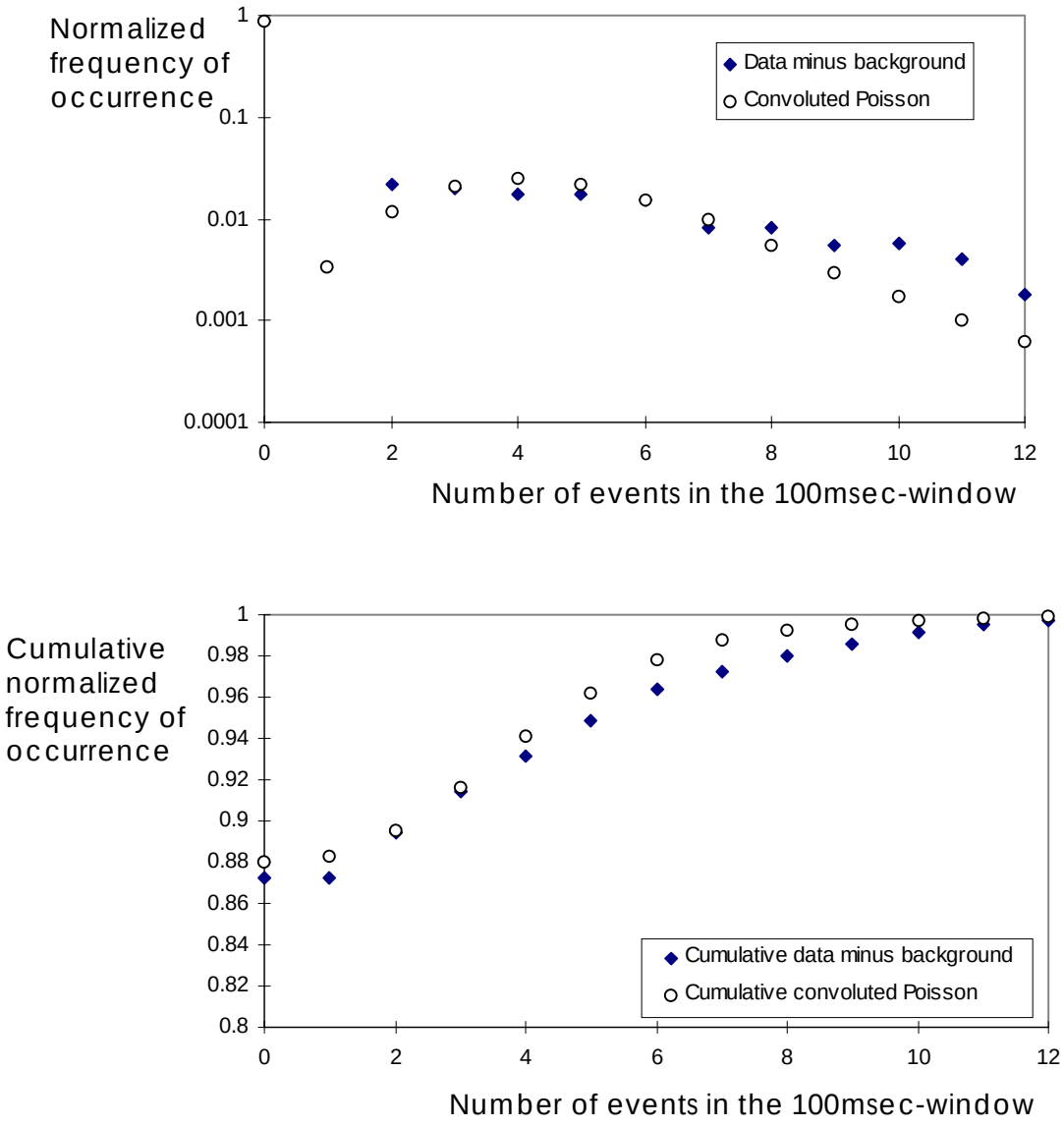

Figure 5.15. Experimental frequencies of occurrence from Figure 5.4 and "Convoluted Poisson" probabilities in the 100msec-window. Diamond-on-sapphire, constant level output.

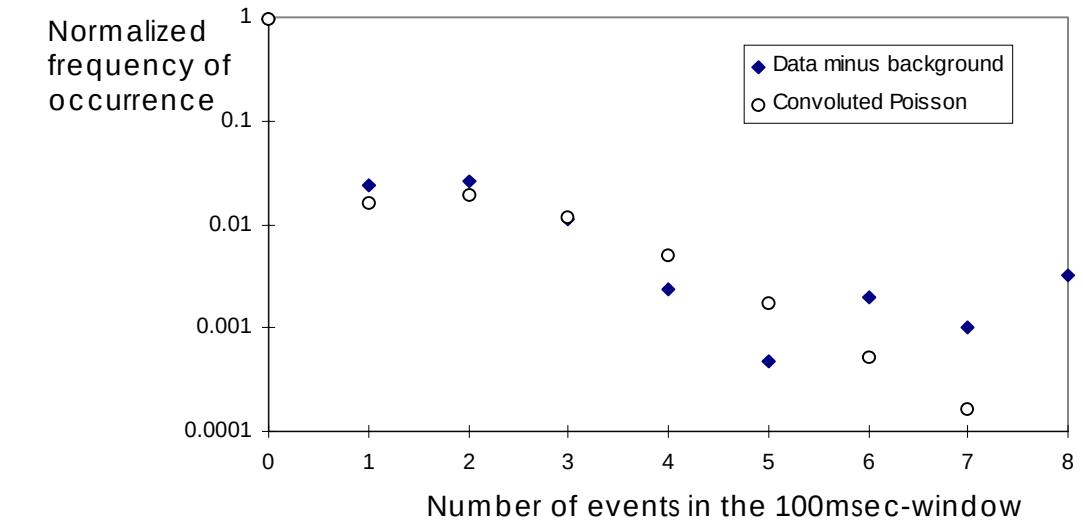

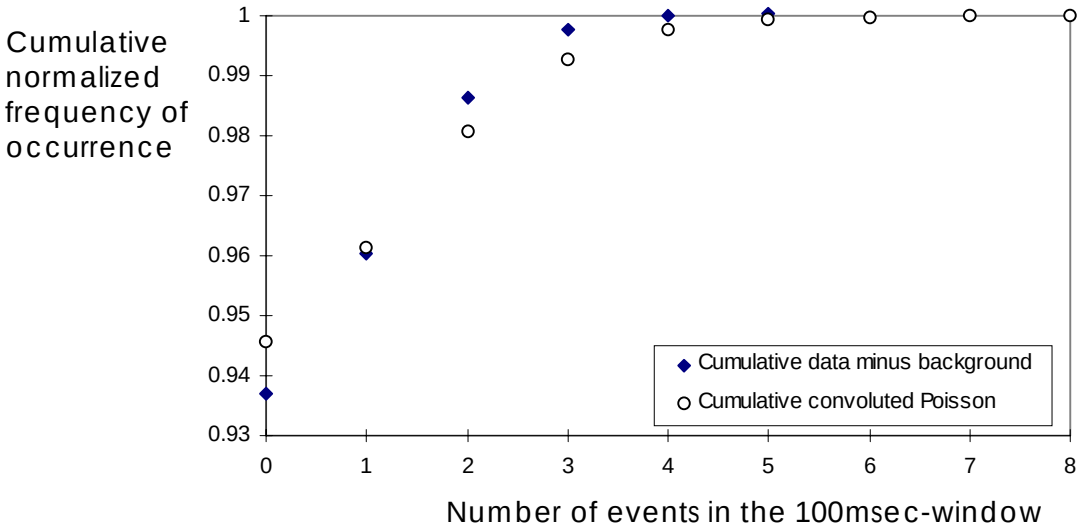

Figure 5.16. Experimental frequencies of occurrence from Figure 5.5 and "Convoluted Poisson" probabilities in the 100msec-window. Diamond-on-alumina, large burst output.

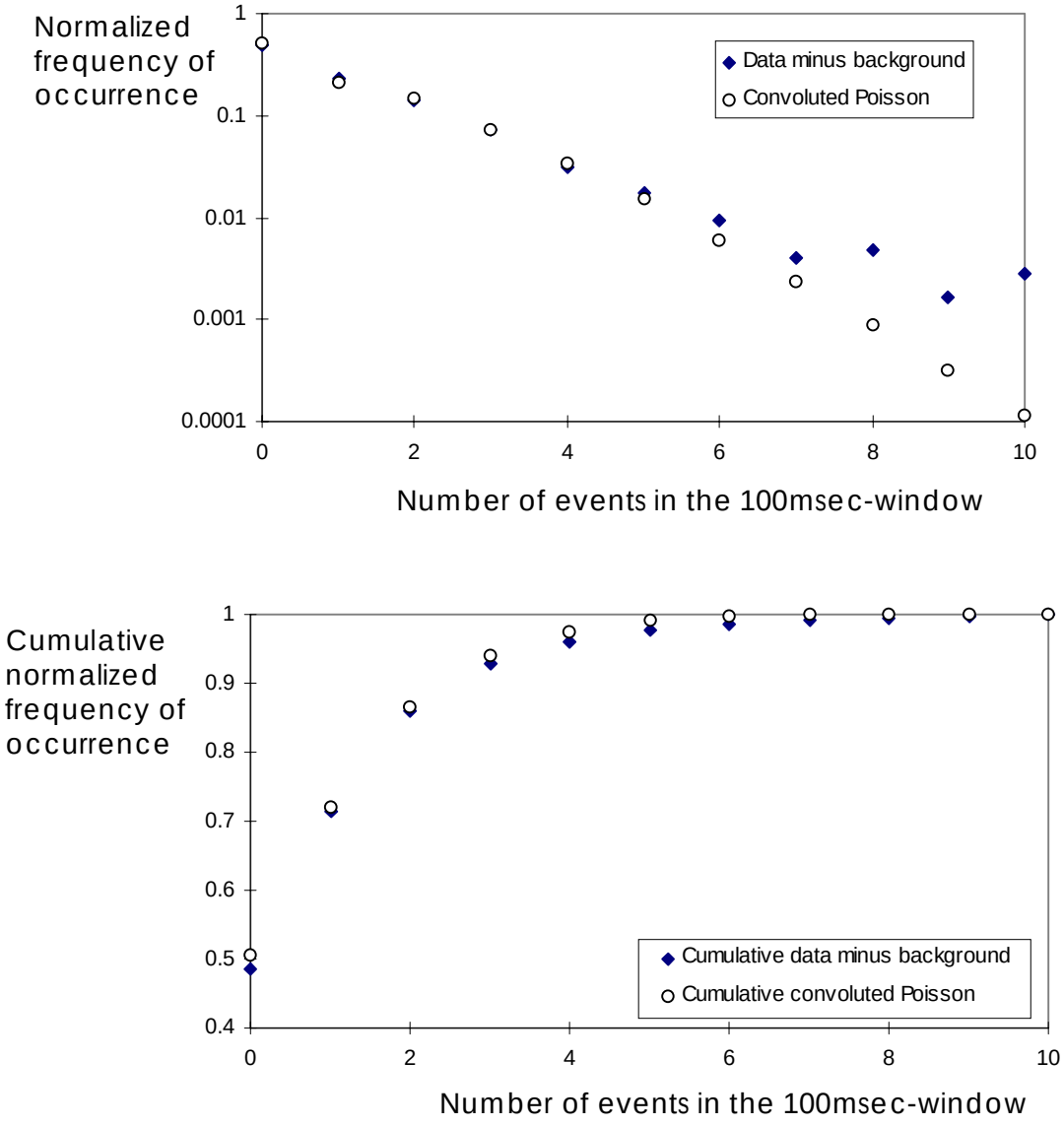

Figure 5.17. Experimental frequencies of occurrence from Figure 5.6 and "Convoluted Poisson" probabilities in the 100msec-window. Diamond-on-sapphire, large burst output.

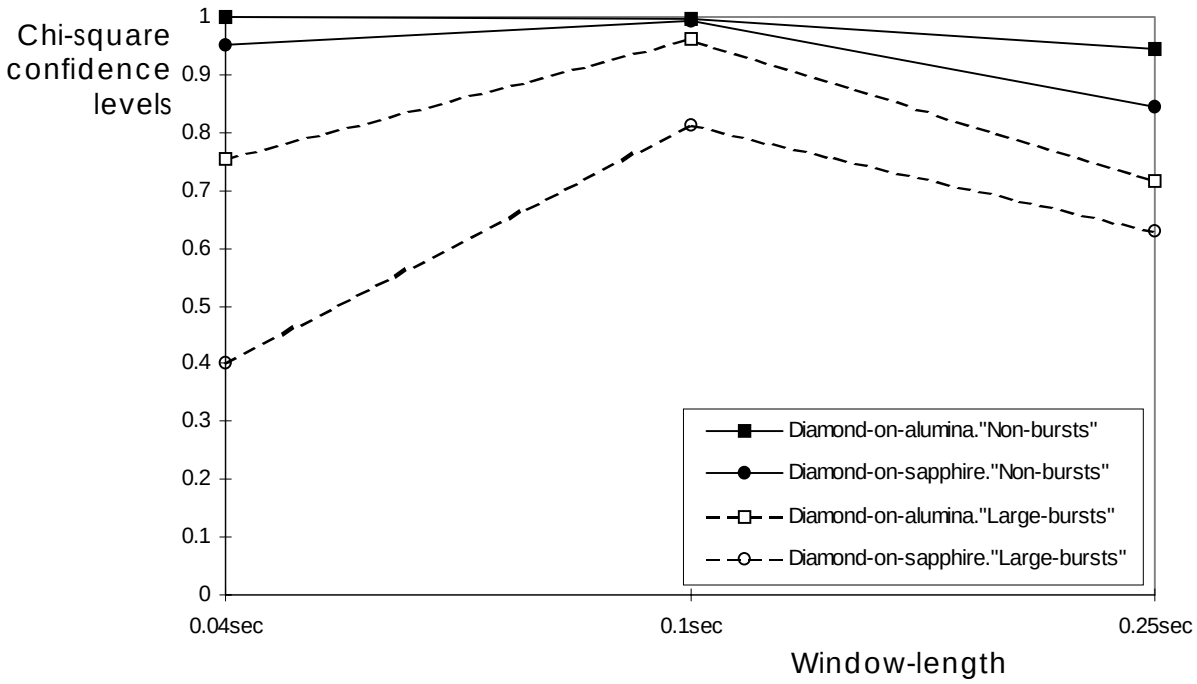

Figure 5.18. Chi-square confidence levels for testing of goodness-of-fit. “Convoluted Poisson” fit to experimental data in three windows of representation.

Good confidence, reasonably independent of window-length, was obtained for the fit of proposed distribution to “constant-level” experimental data. However, for the cases of “large-burst” type of data, the fit of the proposed distribution may not be completely independent of window-length.

5.2.4. Discussion of the proposed “Convoluted Poisson” distribution

The above testing of section 5.4.3 indicates that the proposed “Convoluted Poisson” probability distribution is adequate to describe triboemission data, at least the fraction of triboemitted electrons pertaining to the constant level of small-burst emission. The sporadic high-bursts of triboemission are not, however, well described by the proposed distribution. In the latter case, the proposed fit of “Convoluted Poisson” distribution does not include the fraction of data above the twelve-event cutoff. This may influence the testing since, for “large-burst” data, the amount of non-included information above cutoff is of higher relative importance.The frequency domain representation, however, provides a powerful analytical tool to discriminate “constant level” from “large burst” triboemission, because they clearly present different patterns.

The “Convoluted Poisson” probability-distribution is proposed as a model to describe experimental triboemission data. The two "Convoluted Poisson" parameters λ_P and λ_S may have interpretation in terms of the tribological process. It is apparent from the descriptive model that a two-stage tribological process, which is associated with each burst of triboemission, may exist: one stage of “primary-event” triboemission, which is described by a constant independent rate λ_P , closely followed by another stage of “secondary-event” triboemission, which is described by a constant rate λ_S . Therefore, the latter stage must be determined by the former. A variety of surface mechanisms may be proposed to explain such process.

One possible mechanism requires the assumption that triboemission from ceramics would proceed from initiation and growing of surface microfracture. The possibility that exoemission originates from such surface changes was discussed in section 5.1. In this, triboemission primary-events may correspond to the occurrence of an initial surface

microfracture. The triboemission secondary-events that follow may pertain to secondary microfractures, which must be related to the initial microfracture.

Two schemes may be proposed to explain such a relationship: microfracture branching may originate from the initial crack , and/or steps of microfracture growing may proceed after the initial (primary) one. The time-scale in which a primary event and the following secondary events show to evolve (in a period shorter than the 10msec-window) may be compatible with the characteristic time for surface-microfracture evolution. Dickinson et al. [108] found that typical 0.1 mm surface-cracks in Al-oxide layers, when subjected to tensile strain, grew by fast intermittent steps in the 1microsecond-order.

In a following work [109], Dickinson et al. also found that the distribution in time of fractoemitted electrons with respect to originating cracks showed two distinct delay characteristics. One of them presented an exponential distribution for the occurrence of electrons during cracking with a 0.1microsecond time-constant. The second delay-characteristics, however, grouped fractoemitted electrons which occurred after the originating cracking with an exponential decay of 4 microsecond time-constant. These two groups may represent respectively, in the fractoemission field, the two types of events, i.e., primary and secondary events, which are found by frequency analysis of triboemission data in this dissertation research.

Another explanatory mechanism might be based on the initiation and growing of fresh surface, and on the assumption that this surface change, and not microfracture, would originate triboemission. A fresh-surface patch occurrence (e.g., by grain or particle pullout) should be followed by the creation of related secondary surface-patches. In this, it would be possible that an asperity or a loose material particle created new fresh-surface by scratching and interactions with the base surface. However, the time scale for such process would be orders of magnitude longer than that of the found sequence of triboemission primary to secondary events (which occurs within the 10msec or shorter period for the experimental triboemission data, see subsection 5.2.3) .

Although no detailed mechanism links surface microfracture to triboemission, there is a body of evidence, which was reviewed in sections 2.2 to 2.4, relating exoemission to surface microfracture and new surface creation. As discussed in section 5.1,

microfracture during tribological contact ultimately implies creation of fresh-surface and surface changes, which are thought to originate exoemission.

In section 4.2, further characterization of the burst-type triboemission phenomena was needed before investigating the effects of the factors load, speed and time: burst-type emission required a previous identification of adequate quantitative responses to describe random phenomena (See also section 5.1). The two parameters of the proposed characterization, or a combination of both in a single constant rate (as in formulae 5.7), may be such adequate responses. Experimental testing for the factors of interest could then be planned and carried out.

5.2.5. Frequency-domain analysis for retarded-energy data.

Section 4.4 showed that energy-spectra of negatively-charged triboemission from ceramics presented a characteristic decaying shape for increasing retarded-energy of triboemitted particles: an important fraction of triboemitted particles was found in the zero to 5eVolts range of kinetic energy. It has been shown in this chapter that a pattern characterized triboemission-data in the frequency domain, and that the proposed “Convoluted Poisson” probability distribution can describe such patterns.

This subsection presents testing to explore if such frequency-domain pattern may depend on the kinetic-energy of particles. To this, four tests with different retarding-grid voltages, -5Volts, -10Volts, -50Volts and -100Volts, were carried out for negatively-charged triboemission from diamond-on-sapphire sliding contacts. The acquired triboemission outputs were transformed to frequency domain, subtracted background noise and compared to the “Convoluted Poisson” as described in subsection 5.2.1. Figures 5.19 to 5.22 show the frequency-domain description for these experimental data and the fit of “Convoluted Poisson” distribution as per the procedures of subsection 5.2.3.

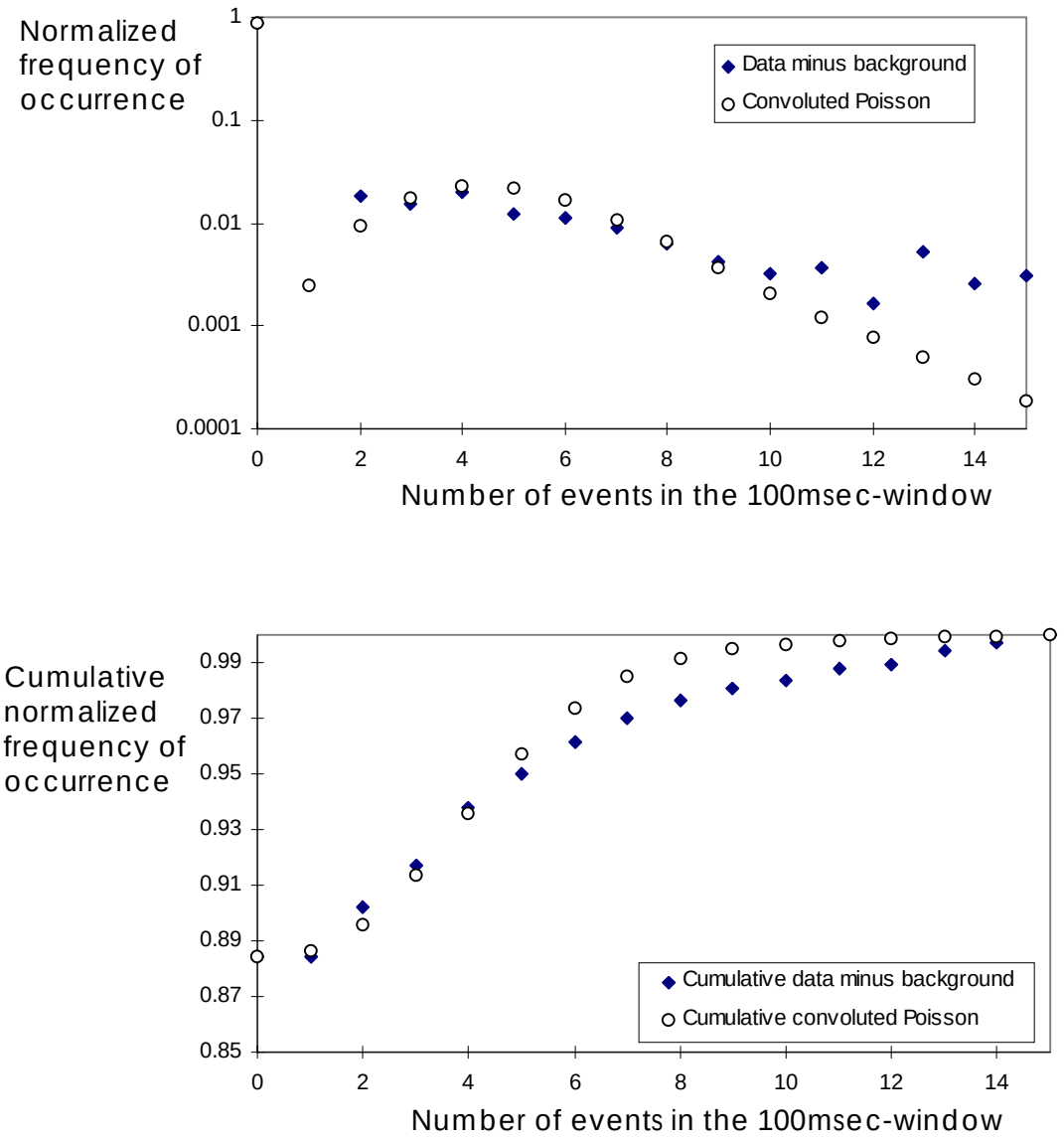

Figure 5.19. “Convoluted Poisson” probabilities in the 100msec-window and experimental frequencies of occurrence for triboemission with grid voltage: -5Volts. Diamond-on-sapphire sliding system.

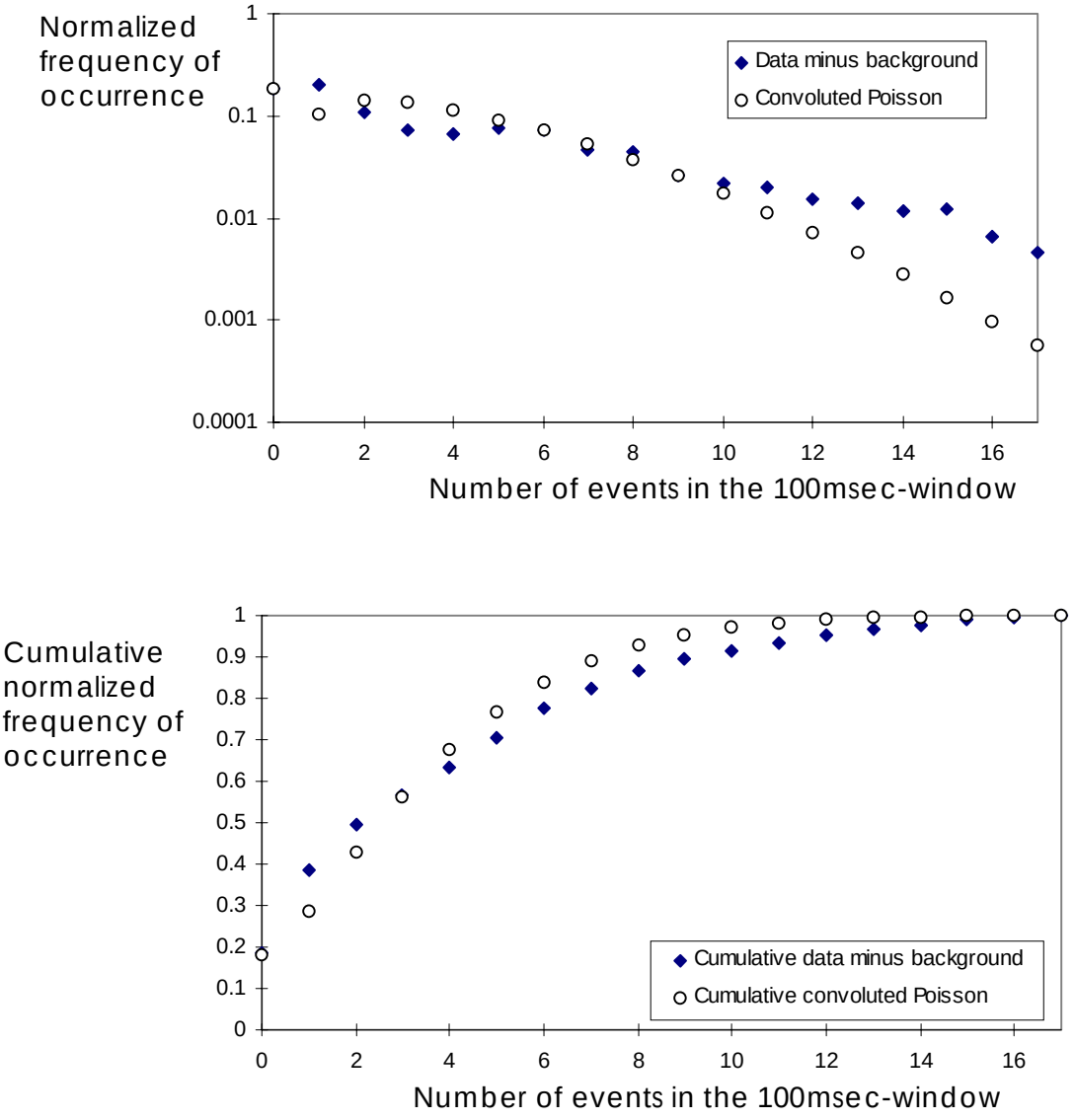

Figure 5.20. “Convoluted Poisson” probabilities in the 100msec-window and experimental frequencies of occurrence for triboemission with grid voltage: -10Volts. Diamond-on-sapphire sliding system.

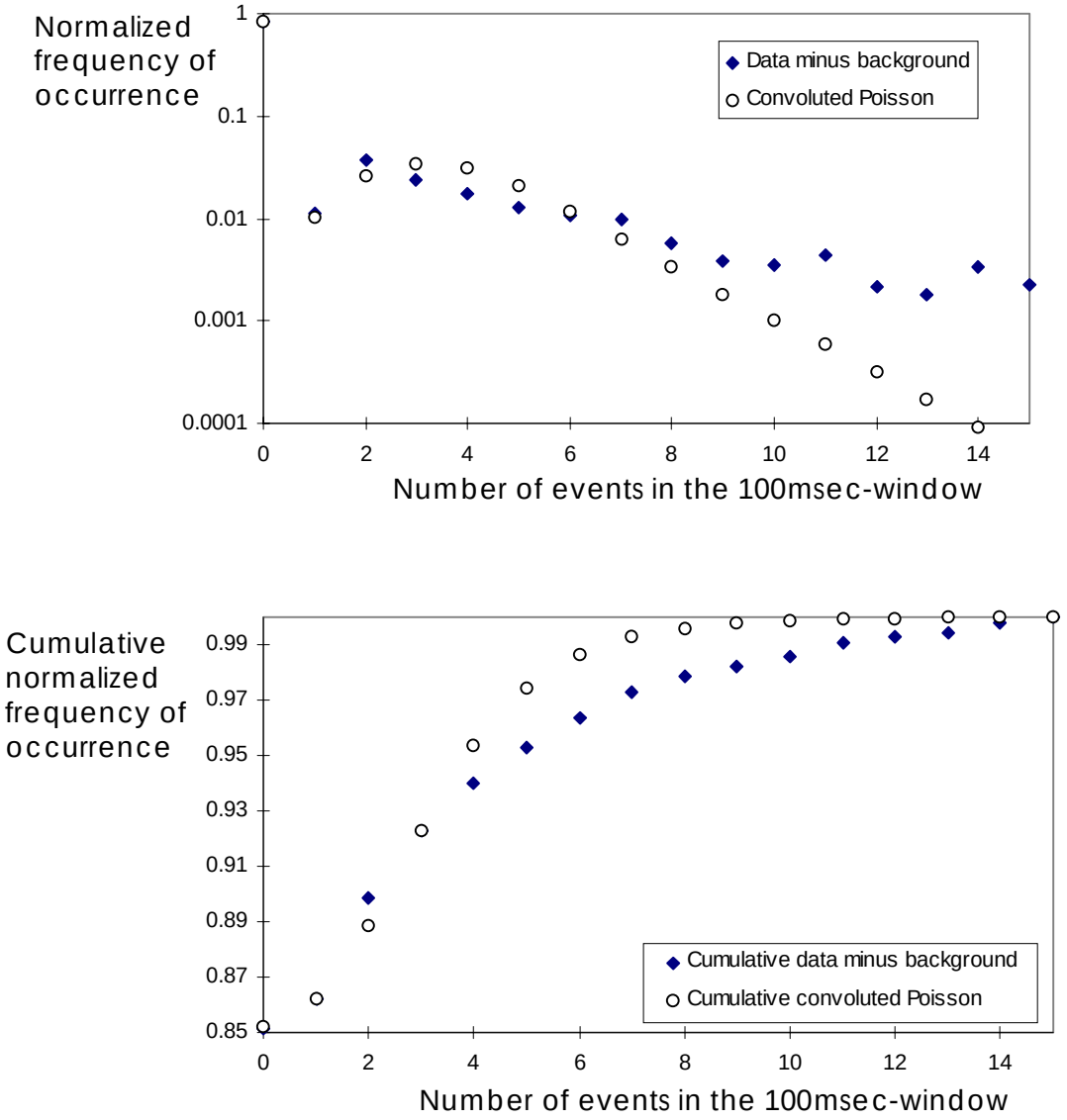

Figure 5.21. “Convoluted Poisson” probabilities in the 100msec-window and experimental frequencies of occurrence for triboemission with grid voltage: -50Volts. Diamond-on-sapphire sliding system.

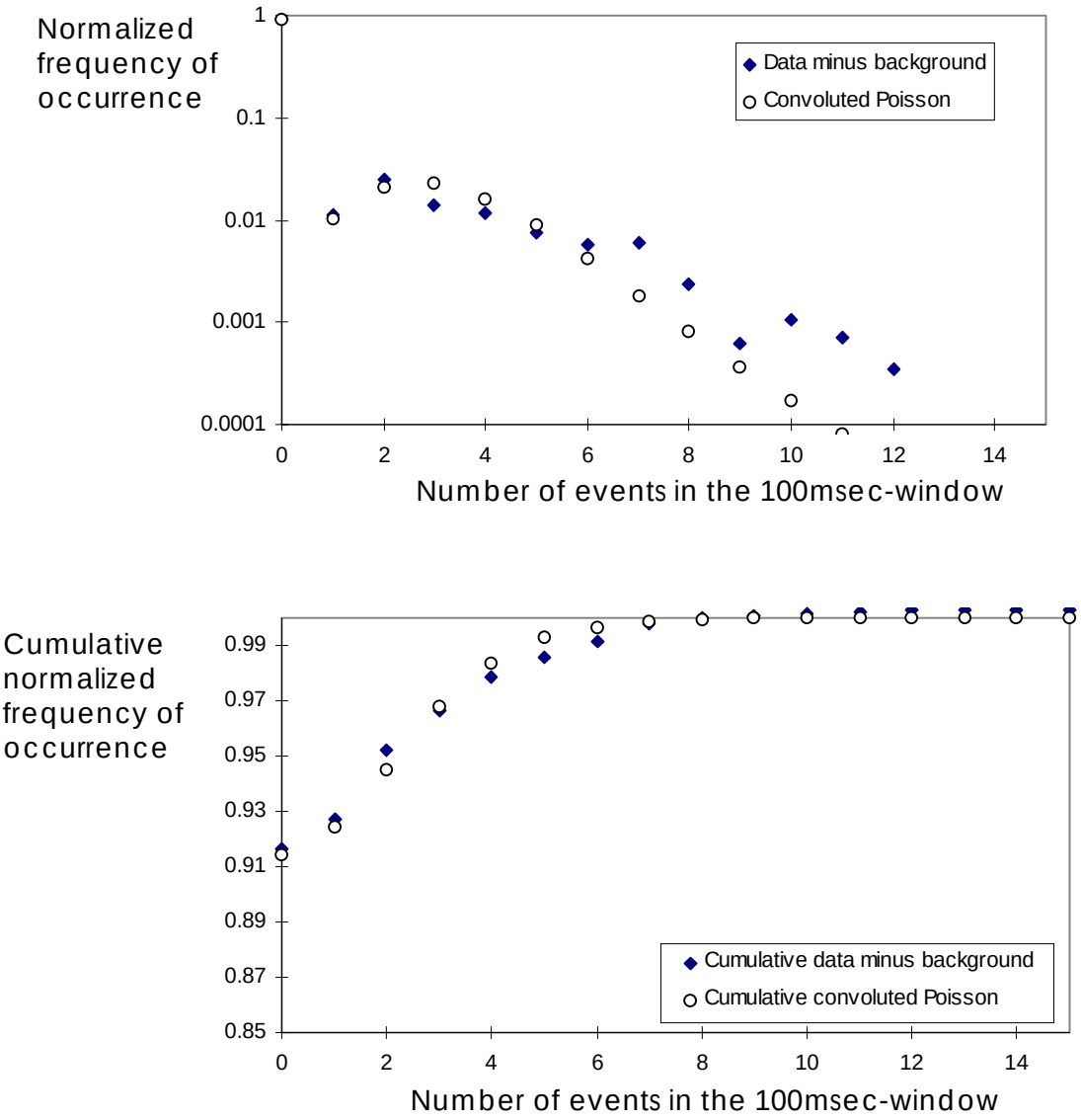

Figure 5.22. “Convoluted Poisson” probabilities in the 100msec-window and experimental frequencies of occurrence for triboemission with grid voltage: -100Volts. Diamond-on-sapphire sliding system

Figures 5.19 to 5.22 show that the characteristic pattern of triboemission data in the frequency-domain is not be substantially affected by screening of low-energy electrons (i.e., by the use of negative-voltage retarding-grid), at least for the retarding potentials used, e.g., as high as -100Volts. Good agreement is observed between the “Convoluted Poisson” probabilities and the experimental estimations of probability of occurrence for these retarding-grid data. The successful use of frequency domain and the “Convoluted Poisson” distribution for the tests in this subsection indicates that both can be tools to analyze energy spectra of triboemission from ceramics.

CHAPTER 6. CONCLUSIONS

One main purpose of the research reported in this dissertation was to design, construct and develop a new triboemission instrument. Appropriate experimental techniques, which accounted for the fast changing burst-type triboemission phenomena, were also designed and developed. This instrument and methodology were employed for the purpose of experimentally measure charged-particles triboemitted from ceramics. These low-energy particles are believed to be important in tribochemical reactions and, in particular, in anionic tribopolymerization of addition-type monomers. In this chapter, conclusions from the design and development of the new triboemission instrument are presented. Also, main conclusions from the triboemission measurements of Chapter 4 and the analysis of Chapter 5 are included.

Initial instrument designs showed that Faraday-cups presented several operational limits, which make them inadequate at the expected picoAmp-level of triboemission currents. In particular, temperature-dependent paths for leakage currents and triboelectric-currents in coaxial cables were found to be major sources of noise. It was concluded that a detector other than a Faraday-cup-type was needed for the very low currents involved in triboemission. Also, a good vacuum was required for low-energy triboemitted electrons to reach such a detector.

The new triboemission instrument designed provides high vacuum between the emitting surface and the particle detector in order to observe low-energy particles. It allows measurements of charge intensity for both negative and positive charge particles, and of kinetic energy of such triboemitted particles. The new instrument is able to accommodate different geometries, including the classical pin-on-disk for contact pairs of either different materials (A-on-B systems) or same material (A-on-A systems). It gives control of load and speed in a broad range of contact conditions.

This new instrument demonstrated the feasibility of performing in-vacuum measurements of charge intensity and retarded-energy of triboemitted charged-particles from ceramics. A channel electron multiplier (CEM) in the pulse-count mode was shown appropriate for such measurement. Pulse counting-technique and data-acquisition sampling rate of 100 Hz were found compatible with the required time-resolution.

Burst-type low-energy electron triboemission was measured from diamond-on-alumina, diamond-on sapphire, and alumina-on-alumina sliding contacts. Decaying electron-triboemission was also observed after the contact ceased in such systems. Although no definitive conclusion was drawn on the effects of operating conditions (e.g., load and sliding speed) on triboemission levels, it is possible that triboemission depend on time and wear, and also on complex interactions of such factors.

Different time-delay values for the occurrence of large bursts of triboemission were found for the triboemission outputs from alumina-on-alumina and those from diamond-on-ceramics, at least for the loads and speeds employed. It is possible that different wear conditions occur, because of the different contacts on the ceramic surfaces (i.e., diamond scratching versus alumina ball sliding). These different wear behaviors may be connected to the occurrence of the largest bursts of triboemission, the measured levels of electron triboemission and the post-contact emission after contact ceased. However, the relation between wear and surface changes and triboemission features is still unclear.

While similar levels of negatively-charged triboemission were observed from diamond-on-alumina and diamond-on-sapphire, both materials of same chemical composition but different crystal structures and properties, lower electron-emission was observed for the same sliding conditions on their metal element (e.g., aluminum). Statistically significant differences were obtained for the negatively-charged triboemission outputs during contact vs. CEM counts during non-contact (i.e., background noise) for these three material systems. However, no statistically significant difference was found for the triboemission outputs during contact of diamond-on-alumina vs. those of diamond-on-sapphire.

The weak emission from aluminum is believed to originate from the wear of the surface oxide-layer. Also, weak positive-ion triboemission is observed from both diamond-on-ceramic and ceramic-on-ceramic system. No statistical difference was found for the positively-charged triboemission outputs during contact vs. CEM count during non-contact (i.e., background noise) for the diamond-on-alumina, diamond-on-sapphire, diamond-on-aluminum, and alumina-on-alumina systems. Given the small differences

between contact positive-ion outputs and background, it is possible that samples larger than the ones employed may be needed to show statistical differences. It is believed, however, that triboemitted electrons interact with remaining gas species (existing at the vacuum level employed) producing positive ions immediately above the wear track. It is concluded that both weak negatively-charged triboemission from aluminum and positive-ion emission from the ceramics are marginal examples of the dominant exoelectron triboemission. On these assumptions, positive-ion and diamond-on-aluminum energy spectra are of less interest for the purposes of this research.

Energy spectra of negatively-charged triboemission from diamond-on-alumina and diamond-on-sapphire extend for energy levels higher than the test maximum-level, 48 eVolts. However, spectra show that important fractions of negatively-charged particles are emitted in the zero to about 5 eVolts, with only a decaying tail extending beyond this 48 eVolts highest retarding potential of the measurement.

Particle triboemission in the zero to about 5eV energy-range may be enhanced by some secondary electron emission from interactions of higher-energy particles in the vicinity of the wear track. Higher-energy emission results from patches of electrostatic charge on the sliding surfaces. The overall effect of triboemission and these added interactions is shown in the measured retarding-energy spectra.

It is concluded that triboemission from alumina and sapphire is essentially a low-energy electron burst-type intermittent phenomenon. In general, large bursts of electron triboemission may appear superimposed on a constant lower level of small-burst emission. This constant level, being higher than background-noise, does not vary significantly between different ceramic specimens, while maximum levels of triboemission-bursts differ by two orders of magnitude between different specimens. The constant low-level of small-burst emission, which is observed for longer periods of time, is an important component of the triboemission phenomenon. Also, the characteristic decay-time of the triboemission bursts is about 100mseconds.

These experiments show that low-energy electrons are emitted from alumina and sapphire surfaces under rubbing contact, the essential first step in the hypotheses of tribopolymerization of certain addition-type monomers presented by Furey and Kajdas. The findings of the present research, that low-energy exoelectrons are significantly triboemitted from alumina under wear conditions, while positively-charged emission is negligible, strongly confirms their line of thought. Furey and Kajdas' main hypothesis – that low-energy electrons initiate and control the formation of radical-anion reactives from some vinyl monomers – receives strong support.

The occurrence of triboemission bursts was found neither related nor coincident to any external or measured variables, but seems to be of random occurrence. It is thought that triboemission originates, at the microscopic scale, from surface changes: in particular, for the severe plowing of diamond-on-ceramics, triboemission may occur during surface microfracture from a mechanism similar to that of fractoemission. However, microfracture during tribological contact proceeds not only by surface cracking but also by grain and particle pullout, both mechanisms that create new surface.

Both the constant small-burst triboemission level, and the large superimposed bursts relate to surface microfracture and/or fresh surface creation. It is believed that the two characteristics stages of alumina wear (i.e., mild and severe stages of wear, see section 5.1) are connected with electron triboemission from alumina. The mild regime of wear, occurring at the beginning of sliding, may correspond to initial low intensity triboemission. The large bursts of triboemission which follow for diamond-on-alumina sliding contact – at least for the load and speed employed – seem to relate to the severe regime of wear, and to surface microfracture.

In the case of the alumina-ball on an alumina-disk, the largest bursts of triboemission may occur after minutes of sliding contact at the onset of microfracture, and during the so-called severe stage of alumina wear. Dickinson et al. [95] related burst occurrences in the reciprocating scratching of MgO by diamond to sporadic stick-slip behavior. However, the sliding speed values employed in the experiments of this dissertation research are not typical of stick-slip regimes.

It is possible that the lower constant-level of triboemission may originate from continuous wear in the sliding process. Although strong connections are found between wear features in ceramics (e.g., microfracture, surface creation) and triboemission of charged particles, the experimental picture is still unclear.

The frequency domain description reveals a characteristic pattern of this triboemission-component. The experimental probabilities of occurrence for a given number of events, minus those for background-noise occurrence, present a similar pattern for all analyzed triboemission data, and a single type of probability distribution of events can describe most of the acquired triboemission data.

A probability distribution, called "Convoluted Poisson", was successfully designed and tested for the description of triboemission data in the frequency domain. This probability-distribution was proved to be an adequate model to describe the experimental triboemission outputs. In particular, this model describes the fraction of triboemission data pertaining to the constant level of triboemission: Good confidence was obtained for the fit of the proposed distribution to the "constant-level" type of experimental data. However, for the cases of "large-burst" type data, the fit of the proposed distribution is not completely independent of window-length, and not all such data are appropriately described by the “Convoluted Poisson” distribution.

The two "Convoluted Poisson" parameters λ_P and λ_S describe any single triboemission burst as a two-stage tribological process. The first stage of primary triboemission is described by λ_P and is followed by another stage of secondary triboemission, which is described by λ_S .

A mechanism can be proposed, based on the assumption that triboemission from ceramics would proceed from initiation and growing of surface microfracture and/or fresh surface. In this, triboemission primary-events would correspond to the initiation of a surface microfracture. The triboemission secondary-events that follow in the same triboemission burst would pertain to secondary microfracture, which should be related to primary-cracks. In terms of surface phenomena, microfracture branches may evolve from the initial (primary) one in growing steps: the time-scale for the proposed mechanism may be compatible with the characteristic time for microfracture evolution.

CHAPTER 7. RECOMMENDATIONS FOR FUTURE RESEARCH

The research work presented in this dissertation provides fundamental experimental knowledge on the charge intensity and energy distributions of triboemitted charged-particles from ceramics. It also explores possible relations of these distributions to operational and material variables. However, the experimental picture relating triboemission to sliding contact and material variables is still incomplete. A new instrument, data acquisition system, and adequate measurement methodologies are made available from this research work to investigate such unknowns regarding triboemission. Further knowledge on triboemission phenomena will be of importance for a deeper understanding of the role of particle emission in tribochemical processes and, in particular, in tribopolymerization as a mechanism of ceramic lubrication.

The possible effects of contact load, sliding speed and time on triboemission from ceramics should be experimentally sorted out. In this, the likely complex interactions between these three factors should be considered when designing experimental testing. Appropriate outcomes to describe triboemission are needed for the design of such experiments: The parameters of the proposed frequency-domain characterization model (in section 5.2), or a convenient combination of them, may be useful.

The correlation of wear to triboemission should be experimentally explored. In this, the evolution in time of both phenomena should be measured in the experiments: The decrease of triboemitted-particle production, which in this research work related to the repeated transit of a diamond or an alumina ball on the same wear-track, should be correlated in time to decreasing wear and/or decreasing creation of fresh surfaces. For this, surface characterization techniques (e.g., profilometry, scanning electron microscopy) should be employed.

Comparative measurements for closely related materials (e.g., alumina, sapphire and aluminum) gave fundamental information about the influence on triboemission of different material contacts. Experimental work should be carried out to extend this knowledge to other ceramic groups (e.g., Si_3N_4 , SiC and Si). Also, triboemission data from some typical semiconductors (e.g., Ge, Si) will be of importance. Semiconductors

have some electrical properties (e.g., electrical conductivity) which range in between those of insulator and conductor materials.

The experimental measurements of triboemission in this dissertation research are in good agreement with Furey and Kajdas' hypotheses and findings about the tribopolymerization mechanism, as discussed in section 5.2. If these hypotheses are true, it should be expected to see correlations between the intensity and charge of triboemitted particles and the efficacy of particular monomers to reduce wear. The particle detector employed is limited, however, to operate at vacuum pressures lower than 10^{-5} Torr. The new triboemission instrument did not allow, at the present stage of development, the simultaneous testing for monomer effects during the measurement of particles.

It is known from previous research [82,115] that photon triboemission may correlate with electron triboemission. Such correlation, if effectively proven for the systems investigated, may be used to measure photons instead of electrons: photon detectors are fully compatible with simultaneous monomer atmospheres and tribopolymerization experiments. Another way of testing tribopolymerization hypotheses may be the use of ultraviolet irradiation on the test specimens to cause low-energy electron emission by the photoelectric effect. Such electron emission, both during and after irradiation, may be employed to initiate tribopolymerization and to investigate the antiwear effects of selected monomers. Although some unknowns need to be answered about such experimental methods, the new triboemission instrument should be used to readily test them.

A probability distribution, called "Convoluted Poisson", was designed and successfully tested for the description of triboemission data in the frequency domain. However, for the cases of "large-burst" type data, the fit of the proposed distribution was not completely independent of window-length, and the data are not well described by the proposed distribution. A general model should be developed to describe also these large-bursts. The model should include time and/or wear as parameters.

Another modeling possibility is a predicting scheme for total rate emission, which may be developed from material and operation conditions as parameters. The assumption of a characteristic stochastic process for the electron triboemission can be made, where the total probability of triboemission occurrence per unit area and the characteristic evolution in time of a triboemission-emitting surface-process should be included. These components may be integrated in a discrete or continuous sense. The values of parameters for such models (e.g., surface properties, applied load and speed, characteristic decay period) should be determined from existing triboemission data, by using parameter estimation methods.

In carrying out the research work of this dissertation, it was found that triboemission may be affected by the effects of electrostatic charges, which are eventually built up on the sliding surfaces and may accelerate triboemitted charged-particles after emission. The phenomenon of surface charge on ceramics should be investigated for its effects on triboemission of charged particles. The work of Dickinson et al. [95,134] proposed some adequate experimental techniques on the use of surface-charge probes (e.g., transient current dynamic-probes) for the measurement of electrostatic charge on tribological systems. Some of the recommendations outlined in this chapter are currently applied in continued research as part of the NSF project [2] that funded this dissertation research.

CHAPTER 8. REFERENCES

[1] Furey,M.J., Kajdas,C., Models of Tribopolymerization as an Anti-Wear Mechanism, Proc. Japan International Tribology Conference, Nagoya, Japan, 1990, pp.1089-1094.

[2] Furey,M.J., Ritter,A., Kajdas,C., Triboemission of Charged Particles from Ceramic Surfaces and Their Role in Tribochemistry, research proposal to National Science Foundation, Surface Engineering and Tribology Program, 1995.

[3] Suh,N.P., Tribophysics, Prentice-Hall, New Jersey, 1986.

[4] Kajdas,C., Physics and Chemistry of Tribological Wear, Proceedings of the 10th International Colloquium on Tribology: Solving Friction and Wear Problems, Plenary lectures, January 9-11, 1996, Technische Akademie Esslingen, Ostfildern, Germany, W.J.Bartz (editor), Vol.1, 1996, pp.37-62.

[5] Heinicke,G., Tribochemistry, Carl Hanser Verlag, Munich, Germany, 1984.

[6] Furey,M.J., Tribology, in: Encyclopedia of Materials Science and Engineering, Bever,M.B.(editor), Pergamon Press, New York, NY, 1986, pp.5145-5157

[7] Carey-Lea,M., Disruption of the Silver Haloid Molecule by Mechanical Force, Philosophical Magazine, 34, 1892, pp.46-50.

[8] Carey-Lea,M., On Endothermic Reactions effected by Mechanical Force (First Part), Philosophical Magazine, 36, 1893, pp.351-354.

[9] Carey-Lea,M., On Endothermic Decompositions obtained by Pressure (Second Part). Transformations of Energy by Shearing Stress, Philosophical Magazine, 37, 1894, pp.31-37.

[10] Carey-Lea,M., Transformations of Mechanical into Chemical Energy (Third Paper). Action of Shearing Stress, Philosophical Magazine, 37, 1894, pp.470-475.

[11] Parker, L.H., Reactions between Solid Substances, J.Chem.Soc., 113, 1918, pp.396-409.

[12] Gilman,J.J., Science, Vol. 274, Oct.4, 1996, p.65.

[13] Shaw,M., The Chemico-Physical Role of the Cutting Fluid, Metal Progress, Vol.42, 1942, pp.85-88.

[14] Grunberg,L, The Formation of Hydrogen Peroxide on Fresh Metal Surfaces, Proceedings of the Physical Society, Vol.66, 1953, pp. 153-161.

[15] St.Pierre,L.E., Owens,R.S., Klint,R.V., Chemical effects in the boundary lubrication of aluminum, Wear, 9, 1966, pp.160-168.

[16] Rosenfeld,L., Gas Release During Wear, Wear, 33, 1975, pp.391-394.

[17] Rosenfeld,L., Gas Release During Wear, Wear, 40, 1976, pp.165-177.

[18] Fox, P. G., Review. Mechanically Initiated Chemical Reactions in Solids, J. Mat. Sci., 10, 1975, pp.340-360.

[19] Singer,I.L., Mechanics and Chemistry of Solids in Sliding Contacts, Langmuir, Vol.12, No.19, 1996, pp.4486-4491.

[20] Preis,G.A., Dziub,A.G., Electrochemical phenomena in metal friction, Trenie i Iznos, Vol.1, No.2, 1980, pp.217-235.

[21] Tamai,Y., Role of mechanochemical activity in boundary lubrication, in: Fundamentals of Tribology, N.P.Suh and N.Saka (editors), MIT Press, Cambridge, MA, 1980, pp. 975-980.

[22] Furey, M.J., Kajdas, C., Tribopolymerization as a Novel Approach to Ceramic Lubrication, Proceedings of the 4th International Symposium on Ceramic Materials and Components for Engines, Carlsson,R., Johansson,T., and Kahlman,L. (editors), Swedish Ceramic Society, Goteborg, Sweden, June 10-12, 1991, pp.1211-1218.

[23] Furey,M.J., The formation of polymeric films directly on rubbing surfaces to reduce wear, Wear, 26, 1973, pp.369-392.

[24] Furey,M.J., The 'in situ' formation of polymeric films on rubbing surfaces, Proceedings Colloques Internationaux du C.N.R.S., Brest, France, 1975, No 233 - Polymeres et Lubrification, Centre National de la Reserche Scientifique, Paris, France, 1975, pp.393-404.

[25] Furey, M.J., Kajdas, C., Tribopolymerization as a Lubrication Mechanism for High-Energetic Contacts of Solids, Proceedings of the 6th International Tribology Colloquium, January 12-14, 1988, Technische Akademie Esslingen, Germany, 1988.

[26] Furey, M.J., Kajdas, C., Ward,T.C., Hellgeth,J.W., Thermal and catalytic effects on tribopolymerization as a new boundary lubrication mechanism, Wear, 136, 1990, pp.85-97.

[27] Furey, M.J., Kajdas, C., Kempinski, R., Tripathy, B.S, Tribopolymerization and the behavior of oxigen-containing monomers in reducing ceramic wear, Proceedings of the Eurotrib'93 Congress, Aug.30-Sept.2, Budapest, Hungary, Vol.2, 1993, pp.477-484.

[28] Furey, M.J., Ghasemi, H., Tripathy, B.S. Kajdas, C., Kempinski, R., Hellgeth, J.W., Tribochemistry of the Antiwear Action of a Dimer Acid/Glycol Monoester on Alumina, Tribology Transactions, 37, 1994, pp.67-74.

[29] Furey, M.J., Kajdas, C., Kempinski, R., Tripathy, B.S, Effects of selected monomers on wear reduction of steel and ceramics under high contact stress lubrication, Proceedings of the Fourth International Tribology Conference Austrib’94, December 5-8, 1994, Perth, Australia, Vol.II, 1994, pp.741-750.

[30] Kajdas, C., Lafleche,P.M., Furey, M.J., Hellgeth,J.W., Ward,T.C., A Study of Tribopolymerization under Fretting Contact Conditions, Lubr.Sc., 6-1, 1993, pp.51-89.

[31] Smith,J.C., Furey, M.J., Kajdas, C., An exploratory study of vapor-phase lubrication of ceramics by monomers, Wear, 181-183, 1995, pp.581-593.

[32] Furey, M.J., Tritt,B.R., Kajdas, C., Kempinski,R., Lubrication of Ceramics by Tribopolymerization. A Designed Experiment to Determine Effects of Monomer Structure, Load, and Speed on Wear, Tribology Transactions, Vol.42, 4, 1999, pp.833-841.

[33] Kajdas,C., On a Negative-Ion Concept of EP Action of Organo-Sulfur Compounds, ASLE Transactions, 28, 1983, pp.21-30

[34] Kajdas,C., About a Negative-Ion Concept of the Antiwear an Antiseizure Action of Hydrocarbons During Friction, Wear, 101, 1985, pp.1-12.

[35] Kajdas,C., About an Ionic-Radical Concept of the Lubrication Mechanism of Alcohols, Wear, 116, 1987, pp.167-180.

[36] Kajdas, C., Importance of Anionic Reactive Intermediates for Lubricant Component Reactions with Friction Surfaces, Lubrication Science, 6-3, 1994, pp.203-228.

[37] Kajdas, C., Furey, M.J., Kempinski, R., Tribopolymerization: II. NIRAM Applications to the Antiwear Action of Addition-Type Monomers, Proceedings of the 2nd International Symposium on Tribochemistry, Sept. 15-17, 1997, Janowice near Cracow, Poland, Polish Tribology Society, 1997, pp.127-139.

[38] Furey, M. J., Kajdas, C., Kempinski, R., Tripathy, B., Action Mechanism of Selected Vinyl Monomers Under Boundary Lubrication of an Alumina-on-Alumina System, Lubrication Science, 10, 1997, pp.3-25.

[39] Tripathy,B.S., A New Approach to Ceramic Lubrication: Tribopolimerization, Ph.D. dissertation, Virginia Polytechnic Institute and State University, Blacksburg, Virginia, July 1995.

[40] Kajdas,C., Furey,M.J., Kempinski,R., Tribopolymerization: I. Surface Temperatures and the Antiwear Action of Condensation-Type Monomers, Proceedings of the 2nd International Symposium on Tribochemistry, Sept. 15-17, 1997, Janowice near Cracow, Poland, Polish Tribology Society, 1997, pp.115-125.

[41] Furey,M.J., Vick, B., Foo,S.J., Weick,B.L., A Theoretical and Experimental Study of Surface Temperatures Generated During Fretting, Proceedings of the Japan International Tribology Conference, Nagoya, Japan, 1990, Vol. II, pp. 809-814.

[42] Vick,B., Furey,M.J., Iskandar,K., Surface Temperatures Generated by Friction with Ceramic Materials, Tribology Transactions, Vol.42, 4, 1999, pp.888-894.

[43] Herring,C., and Nichols,M.H., Thermionic Emission, Review of Modern Physics, Vol.21, No.2, 1949, pp.185-270.

[44] Cardona,M., Ley,L., Photoemission in Solids I. General Principles, M.Cardona and L.Ley (editors), Topics in Applied Physics Vol.26, Springer-Verlag, Berlin, Germany, 1978, pp.1-104.

[45] Bell,A.E., Barofski,D.F., Field Emission and Field Ionization, in: Encyclopedia of Applied Physics, Vol.6, CH Publishers, New York, NY, 1993, pp.379-391

[46] Ohmae,N., Nakayama,K., Mori, S., Exoelectrons and Tribology, Japanese J. of Tribology, Vol.40, No5, 1995, pp.355-362.

[47] Robertson, A.J.B., Exoelectron emission from solids, Int. J. Electronics, Vol.51, No5, 1981, pp.607-619 .

[48] McLennan, J.C., On a kind of Radioactivity imparted to certain Salts by Cathode Rays, The Philosophical Magazine and Journal of Science, Vol.III, Sixth series, January-June 1902, pp.195-203.

[49] Kramer,J., Der metallische Zustand, Vanderhoek and Ruprecht, Goettingen, Germany, 1950.

[50] Nakayama,K., Andino Leiva,J., Hashimoto,H., Chemi-Emission of Electrons from Metal Surfaces in the Cutting Process Due to Metal/Glass Interactions, Tribology International, Vol.28, No8, 1995, pp.507-515.

[51] Sato,N., Seo,M., Chemically Stimulated Exo-Emission from a Silver Catalyst, Nature, 216, 1967, pp.361-362.

[52] Moucharafieh, N., Olmsted, J., Chemiemission from Cesium-Oxygen Surface Reaction, J. Phys. Chem., 75, 1971, pp.1928-1936.

[53] Gesell, T.F., Arakawa, E.T., Callcott, T.A., Exo-Electron Emission During Oxygen and Water Chemisorption on Fresh Magnesium Surfaces, Surf. Sc., 20, 1970, pp.174-178.

[54] Gesell, T.F., Arakawa, E.T., Work Function Changes During Oxygen Chemisorption on Fresh Magnesium Surfaces, Surf. Sc., 33, 1972, pp.414-421.

[55] Ferrante J., Exoelectron Emission From a Clean, Annealed Magnesium Single Crystal During Oxygen Adsorption, ASLE Transactions, 20, 4, 1977, pp. 328-332.

[56] Rabinowicz E., Exoelectrons, Scientific American, 236, 1977, pp.74-81.

[57] Baxter,W.J., Measurement of Surface Fatigue Damage by Exoelectron Emission, Metallurgical Transactions A, Vol.6A, 1975, pp.749-754

[58] Baxter,W.J., Rouze,S.R., Photo Electron Microscopy of Plastic Zone Around a Fatigue Crack, Metallurgical Transactions A, Vol.7A, 1976, pp.647-654.

[59] von Voss, W.D., Brotzen, F.R., Electron Emission from Plastically Strained Aluminum, J. Appl. Phys., Vol.30, No11, 1959, pp.1639-1645.

[60] Dus-Sitek, M., Olszowski, Z., Sujak, B., Optically Stimulated Exoelectron Emission for Determining the Degree of Hydrogen Embrittlement of Nickel, Proceedings of the 8th International Symposium on Exoelectron Emission and Applications, Japanese J. Appl. Phys., Vol.24, Supplement 24-4, 1985, pp.176-180.

[61] Markowski, L., Sujak, B., Possibilities of Optically Stimulated Emission (OSEE) Registration in the Nano- and Microsecond Range from CsCl, Phys. Stat. Sol.(a), 124/1, 1991, pp.273-278.

[62] Veerman,C., Registration and Mapping of Plastically Deformed Metal Surfaces by means of Photoelectrons, Materials Science and Engineering, 4, 1969, pp.329-342.

[63] Tomita, A., Fukuda, Y., Kutomi, Y., Takeuchi, N., Emission Processes in Thermally Stimulated Exoelectron Emission and Thermoluminescence of KCl: Ag Single Crystals. Phys. Stat. Sol.(b), 158, 1990, pp.383-389.

[64] Kamada, M., Yoshiara, K., Tsunumi, K., Energy Spectra of Thermally Stimulated Exoelectrons from KCl:Tl X-Irradiated at 77 K, Japanese J. Appl. Phys., Vol.23, No3, 1984, pp.286-290.

[65] Tagawa,M., Umeno,M., Ohmae,N., Takenobu,S., The Trap-Level of Exoelectron and Field-Stimulated Exoelectron Emission of High Purity Al, Japanese J. of Tribology, Vol.34, No10, 1989, pp.1175-1184.

[66] Hibbert, D. B., Goodman, A., Theoretical study of field-stimulated exoelectron emission, Int. J. Electronics, Vol.59, No6, 1985, pp.701-709.

[67] Enomoto, Y., Hashimoto, H., Photo-stimulated Exoelectron from Abraded Metals in Atmospheric Conditions, Japanese J. of Tribology, Vol.35, No3, 1990, pp.381-389.

[68] Scharmann,A., Grasser,R., Bohm,M., Thermally stimulated processes in solids, Proceedings of the International Workshop in Thermally Stimulated Processes in Solids, June 25-25, 1976, Montpellier, France, Fillard,J.P., van Turnhout,J.(editors), Elsevier, New York, 1977, pp.1-14.

[69] Shigekawa, H., Hyodo, S., Storage Effect in Photostimulated Exoelectron Emission from Scratched Aluminum, Japanese J. Appl. Phys., Vol.21, 1982, pp.1278-1282.

[70] Shigekawa, H., Iwatsu, R., Okada, M., Hyodo, S., Change of Energy Level Distribution of Photoemission Sources in Al and Zn Caused by Scratching, Japanese J. Appl. Phys., Vol.22, 1983, pp.42-45.

[71] Kreigseis, W., Sharman, A., Exoelectron Emission of ZnO, Phys. Stat. Sol. (a), Vol.29, 1975, pp.407-414.

[72] Grunberg, L., A survey of exoelectron emission phenomena, British Journal of Applied Physics, Vol.9, 1958, pp.85-93.

[73] Kobzev, N.I., Exoelectronic Emission, The Foreign Literature, Moscow, 1962.

[74] Ramsey, J.A., Garlick,G.F.J., Sensitized photoelectric emission during oxidation of aluminium, Brit. J. Appl. Phys., Vol.15, 1964, pp.1353-1360.

[75] Ramsey, J.A., Exoelectron Emission from Abraded Metal Surfaces at High and Ultrahigh Vacuums, J. Appl. Phys., 37, 1966, pp.452-453.

[76] Ramsey, J. A., The Emission of Electrons from Aluminium Abraded in Atmospheres of Air, Oxygen, Nitrogen and Water Vapour, Surf. Sci., 8, 1967, pp.313-322

[77] Momose,Y., Noguchi,M., Electron Emission during Frictional Contact between Metals and Polymers, Phys.Stat.Sol.(a), 82, 1984, pp.K83-K86.

[78] March,P.A., Rabinowicz,E., Exoelectron Emission for the Study of Surface Fatigue Wear, ASLE Transactions, Vol.20, No 4, 1977, pp.315-320

[79] Tagawa, M., Mori, M., Ohmae, N., Umeno, M., Takenobu, S., Tribo- and photo-stimulated electron emission from graphite, Tribology International, Vol.26, No.1, 1993, pp.57-60

[80] Nakayama,K., Fujiwara,T., Hashimoto,H. Exoelectron measurement in a scanning electron microscope, J. of Physics E, 17, 1984, pp.1199-1203.

[81] Nakayama,K., Hashimoto,H., Fukuda,Y., Triboemission from Aluminum Oxide Film in Atmosphere, Proceedings Japan International Tribology Conference, Nagoya, Japan, 1990, pp.1141-1146

[82] Nakayama,K., Hashimoto,H., Triboemission from various materials in atmosphere, Wear, Vol. 147, 1991, pp.335-343.

[83] Nakayama,K., Hashimoto,H., Susuki,T., Triboemission of Charged Particles and Photons from Solid Surfaces During Frictional Damage, J. of Physics D, Vol.25, 1992, pp.303-308.

[84] Nakayama,K., Hashimoto,H., Triboemission of Charged Particles and Photons from Wearing Ceramic Surfaces in Various Gases, Tribology Transactions, Vol.35, 4, 1992, pp.643-650.

[85] Nakayama,K., Triboemission of Charged Particles from Various Solids Under Boundary Lubrication Conditions, Wear, Vol.178, 1994, pp.61-67.

[86] Nakayama,K., Hashimoto,H., Effect of Surrounding Gas Pressure on Triboemission of Charged Particles and Photons from Wearing Ceramics Surfaces, Tribology Transactions, Vol.38, No1, 1995, pp.35-42.

[87] Nakayama,K., Hashimoto,H., Triboemission of Charged Particles and Photons from Wearing Ceramic Surfaces in Various Hydrocarbon Gases, Wear, Vol.185, 1995, pp.183-188.

[88] Nakayama,K., Hashimoto,H., Triboemission of Electrons and Ions During Wear of Solids Under Boundary Lubrication with Saturated Hydrocarbon Liquids, Tribology Transactions, Vol.38, 3, 1995, pp.541-548.

[89] Nakayama,K., Hashimoto,H., Triboemission, tribochemical reactions, and friction and wear in ceramics under various n-butane gas pressures, Tribology International, Vol.29, No 5, 1996, pp.385-393.

[90] Nakayama,K., Ikeda,H., Triboemission characteristic of electrons during wear of amorphous carbon and hydrogenated amorphous carbon films in a dry air atmosphere, Wear, Vol.198, 1996, pp.71-76.

[91] Nakayama,K., Hashimoto, H., Friction, Wear, and Triboelectron Emission of Hydrogenated Amorphous Carbon Films, Tribology Transactions, Vol.40, No3, 1997, pp.507-513.

[92] Dickinson,J.T., Jensen,L.C., Jahan-Latibari,A., Fracto-emission: The role of charge separation, J. Vac. Sci. Technol., A2(2), 1984, pp.1112-1116.

[93] Nakayama, K., Bou-Said, B., Ikeda, H., Tribo-Electromagnetic Phenomena of Hydrogenated Carbon Films. Tribo-Electrons, -Ions, -Photons, and -Charging, Journal of Tribology, Vol.119, Oct 1997, pp.764-768.

[94] Nakayama, K., Triboelectromagnetic phenomena in sliding contacts, Proceedings of the 2nd Symposium on Tribochemistry, 15-17 September 1997, Katowice near Cracow, Poland.

[95] Kim, M., Langford, S.C., Dickinson, J.T., Electron and photon emission accompanying the abrasion of MgO with diamond, Trib. Letters 1, 1995, pp.147-157.

[96] Dickinson, J.T., Scudiero, L., Yasuda,K., Kim,W., Langford, S.C., Dynamic tribological probes: particle emission and transient electrical measurements, Tribology Letters 3, 1997, pp.53-67.

[97] Scudiero, L., Dickinson, J.T., Enomoto, Y., The electrification of flowing gases by mechanical abrasion of mineral surfaces, Phys. Chem. Minerals, 25, 1998, pp.566-573.

[98] Grunberg,L., The study of freshly deformed metal surfaces with the aid of exo-electron emission, Wear, Vol.1, 1957/58, pp.142-154.

[99] Sujak, B, Gieroszynski, A., Gajda, R., Effect of oxide and of measuring parameters on the decay of photostimulated (exo)electron emission in vacuum from plastically deformed aluminum (Part I), Acta Physica Polonica, Vol.28, 3(9), 1965, pp.329-335.

[100] Gieroszynski, A., Sujak, B., Effect of oxide and of measuring parameters on the decay of photostimulated (exo)electron emission in vacuum from plastically deformed aluminum (Part II), Acta Physica Polonica, 28, 3 (9), 1965, pp.337-342.

[101] Sujak,B., Gierozynski,A., Dark emission of exoelectrons from plastically deformed aluminium covered with oxide and excited by electrons, Acta Physica Polonica, Vol.35, 1969, pp.667-678.

[102] Gieroszynski, A., Sujak, B., Exoelectron Emission in Vacuum in the Absence of Light During Plastic Deformation of Aluminum Thickly Coated with Oxide, Acta Physica Polonica, 28, 1965, pp.311-327

[103] Sujak,B., Gierozynski,A., Exoelectrons emission of surface-oxidized nickel during plastic deformation in vacuum, Acta Physica Polonica, Vol.A37, 1970, pp.733-740.

[104] Rosemblum,B., Carrico,J.P., Braunlich,P., Himmel,L., Measurement of tribo-emission from oxide-covered metals, Journal of Physics E, Vol.10, 1977, pp.1056-1062.

[105] Arnott,D.R., Ramsey, J.A., Electron emission from anodically oxidised aluminium due to tensile deformation, Surface Science, Vol.28, 1971, pp.1-18.

[106] Dickinson,J.T., Braunlich,P.F., Larson,L.A., Marceau,A. Characteristic Emission of Negatively Charged Particles During Tensile Deformation of Oxide-Covered Aluminum Alloys, Applications of Surface Science, 1, 1978, pp.515-537

[107] Larson,L.A., Dickinson,J., Braunlich,P.F., Snyder,D.B., Emission of neutral particles from anodized aluminum surfaces during tensile deformation, J. Vac. Sci. Technol., 16(2), 1979, pp.590-593.

[108] Dickinson, J.T., Donaldson,E.E., Snyder,D.B., Acoustic emission and electron emission during deformation of anodized aluminium, J. Vac. Sci. Technol., 17(1), 1980, pp.429-432

[109] Dickinson, J.T., Donaldson,E.E., Snyder,D.B., Emission of electrons and positive ions upon fracture of oxide films, J. Vac. Sci. Technol., 18(2), 1981, pp.238-242.

[110] Doering, D.L., Oda, T., Dickinson, J.T., Braunlich, P.F., Characterization of Anodic Oxide Coatings on Aluminum by Tribostimulated Exoemission, Applications of Surface Science, 3, 1979, pp.196-210

[111] Dickinson, J.T., Jensen, L.C., Park,M.K., Mass-to-charge ratio and kinetic energy of positive emission accompanying fracture of a filled elastomer, Appl. Phys. Lett., 41(9), 1982, pp.827-829.

[112] Dickinson, J.T., Jensen, L.C., Miles,M.H., Fractoemission accompanying adhesive failure between rocket propellant constituents, J. Appl. Phys., 62(7), 1987, pp.2965-2971.

[113] Yoo, K.C., Rosemeier, R.G., Dickinson, J.T., Langford, S.C., Anisotropic effects on fracto-emission from MgF_2 single crystals, App. Phys. Letters, 55(4), 1989, pp.354-356.

[114] Dickinson, J.T., Jensen, L.C., Langford, S.C., Hirth, J.P., Atomic and molecular emission following fracture of alkali halides: A dislocation driven process, J. Mat. Res., Vol.6, No1, 1991, pp.112-125

[115] Ma, Z., Dickinson, J.T., Fracto-emission from embedded surfaces, J. Appl. Phys., 70(9), 1991, pp.4797-4807

[116] Zimmerman,K.A., Langford,S.C., Dickinson, J.T., Electrical transients during interfacial debonding and pullout of a metal rod from an epoxy matrix, J. Appl. Phys., 70(9), 1991, pp.4808-4815.

[117] Dickinson, J.T., Jensen, L.C., Fractoemission from high density polyethylene: Bond breaking versus tribological stimulation, J. Appl. Phys., 73(6), 1993, pp.3047-3053

[118] Dickinson, J.T., Jensen, L.C., Lee, S., Scudiero, L., Langford, S.C.: Fractoemission and electrical transients due to interfacial failure, J. Adhesion Sci. Tech., Vol.8, No11, 1994, pp.1285-1309

[119] Dickinson,J.T., Langford, S.C., Nakahara,S., Scudiero,L., Hipps,K.W., Kim,M., Park,N., Spatial and temporal probes of fracture, wear and deformation, in: Fractography for Glasses and Ceramics III, J.R.Varner, V.D.Frechette and G.D.Quinn (editors), Ceramics Transactions, Vol.64, Westerville, Ohio, American Ceramic Society, 1995, pp.193-256.

[120] Dickinson, J.T., Jensen, L,C., Langford, S.C., Hoagland, R.G., Chemisorptive Exoelectron emission as a probe of plastic deformation in reactive metals, J. Mater. Res., 9, 1994, pp.1156-1165.

[121] Dickinson,J.T., Langford, S.C., Jensen,L.C., Recombination on fractal networks: Photon and electron emission following fracture of materials, J. Mater. Res., Vol.8, No11, 1993, pp.2921-2932.

[122] Enomoto,J., Hashimoto,H., Emission of Electrons and Ions during Indentation and Scratching of Brittle Crystals at Elevated Temperature Up to 400C in Air, Proceedings of the Japan International Tribology Conference, Nagoya, Japan, 1990, pp.1189-1194.

[123] C.Kajdas, M.J.Furey, A.L.Ritter, G.J.Molina, Triboemission as a Basic Part of the Boundary Friction Regime, Proceedings of the 12th International Colloquium Tribology 2000-Plus, Technische Akademie Esslingen, Ostfildern, Germany, January 11-13, 2000, Vol. III, pp.2075-2096.

[124] Keithley Instruments, Low Current Measurements, Keithley Application Note Series, No100, Test Instrumentation Group, Keithley Instruments, Inc., Cleveland, OH, 1994.

[125] Furey, M.J., Ritter, A.L., Vick, B., Molina, G.J., Kajdas, C., Triboemission and Surface Temperatures Generated in a Ball-in-Cone Tribocontact, Proc. 5th International Tribology Conference Austrib ’98, Brisbane, Australia, Dec. 6-9, 1998, The Institution of Engineers, Australia, Hargreaves, D.J., Scott, W. (editors), 1999, pp.257-262.

[126] Kurz, E.A., Channel electron multipliers, American Laboratory, March 1979, pp. 67-82.

[127] Schmidt,K.C., The Channeltron Electron Multiplier CEM 4010, Technical Applications Note 9803, Galileo Electro-Optics Corp, Sturbridge, MA, April 1969.

[128] Cho,S.J., Mooon,H., Hockey,B.J., Hsu,S.M., The transition from mild to severe wear in alumina during sliding, Acta metall. mater., Vol.40, No1, 1992, pp.185-192.

[129] Ying,T.N., Shen,M.C., Wang,Y.S., Hsu,S.M., Tribology of Si-Based Ceramics: Wear Mechanisms, Tribology Transactions, Vol.40, 4, 1997, pp.685-693.

[130] Kempinski,R., Malosse,P., Furey,M.J., Kajdas,C., Molina,G.J., Effect of Triboemitted Particles on the Tribological Behavior of Selected Monomers, Proceedings of the 9th Nordic Symposium on Tribology NORDTRIB 2000, June 11-14, 2000, Porvoo, Finland.

[131] Molina, G.J., Furey, M.J., Ritter, A.L., Kajdas, C., Triboemission from Alumina, Single Crystal Sapphire, and Aluminum, Proceedings 9th Nordic Symposium on Tribology NORDTRIB 2000, June 11-14, 2000, Porvoo, Finland.

[132] Molina, G.J., Furey, M.J., Ritter, A.L., Vick, B., Mazilu, D., Kajdas, C., Triboemission and Tribochemistry, Proc. American Physical Society Meeting, March 20-24, 2000, Minneapolis, MN, Bulletin of the APS, Series II, Vol.45, No.1, p.484.

[133] Lapin, L.L., Probability and Statistics for Modern Engineering, 2nd edition, PWS-Kent Publishing Co., Boston, MA, 1990, pp.135-141.

[134] Davenport,W.B., Probability and random processes, McGraw-Hill Book Co., New York, NY, pp.454-458.

[135] Dickinson,J.T., Scudiero,L., Langford,S.C., A Dynamic Probe of Tribological Processes at Metal/Polymer Interfaces: Transient Current Generation, in: Structure and Properties of Glassy Polymers, ACS Symposium Series 710, Tant,M.R., Hill,A.J. (editors), American Chemical Society, Washington, DC, 1998, pp.272-285.

APPENDIX A

Development of the "Convoluted Poisson" probability distribution

A new probability distribution is designed and proposed to describe the occurrence of n events in the window of length t as based in the following assumptions:

(i) "Primary events" occur as described by a classic Poisson probability-distribution for a constant rate of event-occurrence per unit-time λ_p (where the unit-time is the window-length). From this assumption, the pertaining Poisson probability density p(y) (e.g., for the probability of occurrence of y primary events in the bin) is expressed as:

$$p(y) = \frac{(\lambda_P t)\ e^{-(\lambda_P t)}}{y!} = p(y, \lambda_P t) = p_y \qquad (A.1)$$

where: λ_p is the constant rate of event-occurrence per unit-time, i.e., per window-length,

t is the window-length (e.g., the bin length) of representation, and

y is the predicted number of primary events in the bin.

(ii) "Secondary events" occurs as described by a Poisson probability-distribution for a constant rate of secondary event occurrence per primary-event λ_s . This assumption implies the underlying hypothesis that each primary event may independently produce secondary events. The pertaining Poisson probability density s(z) (e.g., for the probability of occurrence of z secondary events in the bin) is expressed as:

$$s(z) = \frac{(\lambda_S y)\ e^{-(\lambda_S y)}}{z!} = s(z, \lambda_S y) = s_{z,y} \qquad (A.2)$$

where : λ_s is the constant rate of event occurrence per primary-event,

y is the predicted number of primary events in the bin, and

z is the predicted number of secondary events in the bin.

By the above definition the probability for secondary event occurrence depends on the primary-event distribution through the number y of primary events. This probability $s_{z,y}$ can be alternatively interpreted as the conditional probability of occurrence of z secondary events, given the occurrence of y primary events.

The above two assumptions mean that for y the number of primary events occurring in a bin of length t and λ_s, the rate of secondary-event occurrence for the s(z) distribution given y primary events is a function of y and the constant rate λ_s as follows:

$$\text{mean}[\,s(z)] = y\ \lambda_S \qquad (A.3)$$

The above means that each primary event would independently produce secondary events at a constant rate λ_S.

(iii) The total number n of predicted events is the sum of primary and secondary events as obtained by the summation of primary and secondary events occurring in the bin:

$$n = y + z \qquad (A.4)$$

An underlying fourth assumption complements the above: secondary events produced by a primary one would show in the same bin of length t where the primary event showed (e.g., there is no carry-out effects on subsequent bins). These assumptions allow the following general formulation.

Assumption (iii) means that n events will be predicted in a bin when any combination of integer values for y and z adds up to exactly n. The probability [p × s (n)] of n events occurring in a bin of length t can be obtained by summation of all the combined probabilities of occurrence of y primary events and z secondary events adding up to n total number of events. A list follows of these combined probabilities for some simple cases.

The probability of occurrence for zero-events in the bin:

$$[p \times s(y+z=0)] = p(y=0) = p_0 \qquad (A.5)$$

Where p_0 is the probability of no primary event occurring in the bin: no secondary event can occur.

The probability of occurrence for one event in the bin:

$$[p \times s(y+z=1)] = p(y=1)\ s(z=0) = p_1\ s_{0,1} \qquad (A.6)$$

Where p_1 is the probability of one primary event occurring in the bin, and

$s_{0,1}$ is the probability of no secondary in the bin, given that one primary event occurred.

The probability of occurrence for two events in the bin:

$$[p \times s(y+z=2)] = p(y=2)\, s(z=0) + p(y=1)\ s(z=1)$$

$$= p_2\ s_{0,2} + p_1\ s_{1,1} \qquad (A.7)$$

Where p_2 is the probability of two primary events occurring in the bin,

$s_{0,2}$ is the probability of no secondary in the bin, given that two primary event occurred,

p_1 is the probability of one primary event occurring in the bin, and

$s_{1,1}$ is the probability of one secondary in the bin, given that one primary event occurred.

The probability of occurrence for three events in the bin:

$$[p \times s(y+z=3)] = p_3 s_{0,3} + p_2 s_{1,2} + p_1 s_{2,1} \qquad (A.8)$$

For increasing value of n, the number of integer combinations of y and z increases. By summation and combination of probabilities as the above, the probability of occurrence for any total number n of events in the bin can be computed as a function of only primary-event and secondary-event probabilities. The procedure can be generalized in the following formula for the probability density of the “Convoluted Poisson” distribution:

$$[p \times s(n)] = \sum_{j=1}^{n} p_j \; s(n-j, \lambda_S j) \qquad (A.9)$$

The above formula (A.9) predicts the combined probability of occurrence for both primary and secondary events as function of just two parameters (e.g., λ_p and λ_s) in a bin of length t.

The Cumulative Probability [$P \times S$ (n)] for this “Convoluted Poisson” distribution is simply:

$$[P \times S(n)] = \sum_{k=0}^{n} [\, p \times q(k) \,] \qquad (A.10)$$

Figures A.1 and A.2 show examples for the “Convoluted Poisson” distribution when compared to the classic Poisson distribution. The same value is employed for both λ_p (i.e., mean rate of primary-events) in the former and for the single parameter (i.e., the mean) of the latter. The figures show how the addition of “secondary-event” occurrence, which is determined by both λ_S and λ_p , affects both the probability density and cumulative probability of the “Convoluted Poisson”. For the range of parameter values in the examples, the addition of λ_S decreases the “Convoluted Poisson” probabilities for event occurrence in the range of 2 events, while increases these probabilities for 3 or higher number of events in the bin, as relative to the classic Poisson distribution probabilities.

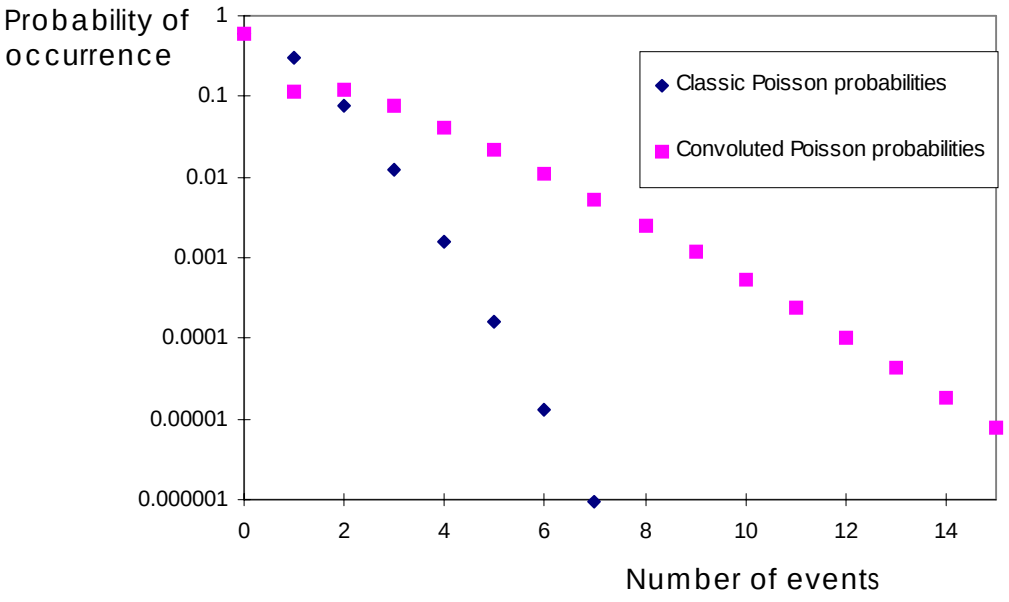

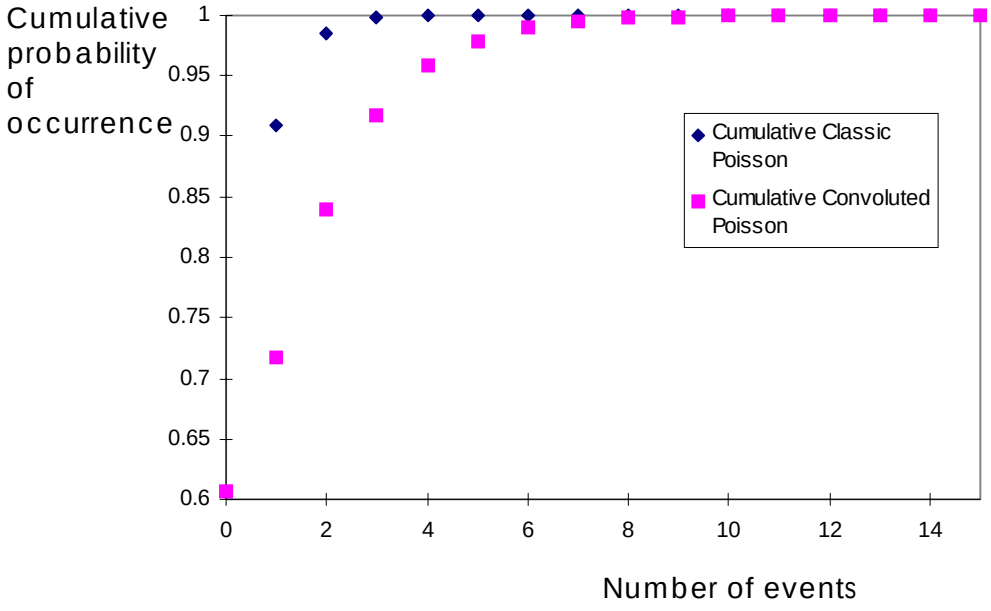

Figure A.1. Classic Poisson distribution for mean = 0.5,

and "Convoluted Poisson" distribution for $\lambda_P = 0.5$ and $\lambda_S = 1$.

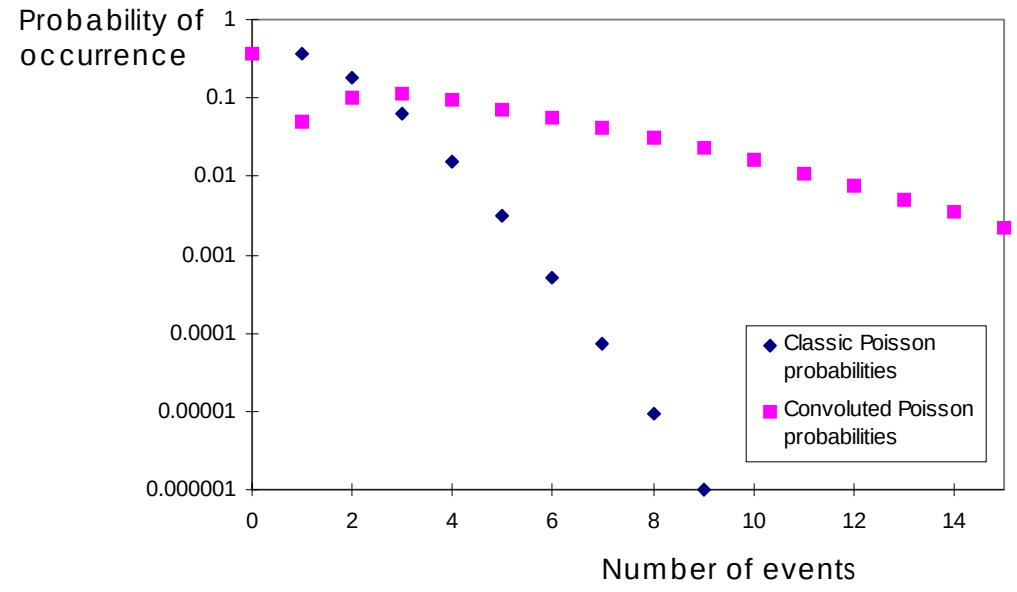

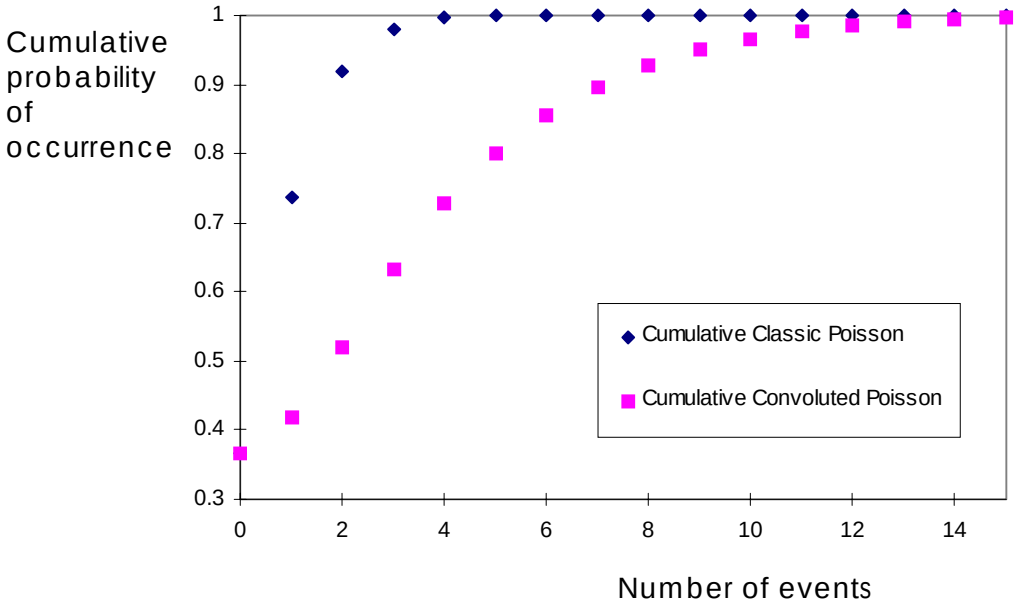

Figure A.2. Classic Poisson distribution for mean = 1,
and "Convoluted Poisson" distribution for $\lambda_P = 1$ and $\lambda_S = 2$.

The definition of the "Convoluted Poisson" allowed induction of its mean and standard deviation formula from numerically generated data:

$$\text{mean}[\,p\times s(n)] = (\lambda_P t)(1+\lambda_S) \qquad \text{(A.11)}$$

$$\text{variance}[\,p\times s(n)] = (\lambda_P t)(\lambda_S+(1+\lambda_S)^2) \qquad \text{(A.12)}$$

It is apparent from the above that both mean and variance of the “Convoluted Poisson” can be substantially larger than that of the original classic Poisson distribution.

Since both primary and secondary events (particles) are independently described by classic Poisson distributions, both should independently proceed as Poisson processes. The Poisson process has the following properties [133]:

- The number of events occurring in any bin is independent of the number of events in any non-overlapping bin (The Poisson process has no memory).

- The mean process rate is constant for the entire time span considered.

- The smaller the considered time-window, the less likely for one or more events to occur in the window (i.e., in the bin).

APPENDIX B

Table B.1. Schedule for the application of load, speed, and grid-voltage (bias) sub-sequences for the retarded-energy measurement of triboemissions from the diamond-on-alumina system.

REPEATED MEASUREMENTS	LOAD (*)	SPEED (*)	GRID VOLTAGE SUB-SEQUENCE [Lower limit , Upper limit] in Volts					
Order number	[N]	[cm/s]	1st sample	2nd sample	6th sample	3rd sample	5th sample	4th sample
1	2	0.14	[0, -3]	[0, -48]	[0, -48]	[0, -12]	[0, -3]	[0, -12] (4)
2	2	0.14	[0, -12]	[0, -12]	[0, -12]	[0, -48]	[0, -12]	[0, -3] (4)
3	2	0.14	[0, -48]	[0, -3]	[0, -3]	[0, -3]	[0, -48]	[0, -48] (4)
4	2	0.96	[0, -3]	[0, -48]	[0, -48]	[0, -12]	[0, -3]	[0, -12]
5	2	0.96	[0, -12]	[0, -12]	[0, -3]	[0, -3]	[0, -12]	[0, -48]
6	2	0.96	[0, -48]	[0, -3]	[0, -12]	[0, -48]	[0, -48]	[0, -3]
7	2	1.92	[0, -3]	[0, -48]	[0, -48]	[0, -12]	[0, -3] (2)	[0, -12] (5)
8	2	1.92	[0, -12]	[0, -12]	[0, -12]	[0, -48]	[0, -12] (2)	[0, -3] (5)
9	2	1.92	[0, -48]	[0, -3]	[0, -3]	[0, -3]	[0, -48] (2)	[0, -48] (5)
10	10	1.92	[0, -3]	[0, -48]	[0, -48]	[0, -12] (1)	[0, -3] (3)	[0, -12] (1)
11	10	1.92	[0, -12]	[0, -12]	[0, -3]	[0, -3] (1)	[0, -12] (3)	[0, -48] (1)
12	10	1.92	[0, -48]	[0, -3]	[0, -12]	[0, -48] (1)	[0, -48] (3)	[0, -3] (1)

(*) Exceptions:
(1) 10N, 0.48cm/second
(2) 10N, 0.96cm/second
(3) 20N, 0.96cm/second
(4) 2N, 0.48cm/second
(5) 10N, 0.14cm/second

Table B.2. Schedule for the application of load, speed, and grid-voltage (bias) sub-sequences for the retarded-energy measurement of triboemissions from the diamond-on-sapphire system.

REPEATED MEASUREMENTS	LOAD	SPEED	GRID VOLTAGE SUB-SEQUENCE [Lower limit , Upper limit] in Volts		
Order number	[N]	[cm/s]	1st sample	2nd sample	3rd sample
1	2	0.14	[0, -3]	[0, -48]	[0, -48]
2	2	0.14	[0, -12]	[0, -12]	[0, -3]
3	2	0.14	[0, -48]	[0, -3]	[0, -12]
4	5	0.14	[0, -12]	[0, -12]	[0, -3]
5	5	0.14	[0, -48]	[0, -3]	[0, -12]
6	5	0.14	[0, -3]	[0, -48]	[0, -48]
7	10	0.14	[0, -48]	[0, -3]	[0, -12]
8	10	0.14	[0, -3]	[0, -48]	[0, -48]
9	10	0.14	[0, -12]	[0, -12]	[0, -3]
10	2	0.48	[0, -3]	[0, -48]	[0, -48]
11	2	0.48	[0, -12]	[0, -12]	[0, -3]
12	2	0.48	[0, -48]	[0, -3]	[0, -12]
13	5	0.48	[0, -12]	[0, -12]	[0, -3]
14	5	0.48	[0, -48]	[0, -3]	[0, -12]
15	5	0.48	[0, -3]	[0, -48]	[0, -48]
16	10	0.48	[0, -48]	[0, -3]	[0, -12]
17	10	0.48	[0, -3]	[0, -48]	[0, -48]
18	10	0.48	[0, -12]	[0, -12]	[0, -3]
19	5	0.96	[0, -3]	[0, -48]	[0, -48]
20	5	0.96	[0, -12]	[0, -12]	[0, -3]
21	5	0.96	[0, -48]	[0, -3]	[0, -12]
22	10	0.96	[0, -12]	[0, -12]	[0, -3]
23	10	0.96	[0, -48]	[0, -3]	[0, -12]
24	10	0.96	[0, -3]	[0, -48]	[0, -48]
25	20	0.96	[0, -48]	[0, -3]	[0, -12]
26	20	0.96	[0, -3]	[0, -48]	[0, -48]
27	20	0.96	[0, -12]	[0, -12]	[0, -3]
28	5	1.92	[0, -3]	[0, -48]	[0, -48]
29	5	1.92	[0, -12]	[0, -12]	[0, -3]
30	5	1.92	[0, -48]	[0, -3]	[0, -12]
31	10	1.92	[0, -12]	[0, -12]	[0, -3]
32	10	1.92	[0, -48]	[0, -3]	[0, -12]
33	10	1.92	[0, -3]	[0, -48]	[0, -48]
34	20	1.92	[0, -48]	[0, -3]	[0, -12]
35	20	1.92	[0, -3]	[0, -48]	[0, -48]
36	20	1.92	[0, -12]	[0, -12]	[0, -3]

APPENDIX C

Testing of hypotheses for the statistical significance of triboemission results

This appendix presents the testing of the hypotheses that the experimental differences measured for the triboemission outputs during contact vs. the CEM-count during non-contact are statistically significant for the material systems investigated. For this, the two-sample t-test (with no assumption of equal variances for the samples) [133] is used.

Each sample is composed of a small number of pin-on-disk specimens (i.e., experimental units) of the same material system (i.e., diamond-on-alumina, diamond-on-sapphire, diamond-on-aluminum, and alumina-on-alumina systems). The hypotheses that negatively- and positively-charged triboemission outputs are significant are tested separately with different samples. From each of the specimens in each sample, one non-contact output and one triboemission output were obtained as per the procedures of Section 3.2. Some of these triboemission outputs were presented in Chapter 4 (See Figures 4.10 to 4.17 and 4.23 to 4.25).

For each of these triboemission and non-contact outputs, the average CEM-count (i.e., the response for these tests) is computed as the accumulated CEM-count divided the pertaining time (i.e., the time during contact or non-contact). Sample means of these averages are computed within each sample. The test statistics employed is the difference of sample means for the contact and non-contact situations [133].

Following Table C.1 summarizes for the material systems investigated, the tested hypotheses and sample sizes, and the t-values and pertaining p-values of the computed statistical tests.

Table C.1. Summary of the testing of hypotheses for the statistical significance of positively- and negatively-charged triboemission outputs.

H (-) : Sample mean for the average negatively-charged triboemission outputs.
H (+) : Sample mean for the average positively-charged triboemission outputs.
H (0) : Sample mean for the average background (during non-contact) outputs.

Material system	**Tested hypothesis**	**Sample size**	**t-value**	**p-value**
Diamond-on-alumina	H (-) $\neq$ H (0)	2	4.47	0.14
Diamond-on-sapphire	H (-) $\neq$ H (0)	3	2.35	0.14
Diamond-on-alumina (i) vs. diamond on sapphire (ii) (*)	H (-) (for i) $\neq$ H (-) (for ii)	2 and 3	1.04	0.41
Diamond-on-alumina (i) and diamond on sapphire (ii) (**)	H (-) (for i + ii) $\neq$ H (0)	2 + 3	3.10	0.036
Diamond-on-aluminum	H (-) $\neq$ H (0)	3	3.53	0.072
Alumina-on-alumina	H (-) $\neq$ H (0)	3	6.15	0.025
Diamond-on-alumina	H (+) $\neq$ H (0)	2	2.47	0.24
Diamond-on-sapphire	H (+) $\neq$ H (0)	2	0.46	0.72
Alumina-on-alumina	H (+) $\neq$ H (0)	2	0.66	0.63

(*) For testing of the hypothesis that the experimental difference measured for the triboemission outputs during contact of diamond-on-alumina vs. diamond-on-sapphire is statistically significant.
(**) Since above test (*) shows no significant difference for the measured diamond-on-alumina triboemission output vs. the diamond-on-sapphire triboemission output, samples from the two material systems are pooled for this test.

APPENDIX D

Table D.1. Material system, applied load, sliding speed, contact schedule and type of measurement for the measurements of triboemission reported in this dissertation research

Figure for test	Material system	Load [N]	Sliding speed [cm/s]	Contact schedule	Type of measurement
4.1	Diamond-on-alumina	2	1.4	20s-periods of contact alternated with 10s-periods of non-contact	Non-grid negatively-charged CEM output
4.2	Diamond-on-alumina	2	0.12	Three-first turns of contact	Non-grid negatively-charged CEM output
4.3	Diamond-on-alumina	2	(*)	100sec-period of contact	Non-grid negatively-charged CEM output
4.4	Diamond-on-alumina	2	(*)	100sec-period of contact	Non-grid positively-charged CEM output
4.5, 4.6, 4.7	Diamond-on-alumina	2	0.12	Three-first turns of contact	Negatively-charged triboemission
4.8	Diamond-on-alumina	2	(*)	100sec-period of contact	Negatively-charged triboemission
4.9	Diamond-on-alumina	10	(*)	100sec-period of contact	Negatively-charged triboemission
4.10	Diamond-on-alumina	2	0.48	320sec-period of contact	Negatively-charged triboemission
4.11	Diamond-on-alumina	2	0.48	260sec-period of contact	Negatively-charged triboemission
4.12	Diamond-on-sapphire	2	0.48	320sec-period of contact	Negatively-charged triboemission

(*) Constant acceleration of 0.048 cm/sec^2 for sliding speed from 0.12cm/sec to 4.8cm/sec.

Table D.1. (Continued from previous page)

4.13	Diamond-on-sapphire	2	0.48	280sec-period of contact	Negatively-charged triboemission
4.15	Diamond-on-aluminum	2	0.48	160sec-period of contact	Negatively-charged triboemission
4.16	Diamond-on-alumina	10	0.96	320sec-period of contact	Positively-charged triboemission
4.17	Diamond-on-sapphire	2	0.48	300sec-period of contact	Positively-charged triboemission
4.20	Alumina-on-alumina	2	0.48	320sec-period of contact	Negatively-charged triboemission
4.21	Alumina-on-alumina	2	0.48	320sec-period of contact	Negatively-charged triboemission
4.22, 4.23	Alumina-on-alumina	2	0.48	45sec-periods of contact	Negatively-charged triboemission
4.24	Alumina-on-alumina	2	0.48	300sec-period of contact	Positively-charged triboemission
4.25	Alumina-on-alumina	20	0.48	300sec-period of contact	Positively-charged triboemission

(*) Constant acceleration of 0.048 cm/sec^2 for sliding speed from 0.12cm/sec to 4.8cm/sec.

NOTE: Information pertaining to retarded-energy measurements is given in Appendix B.

Vita

Mr. Gustavo J. Molina received his Diploma in Mechanical and Electrical Engineering from National University of Cordoba, Argentina in 1986. From 1987 to 1992 he was in the Argentina's National Institute for Industrial Technology, where he acquired extensive expertise in mechanical design of experimental equipment, CAD and vacuum techniques. He also did applied research on the areas of surface modifications, physical vapor deposition coatings, and sintered rare-earth magnets.

In 1994 he received a master's degree in Mechanical Engineering from the University of Ottawa, Canada, where he conducted research on the characterization of impact properties of polymers and polymer-matrix composites, and on the application of pattern recognition and classification to nondestructive data.

He came to Virginia Polytechnic Institute and State University in 1996 as a Ph.D. candidate, and he has been since then involved in the project "Triboemission of Charged Particles from Ceramic Surfaces and Their Role in Tribochemistry", funded by the National Science Foundation, Surface Engineering and Tribology Program. He designed and developed the triboemission device and system and carried the experimental testing and data analysis described in this dissertation. Mr. Molina is the author of 16 journal and congress publications. He has been appointed Assistant Professor at Georgia Southern University, School of Technology, Engineering Studies Program, Statesboro, Georgia, and he will start in this faculty position upon completion of the requirements for the Ph.D. degree.

_____

Gustavo J. Molina